Mathematical and computational methods in R-matrix theory

Edited by

Martin Plummer
Jimena D Gorfinkiel
Jonathan Tennyson

Mathematical and computational methods in R-matrix theory

Edited by

Martin Plummer

Computational Science and Engineering,
STFC Daresbury Laboratory,
Daresbury,
Warrington, WA4 4AD,
United Kingdom

Jimena D Gorfinkiel

Department of Physics and Astronomy,
The Open University,
Walton Hall, Milton Keynes, MK7 6AA,
United Kingdom

Jonathan Tennyson

Department of Physics and Astronomy,
University College London,
Gower Street, London, WC1E 6BT,
United Kingdom

Suggested Dewey classification: 539.7, 541.2

ISBN 978-0-9556616-3-1

Published by

Collaborative Computational Project
on Continuum States of Atoms and Molecules (CCP2),
STFC Daresbury Laboratory,
Daresbury,
Warrington, WA4 4AD,
United Kingdom

Introduction

The UK Collaborative Computing Project 2 (CCP2), supported by EPSRC, has as its area of interest: 'Continuum states of atoms and molecules'. This includes multiphoton processes involving atoms and molecules and electron and positron scattering by atoms and molecules. CCP2 is also involved in work on electron scattering by solids, the theory of Bose–Einstein condensation and the interaction of antihydrogen with simple atoms and molecules.

This booklet is the result of a CCP2 workshop held at University College London over 13–15 September 2007 and contains a variety of articles contributed by invited speakers. We were very pleased to have an international range of speakers despite the limitations of the CCP2 budget and we would like to thank the speakers for their time and for a most stimulating workshop. The specialist articles are designed primarily to provide an insight into diverse technical aspects of theory and calculations, but also demonstrate the broad range of scientific applications of R-matrix theory in atomic, molecular and optical physics and theoretical chemistry. We note that R-matrix theory essentially means a variational *ab initio* solution of the Schrödinger equation with configuration space usefully divided into two or more regions in which the most effective techniques for solution may be used.

The aim of the workshop was to bring together members of the R-matrix community to exchange ideas and techniques, and also to remind each other of the range and success of applications of R-matrix theory. In particular the workshop provided an opportunity for the respective atomic and molecular R-matrix communities to come together: we believe such interaction is extremely valuable and should be encouraged, especially by CCP2 with its emphasis on support for 'collaborative computation'.

We hope the booklet will be of use to researchers in the field who may be interested in the techniques presented, and also to research students who have been introduced to the basics of R-matrix theory and who can use the booklet as a starting point for the study of more specialist applications. We should emphasize that despite the diversity of the articles, the booklet is not intended to be an exhaustive record of the current world-wide state of R-matrix theory, rather the range of topics reflects the interests of the speakers. There is a distinct bias towards discussion of the 'inner-region diagonalization' version of R-matrix theory, although we are pleased to include articles which incorporate a direct variational approach. Following a review by Professor P G Burke, we present the specialist articles in alphabetical order of the speakers.

Martin Plummer, Jimena D Gorfinkiel and Jonathan Tennyson

M Plummer, J D Gorfinkiel and J Tennyson (eds.)
Mathematical and computational methods in R-matrix theory

R-matrix theory: applications and challenges

P G Burke

School of Mathematics and Physics,
The Queen's University of Belfast, Belfast BT7 1NN, UK

I. INTRODUCTION

The development and application of R-matrix theory in the study of atomic, molecular and optical processes was based on fundamental ideas first introduced in electron-atom collisions and in nuclear reaction theory. In electron-atom collisions, Massey and Mohr [1,2] in the early 1930s introduced the close coupling expansion and Seaton [3] in the early 1950s showed how exchange effects could be included in this expansion by extending the Hartree-Fock equations to continuum states. Both of these developments are essential components in R-matrix theory of electron collisions with atoms, ions and molecules. In nuclear reaction theory, Wigner and Eisenbud [4–6] in the late 1940s introduced the R-matrix on the boundary of an internal region as a means of representing the complex nuclear reactions that occur in this region, and Lane and Thomas [7] showed how this theory could describe a wide range of nuclear reactions. Following these developments, R-matrix theory was introduced in the early 1970s [8,9] as an *ab initio* procedure for calculating accurate electron-atom and electron-ion collision cross sections, where the Coulomb interactions between the electrons and the nucleus are accurately included in the internal region. R-matrix theory has been extended to treat a wide range of collision processes, supported by CCP2, since the first meeting of the CCP2 Working Group on 17 February 1978.

II. OVERVIEW OF *R*-MATRIX THEORY

In order to describe electron collisions with atoms, ions and molecules, configuration space is partitioned into three regions, as illustrated in Figure 1 (adapted from [10], Figure 2).

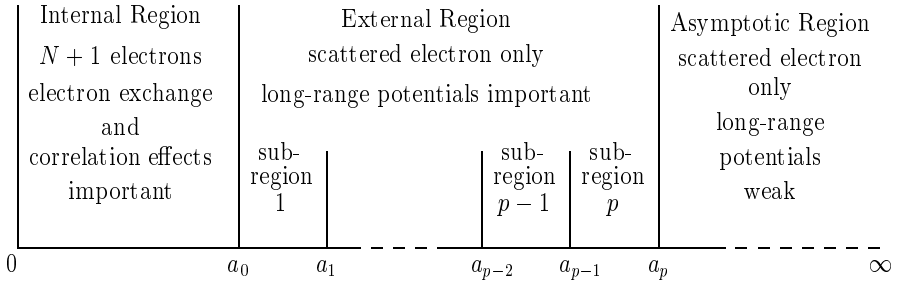

FIG. 1. The partitioning of configuration space in electron-atom collisions

In the internal region $0 \leq r \leq a_0$, where r is the radial coordinate of the scattered electron, electron exchange and electron-electron correlation effects are important and the total wave function is expanded in a CI basis which takes the following form for each total orbital angular momentum, spin and parity combination

$$\psi_k(\boldsymbol{X}_{N+1}) = \mathcal{A}\sum_{ij}\overline{\Phi}_i(\boldsymbol{X}_N;\hat{\boldsymbol{r}}_{N+1}\sigma_{N+1})r_{N+1}^{-1}u_{ij}(r_{N+1})a_{ijk} + \sum_j \chi_j(\boldsymbol{X}_{N+1})b_{jk}\ , \quad k=1,\ldots,n_t\ , \tag{1}$$

where $\mathcal{A}$ is the usual antisymmetrization operator. The functions $\overline{\Phi}_i$ are formed by coupling the target states with the spin-angle functions of the scattered electron, u_{ij} are radial basis functions representing the scattered electron and χ_j are L^2 integrable correlation functions. The coefficients a_{ijk} and b_{jk} are obtained by diagonalizing the $N+1$-electron Hamltonian in the basis ψ_k.

$$\langle\psi_k|H_{N+1}+\mathcal{L}_{N+1}|\psi_{k'}\rangle_{int} = E_k\delta_{kk'}, \tag{2}$$

where $\mathcal{L}_{N+1}$ is a Bloch surface operator [11] which ensures that $H_{N+1}+\mathcal{L}_{N+1}$ is hermitian in the internal region and where the boundary $r=a_0$ is chosen so that $\overline{\Phi}_i$ and χ_j in (1) vanish for $r \geq a_0$. The R-matrix is then defined by

$$R_{ij}(E) = \frac{1}{2a_0}\sum_k \frac{w_{ik}w_{jk}}{E_k - E}, \tag{3}$$

where the surface amplitudes

$$w_{ik} = \sum_j u_{ij}(a_0)a_{ijk}. \tag{4}$$

In the external region the reduced radial wave functions $F_{ij}(r)$, describing the motion of the scattered electron, satisfies a set of coupled second-order differential equations, subject to the R-matrix boundary condition at $r = a_0$.

$$F_{ij}(a_0) = \sum_k R_{ik}(E)\; a_0 \frac{\mathrm{d}F_{kj}}{\mathrm{d}r}\bigg|_{r=a_0} . \tag{5}$$

The coupled differential equations are then integrated from $r = a_0$ to $r = a_p$, using a standard procedure, and the solution fitted to an asymptotic expansion to yield the K-matrix, S-matrix, scattering amplitudes and cross sections. This theory and its applications are described in a recent review [10].

III. LOW-ENERGY ELECTRON COLLISIONS WITH ATOMS AND IONS

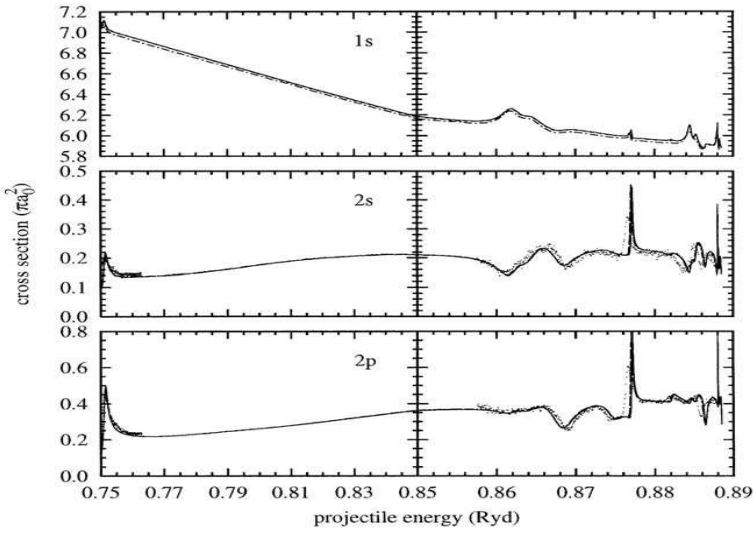

FIG. 2.
Total electron-hydrogen atom 1s–1s, 1s–2s and 1s–2p cross sections between the $n = 2$ and $n = 3$ thresholds. *Full curve*, RMPS; *broken curve*, IERM; *chain curve*, CCC. The dots represent the experimental data of Williams [13]

Since the early 1970s R-matrix theory has been applied to a wide range of low-energy electron-atom and electron-ion collisions of importance in applications, and general computer programs have been developed which enable these

processes to be calculated [10]. In this section two applications are described which illustrate both the accuracy now attainable in low-energy collisions and the challenges which still exist.

The first application considered is electron collisions with atomic hydrogen. The total elastic scattering and 1s–2s and 1s–2p excitation cross sections are shown in Figure 2 (adapted from [12], Figure 4) where the R-matrix and convergent close coupling calculations [12] are seen to be in excellent agreement with experiment [13] accurately reproducing the resonance structure just above the $n = 2$ threshold at 0.75 Ryd and just below the $n = 3$ threshold at 0.8889 Ryd. It is found that the cross section for electron collisions with atomic hydrogen can be accurately calculated using the R-matrix method for target states with principal quantum number $n \leq 5$. However, there is still a major computational problem to obtain accurate cross sections for high $n \approx 10$ states, which are important in some astrophysical applications, due to the many coupled channels involved and the very large radial extent of the target atom eigenstates.

As a second example we consider electron collisions with iron peak elements. Electron impact excitation cross sections and related collision strengths for low ionization stages of open d-shell iron peak elements are of crucial importance in the analysis of a wide range of astrophysical spectra and many calculations have been carried out, using the R-matrix programs, as part of the international IRON PROJECT collaboration [14]. Of particular importance are electron collisions with Fe II and we show in Figure 3 (adapted from [10], Figure 7) the low-energy total collision strength for the transition between the two lowest states $3d^6 4s\ a\,^6D \rightarrow 3d^7\ a\,^4F$ neglecting relativistic effects [15]. We see that this calculation,

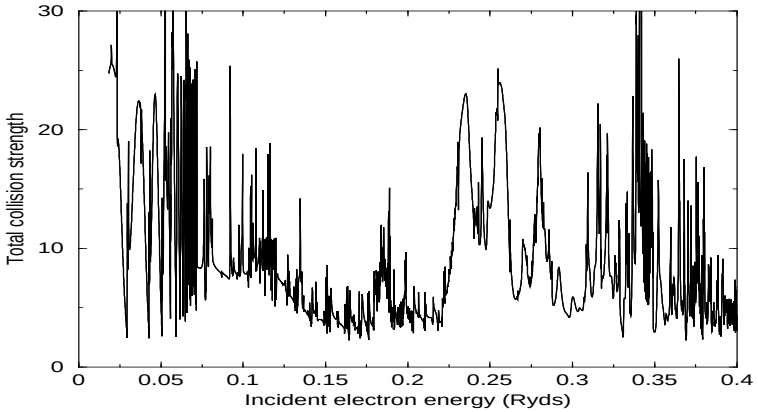

FIG. 3. Total collision strengths for $3d^6 4s\ a\,^6D \rightarrow 3d^7\ a\,^4F$ transition in e^- – Fe II collisions at low energies

which included 113 target states and 301 coupled channels, is dominated by resonances requiring a very fine energy mesh to fully resolve. However, to obtain converged results up to ~ 15 eV many more states would have to be included in the calculation and relativistic terms retained in the Hamiltonian. This would yield over 2000 target states and over 15,000 coupled channels which would correspond to a "grand challenge" calculation.

IV. INCLUSION OF RELATIVISTIC EFFECTS

As the charge number Z on the atomic nucleus increases, relativistic effects become progressively more important in the collision process. There are several procedures for including relativistic effects in low-energy electron collisions. For relatively light targets, these effects are small so that the energy intervals between the fine-structure levels of the target are small compared with the typical intervals between the $LS\pi$ coupled energy levels of the target. In this case the method of Saraph [16,17] which transforms the K-matrix to intermediate coupling was widely used although this method has difficulties since closed channels, which may be important, are omitted in the transformation. This difficulty was overcome by Badnell and Griffin [18] who used Seaton's multichannel quantum defect theory [19] to include the closed channels. Further developments which include relativistic effects in the external region and in the low-lying R-matrix states in the internal region have been proposed [20]. It should however be noted that the above methods are approximations to solving the problem directly using the Breit-Pauli Hamiltonian [21–23]. Finally, for the heaviest atomic targets the Dirac equation must be solved to yield the R-matrix, K-matrix and cross sections [24].

V. INTERMEDIATE ENERGY COLLISIONS

In the examples considered so far, the energy of the incident electron is insufficient to ionize the target. However at higher energies, from close to the ionization threshold to several times this threshold, strong coupling effects will exist between the channels leading to excitation and to ionization. In this so-called "intermediate energy region" theoretical methods which give reliable results must accurately represent this coupling. A successful approach for representing the continuum in electron-atom collisions is the R-matrix with Pseudostates (RMPS) method [25–28]. In this method the first expansion in (1) over target eigenstates is augmented by the inclusion of additional quadratically integrable target pseudostates, representing the continuum, which

are constructed by including additional contracted pseudo-orbitals in the target orbital basis. In this way the exact spectrum of the target is replaced by an approximate discrete spectrum. In practice, it has proved necessary to retain several times more pseudostates than eigenstates in expansion (1) in order to obtain accurate excitation and ionization cross sections at intermediate energies. Also, in order to obtain accurate cross sections close to the ionization threshold it is necessary to have a high density of pseudostate energies in the neighbourhood of this threshold. This can be achieved by allowing two electrons to penetrate into the external region where the corresponding two-dimensional external region is divided into a number of sub-regions. This is the basis of the Intermediate Energy R-matrix Method (IERM) [29,30], which has yielded accurate excitation and ionization cross sections close to threshold.

Finally, both the RMPS and IERM methods involve many coupled target states and hence the calculations can become very large. This is particularly true for calculations involving the iron peak elements and calculations involving highly excited states, both of which provide grand challenges.

VI. ELECTRON-MOLECULE COLLISIONS

The processes that occur in electron-molecule collisions are considerably more varied than those that arise in electron collisions with atoms and ions. Thus, as well as the multicentre nature of the target, the possibility of exciting degrees of freedom associated with the motion of the nuclei must be included in the theory. In practice most calculations commence from the fixed-nuclei approximation and include the nuclear motion in a second step of the calculation. The first fixed-nuclei calculations using R-matrix theory were carried out in the 1970s by Schneider [31,32] and the inclusion of nuclear motion in R-matrix theory was first considered by Schneider *et al* [33]. A recent review of R-matrix theory applications to electron-molecule collisions has been written [34].

Over the last 25 years considerable effort has been directed to developing general R-matrix computer programs for calculating electron collisions with diatomic and polyatomic molecules. Recently, increasing attention has been paid to electron collisions with polyatomic molecules [35,36] and Figure 4 shows calculations of electron impact excitation of H_3^+ [37] which plays a fundamental role in interstellar chemistry and has been observed in planetary aurora and diffuse interstellar media.

In this figure (adapted from [37], Figure 1) the dark full line corresponds to including the lowest 6 target eigenstates in the R-matrix expansion and the light full line includes in addition 58 pseudostates representing the ionizing channels, as discussed in Sect. V. It is seen that including the pseudostates

greatly reduces the cross section above the ionization threshold. Recent work has extended the calculations to more complex polyatomic molecules, including methanol (CH_3OH) of biological interest [38].

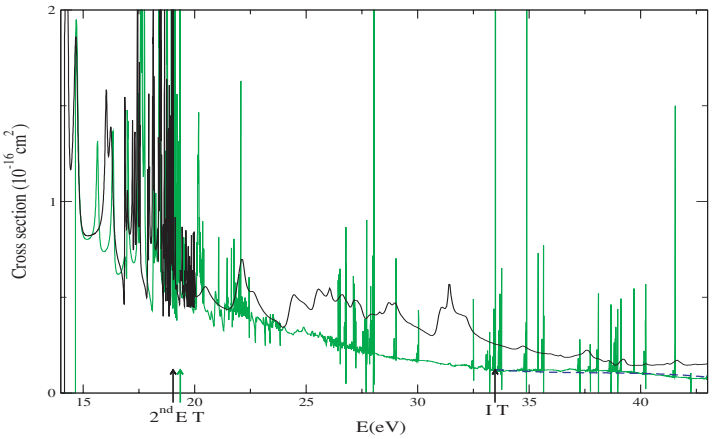

FIG. 4. Integrated cross sections for excitation of the first excited electronic state $^3E'$ of H_3^+ from the ground state X^1A_1'

VII. POSITRON COLLISIONS WITH ATOMS AND IONS

In addition to positron impact excitation and ionization, which also arise in electron impact collisions, PS (positronium) and PS^- formation as well as positron annihilation can occur. There is also considerable interest in the various processes where ortho PS is incident on an atom or ion. Since the positron is distinguishable from the target electrons, there is no need to antisymmetrize the total wave function as in (1). However, this simplification is balanced by the need to include the additional positronium formation channels as discussed in a recent review [39].

R-matrix programs have been developed [39] which have enabled detailed calculations to be carried out for positron collisions with atomic hydrogen and with "one-electron" alkali metal atoms Li, Na, K, Rb and Cs and with the "two-electron" atoms He, Mg, Ca and Zn. In addition detailed calculations for ortho PS collisions with He, Ne, Ar, Kr and Xe have been carried out, where the Ps can be in its 1s, 2s or 2p state and the target is frozen in its ground state. In the case of PS–He collisions good agreement has recently been obtained with experiments at UCL [40].

It is clear that major advances have been made in recent years in both R-matrix collision calculations and in experiment in this area. However there is a challenge to extend the theory and calculations to collisions with general atoms and molecules.

VIII. ATOMIC PHOTOIONIZATION

The extension of R-matrix theory of electron-atom collisions, and the corresponding computer programs, to treat photoionization was first made in the mid 1970s [41]. In this theory the differential cross section for photoionization is written in atomic units in the dipole length form

$$\frac{\mathrm{d}\sigma_{ij}^{\mathrm{L}}}{\mathrm{d}\Omega} = 4\pi^2 \alpha a_0^2 \omega \left| \langle \Psi_{fE}^{-} | \hat{\boldsymbol{\epsilon}}.\boldsymbol{D}_{\mathrm{L}} | \Psi_i \rangle \right|^2 , \tag{6}$$

where $\boldsymbol{D}_{\mathrm{L}}$ is the dipole length operator and Ψ_i and Ψ_{fE}^{-} are the initial bound state and the final continuum state, with ingoing wave boundary conditions, of the target atom. An equivalent expression using the dipole velocity form of the matrix element is also usually used. Both the initial and final states in (6) are obtained using R-matrix expansions, as discussed in Sect. II.

Many calculations for atoms and atomic ions have been carried out over the last 30 years in support of experiments using synchrotron radiation sources. In addition, the international OPACITY PROJECT, led by Seaton [42], developed and used this program as the basis of photoionization calculations for all stages of ionization of elements from He to Ni of importance in the opacity of stellar envelopes. Recent developments in the OPACITY PROJECT have been reviewed by Badnell *et al* [43] and its importance in understanding elemental abundances in the sun has been discussed by Bahcall [44].

In the future the extension of this work to heavy elements of importance in laser-plasma interactions and to photoionization of molecules will be a major challenge.

IX. MULTIPHOTON IONIZATION

The study of the interaction of intense laser fields with atoms and molecules has attracted considerable attention in recent years. In particular, the availability of increasingly intense lasers has made possible the observation of a wide variety of multiphoton processes, including multiphoton ionization, harmonic generation and laser-assisted electron-atom collisions. For longer pulse lasers, which are not too intense ($\geq$ 50 fsec, $\leq 10^{15}$ W cm^{-2}), Floquet theory

has been used to describe the processes. However, for very short pulse intense lasers now available using the "Chirped Pulse Amplification" (CPA) scheme [45], a time-dependent treatment of the collision must be adopted.

Since the early 1990s an R-matrix-Floquet (RMF) theory [46] has been widely used to describe atomic multiphoton processes and has also been applied to molecular multiphoton processes [10]. In addition to many detailed studies of atomic multiphoton ionization over the last 17 years, RMF theory has been successfully applied to atomic harmonic generation [47,48] and to laser-assisted electron-atom collisions [49,50]. In RMF theory the time-dependent wave function is expanded as follows

$$\Psi(\boldsymbol{X}_{N+1}, t) = \mathrm{e}^{-\mathrm{i}Et} \sum_{n=-\infty}^{\infty} \mathrm{e}^{-\mathrm{i}n\omega t} \psi_n(\boldsymbol{X}_{N+1}), \tag{7}$$

where ω is the laser angular frequency. The time-independent functions ψ_n are then determined by partitioning configuration space as in Figure 1 and expanding the wave function in each region as described in Sect. II. The main problem is that now, instead of a single function as in electron-atom collisions, it may be necessary in intense laser fields to retain up to 10 or more terms in expansion (7) to obtain convergence.

Recently a full time-dependent R-matrix theory and computer program have been developed for a general atom and applied to multiphoton ionization of Ar [51].

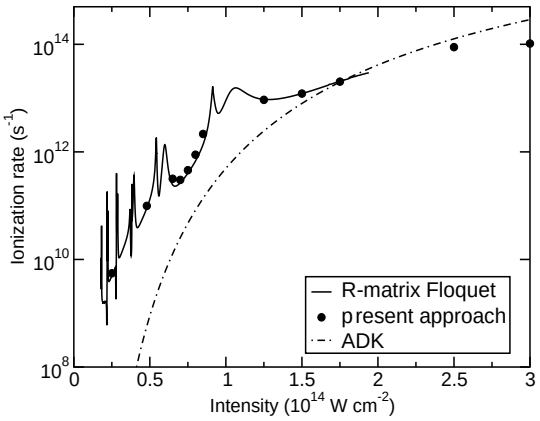

FIG. 5. Comparison of ionization rates for Ar irradiated with 390 nm light as a function of intensity Time-dependent results (solid circles), R-matrix-Floquet results (solid line), ADK results (dashed line)

The results of this time-dependent calculation are compared with Floquet calculations and with an approximate ADK [52] approach in Figure 5 (adapted from [51], Figure 4). There is excellent agreement between the time-dependent and Floquet results, with the time-dependent approach able to extend the calculation to higher laser intensities and, of course, to very short laser pulses. A major challenge for the future is to extend the time-dependent approach to higher intensities and to other complex atoms and ions as well as to molecules, and also to consider processes of current experimental interest where two electrons are ejected from the target due to a re-collision mechanism.

X. CONCLUSIONS

This brief review has shown that R-matrix theory has been successfully applied to a very wide range of atomic, molecular and optical collision processes since the early 1970s. Other applications, which have not been discussed here but are of increasing interest are to low-energy electron collisions with surfaces where some preliminary work has been carried out [53]. Finally, this review has pointed to a number of major challenges which will stimulate further work in this field.

---

[1] Massey, H.S.W. and Mohr, C.B.O., 1932, *Proc. Roy. Soc. A* **136**, 289.
[2] Massey, H.S.W. and Mohr, C.B.O., 1933, *Proc. Roy. Soc. A* **139**, 187.
[3] Seaton, M.J., 1953, *Phil. Trans. Roy. Soc. A* **245**, 469.
[4] Wigner, E.P., 1946, *Phys. Rev.* **70**, 15.
[5] Wigner, E.P., 1946, *Phys. Rev.* **70**, 606.
[6] Wigner, E.P. and Eisenbud, L., 1947, *Phys. Rev.* **72**, 29.
[7] Lane, A.M. and Thomas, R.G., 1958, *Rev. Mod. Phys.* **30**, 257.
[8] Burke, P.G., Hibbert, A. and Robb, W.D., 1971, *J. Phys. B: At. Mol. Phys.* **4**, 153.
[9] Burke, P.G. and Robb, W.D., 1975, *Adv. At. Mol. Phys.* **11**, 143.
[10] Burke, P.G., Noble, C.J. and Burke, V.M., 2007, *Adv. At. Mol. Opt. Phys.* **54**, 237.
[11] Bloch, C., 1957, *Nucl. Phys.* **4**, 503.
[12] Bartschat, K., Bray, I., Burke, P.G. and Scott, M.P., 1996, *J. Phys. B: At. Mol. Opt. Phys.* **29**, 5493.
[13] Williams, J.F., 1988, *J. Phys. B: At. Mol. Opt. Phys.* **21**, 2107.

[14] Hummer, D.G., Berrington, K.A., Eissner, W., Pradhan, A.K., Saraph, H.E. and Tully, J.A., 1993, *Astron. Astrophys.* **279**, 298.
[15] Ramsbottom C.A., Noble C.J., Burke, V.M., Scott, M.P., Kisielius, R. and Burke, P.G., 2005, *J. Phys. B: At. Mol. Opt. Phys.* **38**, 2999.
[16] Saraph, H.E., 1972, *Comput. Phys. Commun.* **3**, 256.
[17] Saraph, H.E., 1978, *Comput. Phys. Commun.* **15**, 247.
[18] Badnell, N.R., and Griffin, D.C., 1999, *J. Phys. B: At. Mol. Opt. Phys.* **32**, 2267.
[19] Seaton, M.J., 1983, *Rep. Prog. Phys.* **46**, 167.
[20] Burke, P.G. and Burke, V.M., *J. Phys. B: At. Mol. Opt. Phys. to be published.*
[21] Scott, N.S. and Burke, P.G., 1980, *J. Phys. B: At. Mol. Phys.* **13**, 4299.
[22] Berrington, K.A., Eissner, W.B. and Norrington, P.H., 1995, *Comput. Phys. Commun.* **92**, 290.
[23] Zatsarinny, O., 2006, *Comput. Phys. Commun.* **174**, 273.
[24] Norrington, P.H. and Grant, I.P., 2007, *Comput. Phys. Commun.* to be published, see also http://www.am.qub.ac.uk/DARC/.
[25] Bartschat, K., Hudson, E.T., Scott, M.P., Burke, P.G. and Burke, V.M., 1996, *J. Phys. B: At. Mol. Opt. Phys.* **29**, 115.
[26] Bartschat, K., Hudson, E.T., Scott, M.P., Burke, P.G. and Burke, V.M., 1996, *Phys. Rev. A* **54**, R998.
[27] Badnell, N.R., and Gorczyca, T.W., 1997, *J. Phys. B: At. Mol. Opt. Phys.* **30**, 2011.
[28] Badnell, N.R., and Gorczyca, T.W., 1997, *J. Phys. B: At. Mol. Opt. Phys.* **30**, 3897.
[29] Burke, P.G., Noble, C.J. and Scott, M.P., 1987, *Proc. Roy. Soc. A* **410**, 289.
[30] Le Dourneuf, M., Launay, J.-M., and Burke, P.G., 1990, *J. Phys. B: At. Mol. Opt. Phys.* **23**, L559.
[31] Schneider, B.I., 1975, *Chem. Phys. Lett.* **31** 237.
[32] Schneider, B.I., 1975, *Phys. Rev. A* **11**, 1957.
[33] Schneider, B.I., Le Dourneuf, M. and Burke, P.G., 1979, *J. Phys. B: At. Mol. Phys.* **12**, L365.
[34] Burke, P.G. and Tennyson, J., 2005, *Molec. Phys.* **103**, 2537.
[35] Morgan, L.A., Tennyson, J. and Gillan, C.J., 1998, *Comput. Phys. Commun.* **114**, 120.
[36] Tennyson, J. and Morgan, L.A., 1999, *Phil. Trans. Roy. Soc. A* **357**, 1161.
[37] Gorfinkiel, J.D. and Tennyson, J., 2004, *J. Phys. B: At. Mol. Opt. Phys.* **37**, L343.
[38] Bouchiha, D.,Gorfinkiel, J.D., Caron, L.G. and Sanche, L., 2007, *J. Phys. B: At. Mol. Opt. Phys.* **40**, 1259.
[39] Walters, H.R.J. and Starret, C., 2007, *NASA Symposium on Atomic and Molecular Physics* Ed. A.K. Bhatia (NASA/CP-2006-214146) 187.
[40] Armitage, S., Leslie, D.E., Garner, A.J. and Laricchia, G., 2002, *Phys. Rev. Lett.* **89**, 173402.
[41] Burke, P.G. and Taylor, K.T., 1975, *J. Phys. B: At. Mol. Phys.* **8**, 2620.
[42] Seaton, M.J., 1987, *J. Phys. B: At. Mol. Phys.* **20**, 6363.
[43] Badnell, N.R., Bautista, M.A., Butler, K., Delahaye, F., Mendoza, C., Palmeri, P., Zeippen, C.J. and Seaton, M.J., 2005, *Mon. Not. R. Astron. Soc.*, **360**, 458.

[44] Bahcall, J.N., 2005, *Physics World* **18** No. 2, 26.
[45] Strickland, D. and Mourou, G., 1985, *Opt. Commun.* **56**, 219.
[46] Burke, P.G., Francken, P. and Joachain, C.J., 1991, *J. Phys. B: At. Mol. Opt. Phys.* **24**, 761.
[47] Plummer, M. and Noble, C.J., 2000, *J. Phys. B: At. Mol. Opt. Phys.* **33**, L807.
[48] Plummer, M. and Noble, C.J., 2002, *J. Phys. B: At. Mol. Opt. Phys.* **35**, L51.
[49] Charlo, D., Terao-Dunseath, M., Dunseath, K.M. and Launay, J.-M., 1998, *J. Phys. B: At. Mol. Opt. Phys.* **31**, L539.
[50] Terao-Dunseath, M. and Dunseath, K.M., 2002, *J. Phys. B: At. Mol. Opt. Phys.* **35**, 125.
[51] van der Hart, H.W., Lysaght, M.A. and Burke, P.G., 2007, *Phys. Rev. A* **76**, 043405.
[52] Ammosov, M.V., Delone, N.B. and Krainov, V.P., 1986, *Sov. Phys. JETP* **64**, 1191.
[53] Jones, P., Inglesfield, J.E., Michiels, J.J.M., Noble, C.J., Burke, V.M. and Burke, P.G., 2000, *Phys. Rev. B* **62**, 13508.

M Plummer, J D Gorfinkiel and J Tennyson (eds.)
Mathematical and computational methods in R-matrix theory

R-matrix for heavy species

N R Badnell

Department of Physics,
University of Strathclyde, Glasgow, G4 0NG, UK

We discuss R-matrix approaches for collisions involving heavy species, viz. elements beyond zinc, where the use of relativistic wavefunctions becomes necessary. We look at extension of the intermediate coupling frame transformation (ICFT) R-matrix approach to use kappa-averaged relativistic radial functions; recent developments of the Dirac R-matrix code (DARC); and thoughts on Dirac R-matrix with pseudo-states (DRMPS).

I. INTRODUCTION

Heavy species, those elements beyond zinc, will play an important role at the ITER fusion device currently under construction at Cadarache, France, but for which plasma modelling studies are already well advanced. The R-matrix approach to electron-impact excitation is ideal for such situations where particle densities are not high enough to cause collisional redistribution of autoionizing states. Then, resonances can be incorporated into the zero-density excitation rate coefficients and so autoionizing levels can be omitted from the collisional–radiative population rate equations. Arguably, a greater effort has gone into R-matrix studies for astrophysics, where the Breit–Pauli approach, and variants thereof, have been the mainstay. For heavy species, the use of non-relativistic wavefunctions is no longer possible. The Dirac R-matrix method now takes centre stage and we need to look at any shortcomings of the current DARC implementation. And, as with Breit–Pauli R-matrix, we also look for faster variants.

In section 2 of this paper we look at a way to extend the ICFT method to use relativistic radial functions. In section 3 we review the DARC code suite that we use, in particular, its parallel developments (PDARC) and extensions to photoionization and radiation damping. Finally, in section 4, we look towards the development of Dirac R-matrix with pseudo-states.

II. ICFTR

Motivation: the ICFT method (Griffin *et al*, 1998) solves most of the problem in LS-coupling (but, including one-body non-fine-structure) viz. H-diagonalization and outer-region solution. It then treats fine-structure mixing asymptotically.

A. The ICFT approach

Uses R-matrix and term-coupling plus Multi-channel Quantum Defect Theory (MQDT) to generate the required scattering matrices:

$$K_{\rm oo} = \mathcal{K}_{\rm oo} - \mathcal{K}_{\rm oc}\left[\mathcal{K}_{\rm cc} - \tan(\pi\nu)\right]^{-1}\mathcal{K}_{\rm co} \tag{1}$$

$$S_{\rm oo} = \mathcal{S}_{\rm oo} - \mathcal{S}_{\rm oc}\left[\mathcal{S}_{\rm cc} - {\rm e}^{-2\pi{\rm i}\nu}\right]^{-1}\mathcal{S}_{\rm co} \tag{2}$$

$$D_{\rm o} = \mathcal{D}_{\rm o} - \mathcal{S}_{\rm oc}\left[\mathcal{S}_{\rm cc} - {\rm e}^{-2\pi{\rm i}\nu}\right]^{-1}\mathcal{D}_{\rm c}\,. \tag{3}$$

Note:

- ICFT terms-couples the entire unphysical $\mathcal{K}$- or $\mathcal{S}$-matrix.
- MQDT applies to *all* closed-channels (Gorczyca and Badnell, 2000).
- Includes long-range coupling potentials by retaining only the finite part of the divergent integrals (Gorczyca *et al*, 1996, Badnell and Seaton, 1999).
- Resonance series converge on levels, ICFT and GFT (since they use level energies in the MQDT formulae), unlike JAJOM.
- Background is correct for ICFT, unlike JAJOM (only term couples open–open) and GFT (omits term-coupling).
- 'Correlation' resonances, which arise in $\mathcal{S}_{\rm oo}$, are well represented still (Badnell and Griffin, 1999).

B. Adding the R to ICFT

As Z increases, the one-body non-fine-structure operators (Mass–Velocity, Darwin) become too large to be treated as a perturbation in H, i.e., the use of non-relativistic radial functions fails.

We start with the Dirac–Slater equations for the large and small components, using a local effective potential (V):

$$\left(\frac{\mathrm{d}}{\mathrm{d}r}+\frac{\kappa}{r}\right)P=\frac{\alpha}{2}\left[\epsilon-V+\frac{4}{\alpha^2}\right]Q \tag{4}$$

and

$$\left(\frac{\mathrm{d}}{\mathrm{d}r}-\frac{\kappa}{r}\right)Q=-\frac{\alpha}{2}\left(\epsilon-V\right)P\,. \tag{5}$$

Eliminate Q to get

$$\left(\frac{\mathrm{d}^2}{\mathrm{d}r^2}-\frac{l(l+1)}{r^2}+(\epsilon-V)\left[1+\frac{\alpha^2}{4}\left(\epsilon-V\right)\right]\right)P$$
$$+\frac{\alpha^2}{4}\left(\frac{\mathrm{d}P}{\mathrm{d}r}-\frac{P}{r}+\frac{(\kappa+1)}{r}P\right)\left[1+\frac{\alpha^2}{4}\left(\epsilon-V\right)\right]^{-1}\frac{\mathrm{d}V}{\mathrm{d}r}=0\,, \tag{6}$$

on using $\kappa(\kappa+1)=l(l+1)$. Then use κ-averaged orbitals: $\kappa=-1$.

This is the basic approach pioneered by Cowan & Griffin (1976) . We then use these orbitals within the standard ICFT or Breit–Pauli approach (not much to be gained in the latter case, so might as well go to fully-relativistic Dirac R-matrix).

1. Some structural comparisons

We compare results from ICR, HFR (Cowan) and relativistic analogue of integrals (RI) with non-relativistic (orbitals) IC and fully relativistic (orbitals) Dirac–Fock (DF) for energy levels in Be-like tungsten, from Jonauskas *et al* (2005). We also compare some IC, ICR and DF radiative and autoionization rates in U^{89+}.

Energy levels (Ry) in W^{70+}.

Index	Level	IC	HFR	DF	RI	ICR
1	2s2 1S0	-14472.2313	-14606.1630	-14661.2007	-14661.2127	-14660.1972
2	2s2p 3P0	11.8033	9.5122	12.7642	13.3690	12.4027
3	2s2p 3P1	14.4817	12.5698	15.6393	16.3163	15.4486
4	2p2 3P0	32.9833	29.5304	35.8501	36.6611	35.0358
5	2s2p 3P2	101.4780	125.3516	123.2548	122.9797	123.2114
6	2s2p 1P1	107.3621	131.9927	129.7459	129.3913	129.8507
7	2p2 3P1	119.6724	141.7643	142.9160	143.2261	142.6208
8	2p2 1D2	121.6674	143.8498	144.8975	145.2266	144.7094
9	2p2 3P2	210.3791	258.4229	254.3276	253.8651	254.5042
10	2p2 1S0	214.6380	262.8561	258.6676	258.1166	258.9496

Decay of the U^{89+} 1s2s2p $^4P_{5/2}$ metastable level.

	ΔE(M1)	ΔE(M2)	S(M1)	S(M2)	$\Delta E(A_a)$	A_a
IC	6972.7	7172.1	0.0255	0.00221	4795.2	1.20(+11)
ICR	7075.5	7407.2	0.0632	0.00231	4989.9	1.03(+11)
DF	7078.0	7409.9	0.0573	0.00236	4951.5	8.50(+11)

The ICR method is more elegant — more self-contained than RI, but gives just as good results. So, we plan to extend to ICFTR by coding for an R-matrix kappa-averaged relativistic continuum basis along the same lines.

III. DRMPS

We have incorporated the set-up of the Dirac R-matrix Hamiltonian (DSTG1, DSTG2 codes) within the OP suite of codes (H-diagonalization and Seaton's outer region suite) and, hence, the parallel versions of said codes (Badnell *et al*, 2004). Furthermore, the DARC dipole matrices have been integrated as well, leading to their use in radiation damped excitation and photoionization calculations (Ballance and Griffin, 2006).

This approach is suitable for highly-charged heavy species, such as those that will arise in the main plasma body at ITER. However, for the edge plasma and divertor regions, neutral and low-charged heavy ions will dominate the diagnostics. As is well known, the close-coupling expansion in physical target states is slowly convergent here and a (large) pseudo-state expansion is often used to achieve sufficient convergence.

A. RMPS

Recall,

$$\Psi = A\sum\!\!\!\!\!\!\int_{\nu} \psi_\nu \phi \,. \tag{7}$$

The R-matrix with pseudo-states approach (like CCC) replaces the sum over high Rydberg states and the integration over continuum states by a quadrature over Laguerre (Sturmian) states. The continuum basis plus Laguerre basis is over complete. The original RMPS implementation of Bartschat *et al* (1996) just Schmidt orthogonalized the two and discarded high-lying basis states. Badnell and Gorczyca (1997) diagonalize the matrix of overlaps and transform to a, reduced, linearly independent basis. The Buttle correction is also transformed appropriately, since the one-body Hamiltonian is no longer diagonal.

The usual Laguerre pseudo-states (Sturmians) are generated from the (non-orthogonal) set of P which satisfy

$$\left(\frac{\mathrm{d}^2}{\mathrm{d}r^2} + \frac{l(l+1)}{r^2} + \frac{\lambda z n}{r} - \frac{\lambda^2 z^2}{4}\right) P(r) = 0 \tag{8}$$

and an orthonormal set is formed by Schmidt orthogonalization, since the basis is not overcomplete. (The physical Coulomb case is recovered via $\lambda = 2/n$.) In RMPS calculations we normally use $\lambda \approx 1$ and so the original orbital energies are a constant, *but* the e-values of H span both negative and positive energies.

B. Adding the D to RMPS

L-spinors (Grant, 2007) are the relativistic analogue of the Sturmians, viz.

$$\left(\frac{\mathrm{d}}{\mathrm{d}r} + \frac{\kappa}{r}\right) P = \frac{\alpha}{2}\left[\epsilon + \frac{4z}{\lambda N r} + \frac{4}{\alpha^2}\right] Q \tag{9}$$

and

$$\left(\frac{\mathrm{d}}{\mathrm{d}r} - \frac{\kappa}{r}\right) Q = -\frac{\alpha}{2}\left(\epsilon + \frac{\lambda z N}{r}\right) P \,, \tag{10}$$

where N is the apparent principal quantum number. Also, the non–rest-mass energy is given by

$$\epsilon = E - 2/\alpha^2 = 2/\alpha^2 \left[\left(1 - \frac{\alpha^2 \lambda^2 z^2}{4}\right)^{1/2} - 1\right] . \tag{11}$$

Note: λ here corresponds to that used in the Laguerre pseudo-states formulation — just expand the above for α small to obtain $\epsilon \approx -\lambda^2 z^2/4$. Again, 'physical' relativistic Coulomb functions are recovered on setting $\lambda = 2/N$.

Following the non-relativistic approach, we take $\lambda \approx 1$ and form an orthonormal basis set by Schmidt orthogonalization. The formation of a linearly independent basis from these states plus the continuum basis follows in a similar fashion to the non-relativistic case.

IV. FUTURE DIRECTIONS

- ICFTR: ICFT breaks down at $\gtrsim$ Zn $\Rightarrow$ use kappa-averaged relativistic wavefunctions.
- Dirac-Coulomb/Breit R-matrix with pseudo-states (DRMPS).
- Port QED/Breit interaction from GRASP to DARC $\Rightarrow$ Dirac-Breit R-matrix.
- Investigate fully-relativistic treatment for the 'outer region'.

Acknowledgements

Queen's Belfast: Patrick Norrington. Rollins: Connor Ballance, Dario Mitnik (now Argentina) & Don Griffin. Sheffield Hallam: Keith Berrington. Strathclyde: Marin O Mullane, Allan Whiteford & Hugh Summers. Western Michigan: Tom Gorczyca.

Badnell N R, Berrington K A, Summers H P, O'Mullane H P, Whiteford A D and Ballance C P 2004 *J. Phys. B: At. Mol. Phys.* **37** 4589

Badnell N R and Gorczyca T W 1997 *J. Phys. B: At. Mol. Phys.* **30** 2011

Badnell N R and Griffin D C 1999 *J. Phys. B: At. Mol. Phys.* **32** 2267

Badnell N R and Seaton M J 1999 *J. Phys. B: At. Mol. Phys.* **32** 3955

Ballance C P and Griffin D C 2006 *J. Phys. B: At. Mol. Phys.* **39** 3617

Bartschat K, Hudson E T, Scott M P, Burke P G and Burke V M 1996 *J. Phys. B: At. Mol. Phys.* **29** 115

Cowan R D & Griffin D C 1976 *J. Opt. Soc. Am.* **66** 1010

Gorczyca T W, Robicheaux F, Pindzola M S and Badnell N R 1996 *Phys. Rev. A* **54** 2107

Gorczyca T W and Badnell N R 2000 *J. Phys. B: At. Mol. Phys.* **30** 2511
Grant I P 2007 *Relativistic Quantum Theory of Atoms and Molecules* (Springer: New York)
Griffin D C, Badnell N R and Pindzola M S 1998 *J. Phys. B: At. Mol. Phys.* **31** 3713
Jonauskas V, Keenan F P, Kisielius R, van Hoof P A M, Foord M E, Heeter R F, Rose S J, Ferland G J and Norrington P H 2005 *J. Phys. B: At. Mol. Phys.* **38** L79

M Plummer, J D Gorfinkiel and J Tennyson (eds.)
Mathematical and computational methods in R-matrix theory

R-matrix Floquet theory for laser-assisted electron–atom scattering

K M Dunseath and M Terao-Dunseath

Laboratoire de Physique des Atomes, Lasers, Molécules et Surfaces,
UMR 6627 du CNRS-Université de Rennes 1,
Campus de Beaulieu, F-35042 Rennes Cedex, France

I. INTRODUCTION

The study of the interaction of atomic systems with intense electromagnetic radiation is a very active field of research. Most work has concentrated on multiphoton ionization, above-threshold ionization and high harmonic generation, with laser-assisted electron-atom scattering receiving somewhat less attention. Experimental and theoretical work in this area has been reviewed by Mason [1] and Ehlotzky *et al* [2] respectively. Most theoretical work can be grouped into methods that relate laser-assisted scattering amplitudes to those for field-free scattering via for example low-frequency approximations [3], and those that approximate the atomic system by a one-electron model. Such approaches however have met with mixed success, being unable to explain a number of experimental results [1].

R-matrix Floquet theory provides the only currently available general, *ab initio* and non-perturbative approach to the study of laser-assisted scattering and multiphoton ionization of complex atomic systems in a linearly polarized laser field. It was first introduced by Burke *et al* [4] and further developed by Dörr *et al* [5]. In the following years, the method was mostly used to study multiphoton ionization. The first application to a collision process was by Dörr *et al* [6], who considered laser-assisted electron–proton scattering. The theory was later refined by Terao-Dunseath and Dunseath [7] through the explicit introduction of field-dressed target states, which greatly simplifies the general formalism.

II. THEORY

We first consider an atomic target composed of a nucleus of charge Z and N electrons, in the presence of a linearly polarized laser field of angular

frequency ω. We assume that the field is monochromatic, monomode, spatially homogeneous with well-defined intensity, described in the dipole approximation by the vector potential $\boldsymbol{A}(t) = \hat{\boldsymbol{z}}\, A_0 \cos\omega t$, with the z-axis parallel to the direction of polarization. The wave function of the atom in the field satisfies the time-dependent Schrödinger equation in the length gauge

$$\mathrm{i}\frac{\partial}{\partial t}\Psi^{\mathrm{T}}(\boldsymbol{X}_N, t) = \left[H_N + \boldsymbol{\mathcal{E}}(t)\cdot\sum_{e=1}^{N}\boldsymbol{r}_e\right]\Psi^{\mathrm{T}}(\boldsymbol{X}_N, t), \tag{1}$$

where the electric field is given by $\boldsymbol{\mathcal{E}}(t) = -\frac{1}{c}\mathrm{d}\boldsymbol{A}(t)/\mathrm{d}t$, H_N is the field-free N-electron Hamiltonian and where $\boldsymbol{X}_N$ represents the space and spin coordinates of all N electrons. Since the time-dependent potential appearing in (1) is periodic, Floquet's theorem states that the solutions can be written in the form

$$\Psi^T(\boldsymbol{X}_N, t) = \mathrm{e}^{-\mathrm{i}E^T t}\sum_{n=-\infty}^{\infty}\mathrm{e}^{-\mathrm{i}n\omega t}\Psi_n^T(\boldsymbol{X}_N), \tag{2}$$

where E^T is the target quasi-energy. The sum is a Fourier-type series, whose n^{th} harmonic can be interpreted as the population of the atomic system dressed by n photons. An important property of the Floquet-Fourier solutions (2) is that of Shirley symmetry, which implies that the solutions (2) can be grouped into different sequences, each characterized by a quasi-energy spectrum of period ω, the same atomic structure and with Floquet components identical apart from a shift in their indices. The *time-independent* Floquet components $\Psi_n^T(\boldsymbol{X}_N)$ are determined by expanding in the basis of the field-free target states and then diagonalizing the Floquet Hamiltonian in this basis.

It is important to note that the presence of the linearly polarized laser field breaks the spherical symmetry of the system by introducing a preferred direction in space. As a consequence, the total atomic angular momentum of the field-dressed target states is no longer defined. Its projection M_T along the polarization axis is however conserved since the system is invariant under rotation around this axis. The parity under inversion with respect to the origin of the total system, atom plus photons, Π_T, is also well defined. This implies that in the expansion over field-free states, the parity of the atomic target state alternates as n increases. As we neglect relativistic corrections, the total atomic spin S_T and projection M_{S_T} are also good quantum numbers. The field therefore mixes all states with the same M_T, S_T and M_{S_T} and correct parity. This is known as ac-Stark or dynamical Stark mixing, and is generally only strong when the energy difference of two states is close to an integral multiple of the photon energy ω.

The above remarks concerning Shirley symmetry and good quantum numbers also apply to the full $(N+1)$-electron scattering system in the field. In particular, the good quantum numbers are the projection M of the total angular momentum

of the (N+1)-electron system along the polarization axis, the total spin S and its projection M_S, as well as the total parity Π of the full (electron + target + photons) system.

As in field-free R-matrix theory, we now define an inner region of the configuration space of the (N+1)-electron system, delimited by the radius a of the most diffuse target state. Inside this region, and for each symmetry $\{M, S, \Pi\}$, we make a Floquet expansion (2) for the full (N+1)-electron wave function, and further expand the Floquet components in a basis of antisymmetrised products of field-free target wave functions and a set of continuum orbitals for the collisional electron. The resulting (N+1)-electron Floquet Hamiltonian matrix is diagonalized and surface amplitudes needed to construct the R-matrix are calculated.

The outer region of the configuration space is defined by $r > a$, where r is the distance of the collisional electron from the nucleus. In this region, exchange with the target electrons becomes negligible, so that the wave function can now be expanded in the basis of simple, non-antisymmetrized products of radial functions for the collisional electron and *field-dressed* channel functions built by coupling the field-dressed target states to the angular and spin functions of the collisional electron to form the symmetry $\{M, S, \Pi\}$. Since the radiative interaction in the length gauge diverges at large distances, the wave function describing the collisional electron in the outer region is transformed into the velocity gauge (in which the electron-laser interaction is described by a term involving $\boldsymbol{A} \cdot \nabla$), the interaction terms for the other (bound) electrons with the field remaining in the length gauge. For a particular collision energy, the R-matrix at $r = a$ is first constructed in the inner region basis, then transformed into the field-dressed channel basis and finally into the velocity gauge.

The close-coupling equations for the radial functions in the velocity gauge contain first-order derivative terms arising from the $\boldsymbol{A} \cdot \nabla$ interaction. These can be removed at each propagation step by a transformation similar to a Smith diabatization in molecular collisions. The resulting couplings however now oscillate with r and do not vanish asymptotically. Rather than propagate the R-matrix, we propagate its inverse, the log-derivative matrix, using the method of Johnson and Manolopoulos [8], which is more suited to such oscillating potentials.

In order to define the collisional boundary conditions, all couplings must vanish asymptotically. At large distances, we therefore transform the wave function into the acceleration frame for the collisional electron

$$\Psi^{\mathrm{V}}(\boldsymbol{X}_{N+1}, t) = \exp[-\mathrm{i}\boldsymbol{\alpha}(t) \cdot \boldsymbol{p}]\, \Psi^{\mathrm{A}}(\boldsymbol{X}_{N+1}, t) \equiv \Psi^{\mathrm{A}}(\boldsymbol{X}_N, \boldsymbol{r} - \boldsymbol{\alpha}(t), \boldsymbol{\sigma}, t) \quad (3)$$

where $\Psi^{\mathrm{V}}, \Psi^{\mathrm{A}}$ are the wave functions in the velocity gauge and acceleration frame respectively, and $\boldsymbol{\alpha}(t) = \int^t \boldsymbol{A}(t')/c\, \mathrm{d}t'$ is the oscillation vector of a free electron in the laser field. The wave function Ψ^{A} satisfies the Schrödinger equation

$$\mathrm{i}\frac{\partial}{\partial t}\Psi^{\mathrm{A}}(\boldsymbol{X}_{N+1},t) = \left[H_N + \sum_{e=1}^{N}\boldsymbol{\mathcal{E}}\cdot\boldsymbol{r}_e - \frac{1}{2}\nabla^2 \right. \tag{4}$$
$$\left. -\frac{Z}{\mid \boldsymbol{r}-\boldsymbol{\alpha}(t)\mid} + \sum_{e=1}^{N}\frac{1}{\mid \boldsymbol{r}-\boldsymbol{\alpha}(t)-\boldsymbol{r}_e\mid}\right]\Psi^{A}(\boldsymbol{X}_{N+1},t).$$

The R-matrix is transformed accordingly but as the transformation to the acceleration frame is time-dependent, the equations are particularly cumbersome. We found it much easier to perform the transformation at $r=\infty$ and propagate the boundary conditions inwards in the velocity gauge, using an asymptotic expansion technique. Substituting into the close-coupling equations yields a set of recurrence relations for the coefficients of the asymptotic expansion. The starting values are determined by imposing the scattering boundary conditions in the acceleration frame. The recurrence relations are more complicated than in the field-free case, due to the presence of first-order derivatives arising from the $\boldsymbol{A}\cdot\nabla$ coupling. Finally, matching the propagated solutions from the inner and asymptotic regions at r_{match} provides the K-matrix, from which scattering cross sections can be calculated [7].

III. COMPUTATIONAL ASPECTS

We must first define a set of field-free target state wavefunctions. All Hamiltonian and dipole matrix elements needed for constructing the $(N+1)$-electron Floquet Hamiltonian in the inner region are then provided by the standard field-free R-matrix computer package.

The program `MPB` constructs and diagonalizes this Floquet Hamiltonian. As in the field-free case, all eigenvalues and eigenvectors are required, the latter being used to calculate surface amplitudes necessary for building the R-matrix. This step has to be performed once for each symmetry $\{M,S,\Pi\}$, but is independent of the collision energy. The dimension of the Floquet Hamiltonian can grow considerably, even for relatively simple atomic systems. For example, in a study of electron–helium scattering including the lowest eleven field-free target states, the dimension of the Floquet Hamiltonian for the $M=0$, singlet, even symmetry was almost 25 000. More often, the dimensions of the matrices to be diagonalized are of the order 10 000 to 15 000. These diagonalizations are realized using routines from the parallel linear algebra library `SCALAPACK`, which are generally very efficient. One caveat is that the orthogonality of eigenvectors corresponding to closely-spaced eigenvalues may not be guaranteed. The eigenvectors can be reorthogonalized, but at the cost of supplying very large workspace arrays. In a number of tests however, we have found that the final cross sections obtained when there are orthogonality warnings are the same as when there are no warnings. Nevertheless, it is still preferable to ensure orthogonality.

The next program, `MPSCAT`, defines the R-matrix at energy E at the boundary a of the inner region, transforms it into the field-dressed channel basis and then into the velocity gauge. These transformations involve a series of matrix multiplications. We then invert the R-matrix to form the logarithmic derivative matrix which we propagate outwards using the method developed by Johnson and Manolopoulos [8]. Overall, the propagation over one step requires the solution of two sets of linear equations (matrix inverses) and six matrix multiplications. The calculation of the asymptotic expansion requires the singular value decomposition of a particular matrix for each block of degenerate channels, several matrix-vector and matrix-matrix multiplications as well as the solution of a system of linear equations, and makes use of Padé acceleration techniques. As the number of channels increases, this part of the code begins to dominate the execution time. The program makes heavy use of multi-threaded, vendor-supplied `BLAS` and `LAPACK` routines as well as OpenMP directives.

It should be mentioned that while in principle the various transformations are unitary and the resulting R-matrices are symmetric, in practice truncating the Floquet expansion results in a small loss of unitarity and non-symmetric R-matrices and, eventually, a non-symmetric K-matrix. It is important for example not to symmetrize the K-matrix by hand, as we have found that this leads to spurious oscillations in the results.

IV. SCATTERING FROM DRESSED STATES

In R-matrix Floquet theory, the description of the collisional process is thus based on the use of dressed atomic states. A particular field-free level gives rise to a Shirley sequence of states with quasi-energies $\varepsilon \pm N_\gamma\omega$ which have the same internal atomic structure but which are dressed by a different number of photons. A collision may result in a transition between two dressed states: if these belong to the same Shirley sequence, the process is said to be a free-free transition accompanied by net absorption or emission of photons. The initial state with quasi-energy ε_0 is by definition dressed by zero photons (N_γ=0). If the final state has quasi-energy $\varepsilon_0 - N_\gamma\omega$ then for an incident electron of energy E_i , the energy of the scattered electron is $E_f = E_i + N_\gamma\omega$. If $N_\gamma > 0$, the process corresponds to absorption of N_γ photons, while $N_\gamma < 0$ corresponds to emission of N_γ photons. If the collision energy is not sufficiently large, the emission process cannot occur, whereas absorption is always possible.

Similarly, the transition into a dressed state of quasi-energy $\varepsilon_1 - N_\gamma\omega$ belonging to a different Shirley sequence corresponds to excitation of the target with absorption or emission of photons. Of particular interest is the case when the kinetic energy of the incident electron lies below the threshold for excitation of the upper state dressed by 0 photons, ε_1, but above the threshold for excitation of the upper state dressed by 1 photon, $\varepsilon_1 - \omega$. It is then possible

to excite the target atom into the upper state at a collision energy below the field-free threshold by absorption of one or more photons, a process known as simultaneous electron-photon excitation (SEPE).

A resonance occurs in the field-free scattering cross section if the total energy of the collision system coincides with the energy of a doubly excited state of the $(N+1)$-electron system. In the presence of the laser field, this doubly excited state will also give rise to a Shirley sequence, and hence a series of resonances separated by ω in the scattering cross section.

V. APPLICATIONS

Much theoretical and experimental work has concentrated on free-free collisions, in particular for CO_2 lasers, in order to test the predictions of a low-frequency approximation (LFA) [3]. The derivation of this approximation breaks down for certain collision geometries, although the cross sections are then expected to be very small. Measured cross sections however were found to be several orders of magnitude larger [9]. This disagreement stimulated a number of attempts at refining the LFA, unfortunately with mixed and even contradictory results. Cross sections obtained using R-matrix Floquet theory [10] are very small, and tend to confirm the hypothesis that double scattering is responsable for the large measured cross sections [11].

Another interesting case is the simultaneous electron-photon excitation of helium in the presence of a Nd:YAG laser field, at collision energies near the first field-free excitation threshold. In this case, the photon energy is very close to the energy separation of the lowest field-free ^{3}S and ^{3}P^o states, so that there is strong ac-Stark mixing. The calculated SEPE signal [12,13], dominated by the $He^-(1s2s^2\ ^2S)$ resonance just below threshold, is in good agreement with measurements by Luan *et al* [14] below 20 eV. At higher energies, the computed signal is very small while the measured values become very large and negative. Multiphoton ionization of the excited atoms may explain this difference.

Other work based on the R-matrix Floquet theory includes the demonstration and numerical investigation of general selection rules for differential cross sections in geometries where the laser polarization axis is perpendicular to the scattering plane [15] and electron–helium scattering at very low collision energies [16]. Most recently, the method has been applied to electron-hydrogen scattering in a CO_2 laser at collision energies below the first excitation threshold. We have in particular demonstrated the possibility of suppressing resonances at particular laser intensities and collision geometries, due to the absence of flux in incident channels [17].

[1] N.J. Mason, *Rep. Prog. Phys.* **56** 1275 (1993)
[2] F. Ehlotzky, A. Jaroń, J.Z. Kamiński, *Phys. Rep.* **297** 63 (1998)
[3] N.M. Kroll, K.M. Watson, *Phys. Rev. A* **8**, 804 (1973)
[4] P.G. Burke, P. Francken, C.J. Joachain, *J. Phys. B: At. Mol. Opt. Phys.* **24** 761 (1991)
[5] M. Dörr, M. Terao-Dunseath, J. Purvis, C.J. Noble, P.G. Burke, C.J. Joachain, *J. Phys. B: At. Mol. Opt. Phys.* **25** 2809 (1992)
[6] M. Dörr, M. Terao-Dunseath, P.G. Burke, C.J. Joachain, C.J. Noble, J. Purvis, *J. Phys. B: At. Mol. Opt. Phys.* **28** 3545 (1995)
[7] M. Terao-Dunseath, K.M. Dunseath, *J. Phys. B: At. Mol. Opt. Phys.* **35** 125 (2002)
[8] D.E. Manolopoulos, *J. Chem. Phys.* **85** 6425 (1986)
[9] B. Wallbank, J.K. Holmes, *Can. J. Phys.* **79** 1237 (2001)
[10] K.M. Dunseath, M. Terao-Dunseath, *J. Phys. B: At. Mol. Opt. Phys.* **37** 1305 (2004)
[11] I. Rabadán, L. Méndez, A.S. Dickinson, *J. Phys. B: At. Mol. Opt. Phys.* **29** L801 (1996)
[12] M. Terao-Dunseath, K.M. Dunseath, D. Charlo, A. Hibbert, R.J. Allan, *J. Phys. B: At. Mol. Opt. Phys.* **34** L263 (2001)
[13] K.M. Dunseath, M. Terao-Dunseath, A. Hibbert, to be submitted
[14] S. Luan, R. Hippler, H.O. Lutz, *J. Phys. B: At. Mol. Opt. Phys.* **24** 3241 (1991)
[15] K.M. Dunseath, M. Terao-Dunseath, G. Bourhis, *Phys. Rev. A* **72** 033410 (2005)
[16] K.M. Dunseath, M. Terao-Dunseath, *Phys. Rev. A* **73** 053407 (2006)
[17] K.M. Dunseath, M. Terao-Dunseath, XXV ICPEAC, abstracts of contributed papers, FR139 (2007)

M Plummer, J D Gorfinkiel and J Tennyson (eds.)
Mathematical and computational methods in R-matrix theory

An R-matrix method for positron atom and molecule scattering using explicitly correlated wavefunctions

Jan Franz

Department of Physics and Astronomy,
University College London, London WC1E 6BT, UK

I. INTRODUCTION

The theoretical description of positron molecule scattering is complicated by the fact that, due to the attractive interaction between electron and positron, the correlation between both particles is very strong. Early studies by Danby and Tennyson have shown that the conventional R-matrix method, where products of N-electron wavefunctions and one-positron wavefunctions are used, results in cross sections for positron molecule scattering that are too low as compared with experiment and other *ab initio* results [1,2]. This failure was mainly due to the omission of terms that take the electron-positron distance explicitly into account. Armour and co-workers have shown that such terms are required in order to get accurate cross section and annihilation rates for positron H_2 scattering that allow comparison with experimental data [3–5].

In the R-matrix method the interaction space is divided into two regions. In the inner region the wavefuntion can be expressed as a very complicated function of the projectile and all particles contained in the target. In the outer region the wavefunction can be expressed as a product between the target wavefunction and the projectile in the continuum (see e.g. [1]). This framework allows us to include explicitly correlated wavefunctions in the inner region without changing the computer codes for the outer region.

In this paper we will discuss a few aspects of using explicitly correlated wavefunctions. In the second section we will discuss the R-matrix wavefunction, in the third section the construction of explicitly correlated functions is explained, and in the fourth section we discuss integral evaluation for one example.

II. *R*-MATRIX WAVEFUNCTION

The scattering wavefunction for a given energy E is built up as a linear combination [10]

$$\Psi(E) = \sum_k A_K(E)\Psi_K$$

where the coefficients A_K are obtained by propagating the R-matrix in the outer region. The R-matrix basis functions are represented by a close-coupling expansion [1]

$$\Psi_K = \sum_A \sum_{\overline{x}} b^K_{A\overline{x}} \Xi^{Ne}_A \eta_{\overline{x}} + \sum_B \sum_{\overline{r}} c^K_{B\,\overline{a}} \Phi^{Ne1p}_{B\,\overline{r}} + \sum_C \sum_{i\overline{a}} c^K_C \tilde{\Phi}^{Ne1p}_{C\,i\overline{a}} \ ,$$

where the first sum runs over all products of target wavefunctions Ξ^{Ne}_A and positronic continuum orbitals $\eta_{\overline{x}}$. The second sum runs over conventional square-integrable functions $\Phi^{Ne1p}_{B\,\overline{a}}$ for N electrons and one positron, and the third sum runs over explicitly correlated square-integrable functions $\tilde{\Phi}^{Ne1p}_{C\,i\overline{r}}$.

In the following we briefly describe the three different types of basis functions. The target wavefunctions are obtained by diagonalizing the Hamiltonian for the target molecule containing N electrons. In general the eigenfunctions of the target Hamiltonian are linear combinations of Slater determinants Λ^{Ne}_D

$$\Xi^{Ne}_A = \sum_D d^A_D \Lambda^{Ne}_D(\boldsymbol{r}_1, \cdots, \boldsymbol{r}_N) \ .$$

The coefficients d^A_D, obtained by diagonalising the target Hamiltonian, are kept frozen in the scattering calculation containing the additional positron (see e.g. [2] for an efficient algorithm). The conventional square-integrable functions are given by

$$\begin{aligned} \Phi^{Ne1p}_{B\,\overline{r}} &= \Phi^{Ne1p}_{B\,\overline{r}}(\boldsymbol{r}_1, \cdots, \boldsymbol{r}_N, \boldsymbol{r}_{\overline{1}}) \\ &= \Lambda^{Ne}_B(\boldsymbol{r}_1, \cdots, \boldsymbol{r}_N) \times \chi_{\overline{r}}(\boldsymbol{r}_{\overline{1}}) \ , \end{aligned}$$

where Λ^{Ne}_B is a N-electron function (e.g. a Slater determinant) and $\chi_{\overline{r}}(\boldsymbol{r}_{\overline{1}})$ is a square-integrable positron orbital. Finally, the explicitly correlated square-integrable functions are given by

$$\begin{aligned} \tilde{\Phi}^{Ne1p}_{C\,i\overline{a}} &= \tilde{\Phi}^{Ne1p}_{C\,i\overline{a}}(\boldsymbol{r}_1, \cdots, \boldsymbol{r}_N, \boldsymbol{r}_{\overline{1}}) \\ &= \hat{f}_{i\overline{a}} \left(\Lambda^{Ne}_C(\boldsymbol{r}_1, \cdots, \boldsymbol{r}_N) \times \chi_{\overline{a}}(\boldsymbol{r}_{\overline{1}}) \right) \end{aligned}$$

Here $\hat{f}_{i\overline{a}}$ is the particle-connection operator, which connects the electron in orbital ϕ_i with the positron in orbital $\chi_{\overline{a}}$ by an exponential function which explicitly contains the electron positron distance.

III. EXPLICITLY CORRELATED FUNCTIONS

In first quantization the particle-connection operator can be defined as

$$\hat{f}_{i\overline{a}} = \sum_{I\overline{A}} f(r_{I\overline{A}})|\ \phi_i(I)\chi_{\overline{a}}(\overline{A})\rangle\langle\phi_i(I)\chi_{\overline{a}}(\overline{A})|\ ,$$

where the sums are running over electrons I and positrons $\overline{A}$.

As an example we apply the particle-connection operator onto a wavefunction with two electrons and one positron. A conventional wavefunction is given by

$$\begin{aligned}\Phi^{2e1p}_{C\,\overline{a}}(1,2,\overline{1}) &= \Lambda^{2e}_{C}(1,2) \times \chi_{\overline{a}}(\overline{1}) \\ &= \frac{1}{2}\left(\phi_i(1)\phi_j(2) - \phi_j(1)\phi_i(2)\right) \times \chi_{\overline{a}}(\overline{1})\ .\end{aligned}$$

Now we apply the particle-connection operator $\hat{f}_{i\overline{a}}$ in order to include terms that are containing the distance between the electron in orbital ϕ_i and positrons in the positronic orbital $\chi_{\overline{a}}$

$$\begin{aligned}\tilde{\Phi}^{2e1p}_{C\,i\overline{a}}(1,2,\overline{1}) &= \hat{f}_{i\overline{a}}\Phi^{2e1p}_{C\,\overline{a}}(1,2,\overline{1}) \\ &= \sum_{I\overline{A}} f(r_{I\overline{A}})|\phi_i(I)\chi_{\overline{a}}(\overline{A})\rangle\langle\phi_i(I)\chi_{\overline{a}}(\overline{A})| \\ &\qquad \frac{1}{2}\left(\underline{\phi_i(1)}\phi_j(2) - \phi_j(1)\underline{\phi_i(2)}\right) \times \underline{\chi_{\overline{a}}(\overline{A})} \\ &= \frac{1}{2}\left(f(r_{1\overline{1}})\underline{\phi_i(1)}\phi_j(2) \times \underline{\chi_{\overline{a}}(\overline{A})} - f(r_{2\overline{1}})\phi_j(1)\underline{\phi_i(2)} \times \underline{\chi_{\overline{a}}(\overline{A})}\right)\ ,\end{aligned}$$

where the connected orbitals are underlined for pedagogical reasons. The explicitly correlated functions are antisymmetric with respect to electron exchange

$$\tilde{\Phi}^{2e1p}_{C\,i\overline{a}}(1,2,\overline{1}) = -\tilde{\Phi}^{2e1p}_{C\,i\overline{a}}(2,1,\overline{1})\ ,$$

as required by the Pauli-principle. A similar function

$$\tilde{\Phi}^{2e1p}_{C\,j\overline{a}}(1,2,\overline{1}) = \hat{f}_{j\overline{a}}\Phi^{2e1p}_{C\,\overline{a}}(1,2,\overline{1})$$

can be obtained by connecting electronic orbital ϕ_j and positronic orbital $\chi_{\overline{a}}$.

IV. EVALUATION OF MANY-PARTICLE INTEGRALS

When using conventional many-particle wavefunctions without explicitly-correlated terms, we have to evaluate one- and two-particle integrals only. By

using explicitly-correlated wavefunctions we have to evaluate three- and four-particle integrals. Kutzelnigg and Klopper have shown how these integrals can be approximated by a sum of one- and two-particle integrals. In the following we discuss the evaluation of one type of these integrals (see e.g. [9]). In some of the contributions to the electron-electron interaction we have to compute three-particle integrals of the type

$$\begin{aligned} I_3 = \int & \phi_i^*(\boldsymbol{r}_1)\phi_j^*(\boldsymbol{r}_2)\chi_{\overline{a}}^*(\boldsymbol{r}_{\overline{1}}) \\ & f(r_{1\overline{1}})g(r_{12})f(r_{1\overline{1}}) \\ & \phi_{i'}(\boldsymbol{r}_1)\phi_{j'}(\boldsymbol{r}_2)\chi_{\overline{a}'}(\boldsymbol{r}_{\overline{1}})\mathrm{d}\boldsymbol{r}_1\mathrm{d}\boldsymbol{r}_2\mathrm{d}\boldsymbol{r}_{\overline{1}}\,, \end{aligned}$$

where $g(r_{12}) = \frac{1}{r_{12}}$. By introducing a delta-function $\delta(\boldsymbol{r}_3 - \boldsymbol{r}_1)$ we can seperate the function $g(r_{12})$ from the two factors $f(r_{1\overline{1}})$

$$\begin{aligned} I_3 = \int & \phi_i^*(\boldsymbol{r}_1)\phi_j^*(\boldsymbol{r}_2)\chi_{\overline{a}}^*(\boldsymbol{r}_{\overline{1}}) \\ & f(r_{1\overline{1}})\delta(\boldsymbol{r}_3 - \boldsymbol{r}_1)g(r_{32})f(r_{1\overline{1}}) \\ & \phi_{i'}(\boldsymbol{r}_3)\phi_{j'}(\boldsymbol{r}_2)\chi_{\overline{a}'}(\boldsymbol{r}_{\overline{1}})\mathrm{d}\boldsymbol{r}_1\mathrm{d}\boldsymbol{r}_2\mathrm{d}\boldsymbol{r}_3\mathrm{d}\boldsymbol{r}_{\overline{1}}. \end{aligned}$$

In a nearly complete basis set the delta-function $\delta(\boldsymbol{r}_3 - \boldsymbol{r}_1)$ can be approximated by a sum of orbital products

$$\delta(\boldsymbol{r}_3 - \boldsymbol{r}_1) \approx \sum_\kappa \phi_\kappa^*(\boldsymbol{r}_3)\phi_\kappa(\boldsymbol{r}_1)\ .$$

Inserting the approximation for the delta-function results in

$$\begin{aligned} I_3 \approx \sum_\kappa \int & \phi_i^*(\boldsymbol{r}_1)\phi_j^*(\boldsymbol{r}_2)\phi_\kappa^*(\boldsymbol{r}_3)\chi_{\overline{a}}^*(\boldsymbol{r}_{\overline{1}}) \\ & f(r_{1\overline{1}})g(r_{32})f(r_{1\overline{1}}) \\ & \phi_\kappa(\boldsymbol{r}_1)\phi_{j'}(\boldsymbol{r}_2)\phi_{i'}(\boldsymbol{r}_3)\chi_{\overline{a}'}(\boldsymbol{r}_{\overline{1}})\mathrm{d}\boldsymbol{r}_1\mathrm{d}\boldsymbol{r}_2\mathrm{d}\boldsymbol{r}_3\mathrm{d}\boldsymbol{r}_{\overline{1}}\,. \end{aligned}$$

This can be written as a a sum of products of two particle integrals

$$\begin{aligned} I_3 \approx \sum_\kappa & \int \phi_i^*(\boldsymbol{r}_1)\chi_{\overline{a}}^*(\boldsymbol{r}_{\overline{1}})f(r_{1\overline{1}})f(r_{1\overline{1}})\phi_\kappa(\boldsymbol{r}_1)\chi_{\overline{a}'}(\boldsymbol{r}_{\overline{1}})\mathrm{d}\boldsymbol{r}_1\mathrm{d}\boldsymbol{r}_{\overline{1}} \\ & * \int \phi_j^*(\boldsymbol{r}_2)\phi_\kappa^*(\boldsymbol{r}_3)g(r_{32})\phi_{j'}(\boldsymbol{r}_2)\phi_{i'}(\boldsymbol{r}_3)\mathrm{d}\boldsymbol{r}_2\mathrm{d}\boldsymbol{r}_3 \end{aligned}$$

Several new types of two-particle integrals

$$(ij|\mathrm{Op}(1\overline{1})|\overline{a}\overline{b}) = \int \phi_i^*(\boldsymbol{r}_1)\chi_{\overline{a}}^*(\boldsymbol{r}_{\overline{1}})\mathrm{Op}(r_{1\overline{1}})\phi_\kappa(\boldsymbol{r}_1)\chi_{\overline{a}'}(\boldsymbol{r}_{\overline{1}})\mathrm{d}\boldsymbol{r}_1\mathrm{d}\boldsymbol{r}_{\overline{1}}$$

are required, where $\mathrm{Op}(r_{1\overline{1}})$ being one of the integral kernels $[t,[f(r_{1\overline{1}}),t]]$, $f(r_{1\overline{1}})$, $f(r_{1\overline{1}})^2$, $\frac{f(r_{1\overline{1}})}{r_{1\overline{1}}}$,and $\frac{f(r_{1\overline{1}})^2}{r_{1\overline{1}}}$. Handy expressions can be derived from the Slater-type geminal $f(r_{1\overline{1}}) = \exp(-\alpha r_{1\overline{1}})$, for which Ten-no has developed efficient integral routines [10,11].

Acknowledgements

The author thanks the EPSRC and the Daiwa Anlgo-Japanese Foundation for Funding. The author thanks Jonathan Tennyson and Edward Armour for many helpful discussion, and Seiichiro Ten-no and Akio Takatsuka for help with the computer implementation.

---

[1] G. Danby and J. Tennyson. *J. Phys. B: At. Mol. Opt. Phys.* **23** (1990) 1005–1016. erratum **23** (1990) 2471.

[2] G. Danby and J. Tennyson. *J. Phys. B: At. Mol. Opt. Phys.* **24** (1991) 3517–3529.

[3] E. A. G. Armour and D. J. Baker. *J. Phys. B: At. Mol. Opt. Phys.* **19** (1986) L871-L875.

[4] E. A. G. Armour and D. J. Baker. *J. Phys. B: At. Mol. Opt. Phys.* **20** (1987) 6105-6119.

[5] E. A. G. Armour and J. W. Humberston. *Phys. Rep.* **204** (1991) 165.

[6] P. G. Burke and K. A. Berrington, editors. *Atomic and Molecular Processes, an R-matrix Approach*. Institute of Physics Publishing, Bristol, 1993.

[7] L. A. Morgan, J. Tennyson, and C. J. Gillan. *Computer Phys. Comms.* **114** (1998) 120–128.

[8] J. Tennyson. *J. Phys. B: At. Mol. Opt. Phys.* **29** (1996) 1817–1828.

[9] J. Noga, W. Klopper, and W. Kutzelnigg. *CC-R12 An explicitly correlated coupled cluster theory* in: Recent Advances in Coupled-Cluster Methods, R. J. Bartlett (Ed.), World Scientific, Singapore, 1997, pp. 1-48

[10] S. Ten-no. *Chem. Phys. Lett.* **398** (2004) 56-61.

[11] S. Ten-no. *J. Chem. Phys.* **126** (2007) 014108.

M Plummer, J D Gorfinkiel and J Tennyson (eds.)
Mathematical and computational methods in R-matrix theory

R-matrix methods for electronic and nuclear dynamics in molecules

R Guérout[†], Ch Jungen[†] and M Telmini[‡]

[†] *Laboratoire Aimé Cotton du CNRS, Bâtiment 505 Université de Paris-Sud, F-91405 Orsay, France*
[‡] *LSAMA Department of Physics, Faculty of Sciences of Tunis, University of Tunis El Manar, 2092 Tunis, Tunisia*

We present a brief discussion of problems arising in $\mathcal{R}$-matrix calculations for molecules, related in particular to the inclusion of vibrational and rotational motion.

I. MOLECULAR ASPECTS OF MQDT AND *R*-MATRIX THEORY

Ab initio calculations of molecular quantum defects encounter specific difficulties which are not present in atomic calculations. Most of these are associated with the presence of the nuclear degrees of freedom in molecules, some with the loss of spherical symmetry.

(i) Vibrational coordinates are continuous variables and therefore one must, for a given total energy, obtain quantum defects or the equivalent reaction matrices, as functions of the molecular geometry over an appropriate range of the nuclear coordinates. Since quantum defects depend also on the energy, each element of the quantum defect matrix $\boldsymbol{\mu}(E, Q)$ is in fact a two-dimensional *surface* in a diatomic molecule, and it is a hypersurface in a polyatomic system. The continuous manifold of nuclear geometries of a molecule translates into an infinity of vibrational Rydberg channels that are associated with any single electronic channel. Various ℓ partial waves are mixed by the non-spherical core field. These features are illustrated in Fig. 1 for the highly dipolar CaF molecule for which ℓ- mixing is particularly strong. The figure displays the vibronic level structure near threshold that arises from s, p, d and f Rydberg partial waves associated with the first vibrational levels v^+ of the electronic ground state of CaF^+.

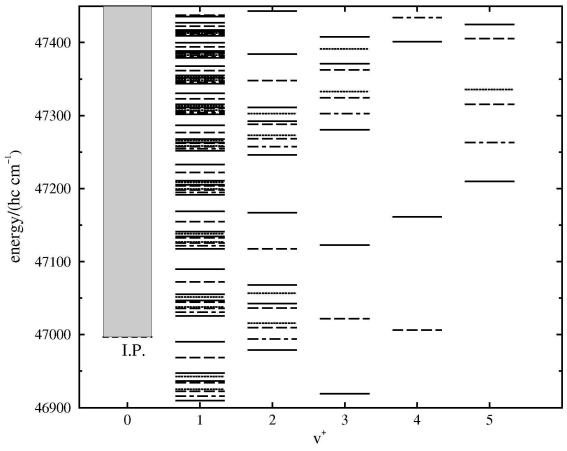

FIG. 1.
Vibronic Rydberg structure of CaF associated with the ground state levels $X^1\Sigma^+, v^+ = 0{-}5$ of CaF^+. The levels shown arise from s, p, d and f partial waves: $^2\Sigma^+$ (full lines), $^2\Pi$ (dashed lines), $^2\Delta$ (dotted lines), $^2\Phi$ (dot-dashed lines). High-n/low-v levels are represented on the left, and low-n/high-v levels on the right hand side of the figure (adapted from [1]).

(ii) Another difficulty arises because the total energy in molecules is the sum of electronic and rotational/vibrational energy. Therefore, both *low* vibrational levels of a Rydberg series with *high* principal quantum number n, and *high* vibrational levels of a Rydberg series with *low* principal quantum number n, may coexist at the same total energy E (cf. Fig. 1). Indeed, the coupling of high-n/low-v to low-n/high-v levels is a characteristic feature of molecular dynamics and constitutes a pathway for the conversion of electronic into vibrational energy. In polyatomic molecules where high vibrational levels occur as dense quasi-continua, this process leads to the phenomenon of *internal conversion*.

(iii) A further complication arises in molecules because an electronic channel which is strongly closed for one geometry, may become weakly closed for another geometry. The core excited $^1\Sigma_g^+$ channels $(1\sigma_u)np\sigma$ and $nf\sigma$ of H_2 afford an example of such a situation, since they are strongly closed for small internuclear distances R, but become weakly closed at large distances. This is illustrated by Fig. 2. The inclusion of the rotational and vibrational degrees of freedom is possible only if such channels can be incorporated into the $\mathcal{R}$-matrix and MQDT formalisms in a unified manner, that makes no distinction between the two regimes.

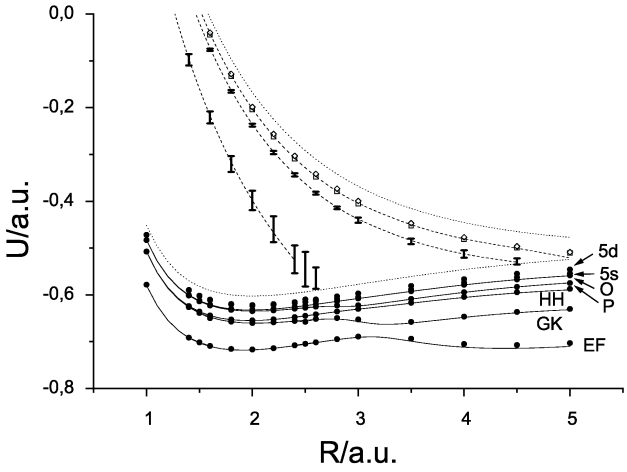

FIG. 2.

Potential energy curves and resonances of $^1\Sigma_g^+$ symmetry in H_2. The core states $1\sigma_g$ and $1\sigma_u$ are indicated by dotted lines. Positions and widths of core excited resonances ($1\sigma_u$) $2p\sigma$, $3p\sigma$, $4p\sigma$ and $4f\sigma$ are indicated by bars, bars, squares and diamonds, respectively. Note how with respect to an energy near threshold (≈ -0.6 a.u.) the core excited channels are strongly closed near $R = 1$ a.u. while they become weakly closed near about $R = 4$ a.u. (adapted from [2]).

(iv) Vibronic interactions between vibrational channels such as those shown in Fig. 1 are a principal focus of interest in the dynamics of highly excited molecular systems. They are usually - and most efficiently - accounted for in the framework of rotational/vibrational frame transformations (see [3] and references in [4], in particular [5] and [6]), in terms of the clamped-nuclei quantum defect matrices. Taking account of the vibrational motion within this framework thus always involves averaging of the clamped-nuclei quantum defect matrix elements over the vibrational motion in some way or another (including the ion levels $v^+ = 0 - 5$ in the example of Fig. 1). It will therefore be easier to obtain meaningful results if the quantum defect functions are smooth functions of the geometry. The frame transformation approach is known to yield an accurate description of electron-ion collisions as long as the quantum defects are nearly independent of the energy. It may fail, however, when strong energy dependences occur, e.g. as the consequence of electronic channel couplings or electronic autoionization. In summary then, it appears that quantum defect matrices appropriate for the use in molecular dynamical calculations (MQDT) should be as smooth functions as possible both of geometry and energy.

II. MOLECULAR *R*-MATRIX CALCULATIONS DESIGNED FOR NUCLEAR DYNAMICS CALCULATIONS

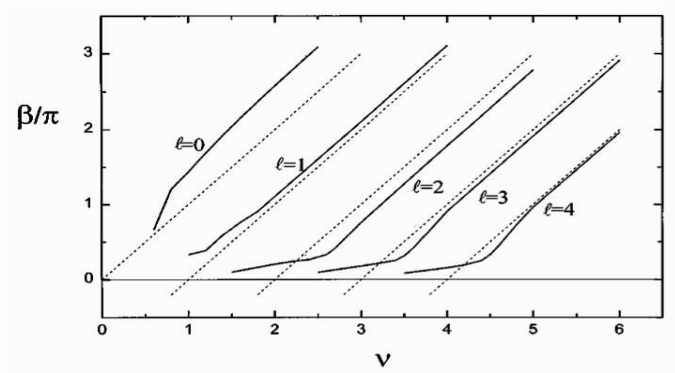

FIG. 3.

Accumulated phase parameters β, in units of π and evaluated numerically in spheroidal coordinates, plotted as functions of the effective principal quantum number $\nu = (-E)^{-1/2}$ for CaF ($^2\Sigma^+$ symmetry). These phase parameters incorporate the effect of the dipole field of the ion core. The dotted lines represent the Coulomb phase parameters corresponding to Seaton's spherical reference Coulomb functions $s(r)$ and $c(r)$ used in ordinary quantum defect theory [8]. Owing to their crossing of the abscissa in the figure these yield unphysical $1p$, $2d$ ... states at low energy (adapted from [7]).

The molecular $\mathcal{R}$-matrix codes which have been developed - or are under development - in a joint effort between Orsay, Tunis and Basel [7] [9] [10] are specifically designed to yield quantum defect matrices $\boldsymbol{\mu}(E, Q)$ which can be used as input for the Orsay molecular spin-rovibronic MQDT code [11]. These codes evaluate the clamped-nuclei quantum defect matrices in spheroidal coordinates. In this way rapidly converging restricted partial wave expansions can be obtained even for strongly dipolar systems [7]. Efforts have been made to devise numerical [12] and analytical [13] schemes that allow the channel phases outside the $\mathcal{R}$-matrix reaction zone to be obtained in a smooth and stable manner, from energies far below the first physical level through the Rydberg region into the ionization continuum. In addition to providing smooth phase parameters, this approach avoids the occurrence of unphysical solutions in the strongly closed range. Fig. 3 illustrates the accumulated phase parameters for the CaF molecule used in the $\mathcal{R}$-matrix calculations of [7].

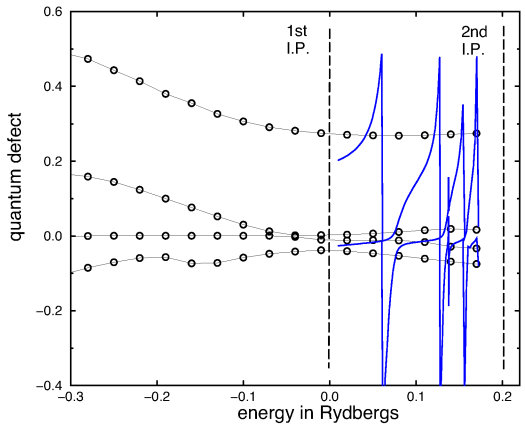

FIG. 4.

Clamped-nuclei eigen-quantum defects/phase shifts for H_2, $^1\Sigma_g^+$ $R = 4$ a.u. as functions of the energy. The calculation has been carried out in spheroidal coordinates and explicitly includes in the outer region the channels $(1\sigma_g)s\sigma_g$, $(1\sigma_g)d\sigma_g$, $(1\sigma_u)p\sigma_u$ $(1\sigma_u)f\sigma_u$ (circles connected by light lines). The heavy lines represent the same calculation, where physical boundary conditions have been applied above the first I.P. $(1\sigma_g)$, i.e. the radial wavefunctions associated with the $1\sigma_u$ core are forced to go to zero asymptotically.

Smooth reference functions for the asymptotic region that account accurately for the physics in the outer zone, including e.g. dipole and quadrupole fields and polarization terms in addition to the dominant Coulomb contribution, are helpful for the evaluation of quantum defect matrices satisfying the criteria discussed in Sec.I. These functions also allow us to include closed channels explicitly in the outer region, which otherwise would lead to a resonant behavior of the quantum defect matrices. This is illustrated in Fig. 4 where the *ab initio* eigen-quantum defects for the H_2 molecule ($^1\Sigma_g^+$ symmetry, $R = 4$ a.u.) are plotted as functions of the energy. The channels associated with the excited core $1\sigma_u$ have been included either implicitly (heavy lines, two channels) or explicitly (circles, four channels). Note that the physical content of the two calculations is exactly the same. The implicit treatment yields continuum eigen-phases that allow us to see where the core excited resonances occur and what their widths are. The advantage of the explicit treatment on the other hand is that the eigen-quantum defects are smooth throughout the bound state and resonance regions. Together with their counterparts computed over a range of relevant R values they can therefore be combined with frame transformation theory to account for the nuclear dynamics.

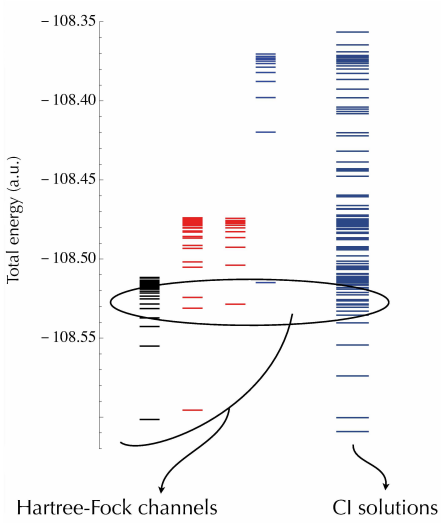

FIG. 5.
Rydberg channel structures in N_2 associated with the $X^{+2}\Sigma_g^+$, $A^{+2}\Pi_u$ and $B^{+2}\Sigma_u^+$ states of N_2^+ ($^1\Pi_u$ symmetry). Hartree-Fock channels are shown on the left, while the mixed CI solutions are shown on the right.

The examples mentioned so far all concern effective one-electron or two-electron systems for which the variational eigen-channel $\mathcal{R}$-matrix scheme [14] has been implemented [7] [9]. Another approach, designed to eventually provide quantum defect matrices for polyatomic multi-electron systems, is currently under development [10]. The method uses artificial well potentials (AWP) which serve as "soft-walled" $\mathcal{R}$-matrix boundaries. Thereby the electronic continuum is made discrete, and, by varying the strength of the AWP, one can move any (Hartree-Fock or CI) solution to a preselected total energy E. The advantage is that the *ab initio* techniques based on Gaussian basis sets can be taken over without change from a standard quantum chemical code. This is so because the integrations extend formally over the full space, and because the form of the AWP is chosen such that the required integrals involving the Gaussian basis also have analytical expressions.

The method has so far been applied in an iterative Hartree-Fock frozen-core version to NO [15] and N_2^- [13], which both have a 14-electron closed-shell core. Fig. 5 illustrates the application of the new CI version of the code to the open-shell core system N_2. The l.h.s. of the figure displays the Hartree-Fock

channels for $^1\Pi_u$ symmetry associated with the $X^{+2}\Sigma_g^+$, $A^{+2}\Pi_u$ and $B^{+2}\Sigma_u^+$ cores. The CI calculation yields the manifold of mixed levels shown on the right. It is to these that the iterative AWP procedure is applied, which shifts a sufficient number of eigen-solutions (e.g. those situated inside the ellipse in the figure), one by one, to a preselected total energy E nearby. The matching of the solutions to the asymptotic reference functions is carried out on an ellipsoidal surface which is placed inside the AWP where the latter vanishes. The result is a non-diagonal reaction or quantum defect matrix that accounts for intra- as well as inter-channel couplings.

---

[1] R. W. Field, C. M. Gittins, N. A. Harris and Ch. Jungen, *J. Chem. Phys.* **122**, 184314 (2005).
[2] S. Bezzaouia, M. Telmini and Ch. Jungen, *Phys. Rev. A* **70**, 012713 (2004).
[3] C. H. Greene and Ch. Jungen, *Adv. At. Mol. Phys.* **21**, 51 (1985).
[4] Ch. Jungen (ed.) *Molecular Applications of Quantum Defect Theory*, Institute of Physics Publishing, Bristol, (1996).
[5] U. Fano, *Phys. Rev. A* **2**, 353 (1970) (reprinted in [4]).
[6] S. C. Ross and Ch. Jungen *Phys. Rev. A* **49**, 4364 (1994) (reprinted in [4]).
[7] M. Arif, Ch. Jungen and A. L. Roche, *J. Chem. Phys.* **106**, 4102 (1997).
[8] M. J. Seaton, *Rep. Prog. Phys.* **46**, 167 (1983) (reprinted in [4]).
[9] M. Telmini and Ch. Jungen, *Phys. Rev. A* **68**, 062704 (2003).
[10] R. Guérout, M. Jungen and Ch. Jungen, *J. Phys. B: At. Mol. Opt. Phys.* **37**, 3043 (2004).
[11] A. Osterwalder, A. Wüest, F. Merkt and Ch. Jungen, *J. Chem. Phys.* **121**, 11810 (2004).
[12] Ch. Jungen and F. Texier, *J. Phys. B: At. Mol. Opt. Phys.* **33**, 2495 (2000).
[13] R. Guérout and Ch. Jungen (2007, in preparation).
[14] C. H. Greene, *Phys. Rev. A* **28**, 2209 (1983) (reprinted in [4]).
[15] R. Guérout, M. Jungen and Ch. Jungen, *J. Phys. B: At. Mol. Opt. Phys.* **37**, 3057 (2004).

M Plummer, J D Gorfinkiel and J Tennyson (eds.)
Mathematical and computational methods in R-matrix theory

A hyperspherical *R*-matrix scheme for two-active-electron systems

L Malegat[1], C Bouri[2] and P Selles[3]

[1] *Laboratoire d'Interaction du Rayonnement X Avec la Matière (UMR 8624 du CNRS), Université Paris-Sud 11, 91405 Orsay, France*
[2] *Quantum Optics and Statistics, Institute of Physics, Albert-Ludwigs-Universität Freiburg, Hermann-Herder-Str 3, D-79104, Germany*
[3] *Laboratoire de Chimie Physique Matière et Rayonnement (UMR 7614 du CNRS), Université P et M Curie, 11 reu P et M Curie, 75231 Paris Cedex 05, France*

The *ab initio* method presented here belongs to the $\mathcal{R}$-matrix family undoubtedly. Yet it departs from the current implementations of the $\mathcal{R}$-matrix approach in many important respects. The focus of this brief report is on these differences. This is at the expense of the results for which we refer to the literature.

The method we wish to present has been designed to deal with two-active-electron systems in the very challenging case when the motion of the two electrons is highly correlated and unbounded. It is best introduced by considering the textbook example of such a situation, that is to say, photo double ionization of helium.

I. A STATEMENT OF THE DOUBLE IONIZATION PROBLEM

This process is governed by a time dependent Schrödinger equation involving a Hamiltonian which is periodic in time. This is why we may look for the solution in the form of a Floquet expansion, the components of which satisfy an infinite set of stationary coupled partial differential equations. We then note that: (i) photoemission is negligible since the transition from the discrete initial state to the continuum final state is quasi-irreversible; (ii) multiphoton absorption is

negligible at the intensities of the incident radiation; (iii) the exciting electric field is negligible compared to the intra atomic field and can be treated to the first order of perturbation. Due to these circumstances, the system reduces to the following stationary inhomogeneous equation which has to be solved for an outgoing wave boundary condition:

$$[H_0 - (E_0 + \omega)]\,\Psi_1 = (\vec{D} \cdot \vec{\mathcal{E}}_0)\Psi_0. \tag{1}$$

In (1), H_0 is the field free Hamiltonian, Ψ_0 and E_0 are the ground state wavefunction and energy respectively, ω is the radiation frequency, $\vec{D}$ the atomic dipole, and $\vec{\mathcal{E}}_0$ the resonant component of the incident electric field at the origin of coordinates. The wavefunction to determine, Ψ_1, which describes the system after photo absorption, will be referred to accordingly as the *photoabsorption wavefunction*. It contains complete information regarding the infinite number of processes which are open at the energy considered, located above the double-ionization theshold: single ionization leaving the ion in the ground state $n = 1$, single ionization leaving the ion in an excited state $n > 1$, and finally double ionization. The inhomogeneous term on the right plays the role of a source term that feeds the photoabsorption wavefunction.

II. A SEPARATION OF CONFIGURATION SPACE INTO TWO REGIONS

It is convenient to express (1) in the center of mass frame using hyperspherical coordinates including the hyperradius $R = \sqrt{r_1^2 + r_2^2}$ and a set of five angles denoted collectively by Ω, which include the radial correlation angle $\alpha = \tan^{-1}(r_2/r_1)$. This indeed makes two interesting features appear: (i) the potential term in H_0 scales as $1/R$, so that for large R, it varies slowly enough with R to allow for a semiclassical treatment of the hyperradial motion; (ii) the source term vanishes as soon as R exceeds the range of the initial state Ψ_0. It is then natural to split configuration space into two regions separated by a hypersphere of appropriate hyperradius R_0. Within this hypersphere, we develop a quantum treatment of all variables and take account of the source term, whereas outside this hypersphere, we combine a quantum treatment of Ω with a semiclassical treatment of R while neglecting the source term. Having split configuration space, we have complied with the first pre-requisite for an $\mathcal{R}$-matrix treatment. However important differences appear with respect to the CCP2 $\mathcal{R}$-matrix. First of all, the separating surface is a hypersphere $R = R_0$ in the full 6D space of the problem, instead of a sphere $r_i = r_0$ in the 3D space attached to an individual particle i in the system. Moreover, the physical criteria which distinguish the two regions, and the approximations which simplify the outer region treatment accordingly, are very different. What is crucial here is

the possibility to treat the size of the system semiclassically, whereas in the CCP2 case, it is to neglect exchange and correlation effects. *

III. INNER REGION TREATMENT

A. $\mathcal{R}$-matrix equation

By making the standard change of function $\Psi_1 = (R^{5/2}\sin 2\alpha)^{-1}\tilde{\Psi}_1$, introducing the fixed-$R$ Hamiltonian $H_R(\Omega)$, multiplying on the left by $R^{5/2}\sin 2\alpha$ and renaming the resulting inhomogeneous term I for brevity, one can recast (1) as

$$\left[-\frac{1}{2}\frac{\partial^2}{\partial R^2} + H_R(\Omega) - E\right]\tilde{\Psi}_1(R;\Omega) = I(R;\Omega). \tag{2}$$

Next, one introduces its companion equation

$$\left[-\frac{1}{2}\frac{\partial^2}{\partial R^2} + B(R) + H_R(\Omega) - E_k\right]\tilde{\Psi}_k(R;\Omega) = 0. \tag{3}$$

The latter, which is made hermitic over the finite inner region by the addition of the Bloch term $B(R)$, defines the $\mathcal{R}$-matrix eigenstates $\tilde{\Psi}_k$ and eigenvalues E_k. It is then easy to anybody familiar with the $\mathcal{R}$-matrix machinery to establish the $\mathcal{R}$-matrix relation

$$F_i(R_0) = \sum_j \mathcal{R}_{ij}F'_j(R_0) + \mathcal{I}_i(R_0), \tag{4}$$

between the hyperradial channel functions $F_i(R)$, defined with respect to some appropriate angular basis $\Phi_i(\Omega)$ by

$$\tilde{\Psi}_1(R;\Omega) = \sum_i F_i(R)\Phi_i(\Omega), \tag{5}$$

and their derivatives. The $\mathcal{R}$-matrix and $\mathcal{I}$ vector are then obtained from the $\mathcal{R}$-matrix eigenstates and eigenvalues according to

$$\mathcal{R}_{ij}(R_0) = \frac{1}{2}\sum_k \frac{F_i^k(R_0)F_j^k(R_0)}{E_k - E}, \qquad \mathcal{I}_i(R_0) = \frac{1}{2}\sum_k \frac{\langle\tilde{\Psi}_k|I\rangle F_i^k(R_0)}{E_k - E}, \tag{6}$$

---

*Note that here, exchange and correlation effects remain important in the outer region.

where the $F_i^k(R_0)$ defined by

$$\tilde{\Psi}_k(R;\Omega) = \sum_i F_i^k(R)\Phi_i(\Omega) \tag{7}$$

are sometimes referred to as the $\mathcal{R}$-matrix amplitudes. $\langle\tilde{\Psi}_k|I\rangle$ denotes the scalar product of the inhomogeneous term and the kth $\mathcal{R}$-matrix eigenstate. Putting aside the already mentioned fact that the inner region boundary is not a sphere but a hypersphere, as well as the presence of the additional term arising from the inhomogeneous nature of the original equation, our $\mathcal{R}$-matrix relation (4) looks perfectly standard.

B. Outgoing wave boundary condition

The $\mathcal{R}$-matrix relation by itself does not determine $\tilde{\Psi}_1$. Clearly, one more relation is required between the channel functions and their derivatives at the boundary. For systems which reduce asymptotically to two-bodies, this relation follows from our full understanding of the long range dynamics of two interacting particles. But for systems which remain three body in character asymptotically, the problem is still an open one, to which we propose an original solution. The idea is as follows: if we expand $\tilde{\Psi}_1$ on some angular basis specially designed to account for the dynamics around R_0, it is likely that the channel functions $G_\lambda(R)$ thus defined will satisfy *locally* much simpler equations than the $F_i(R)$ introduced so far; and this may well open a route to the additional relation we look for. The angular basis we consider is made up of the eigenvectors of the fixed-R Hamiltonian satisfying

$$[H_R(\Omega) - E_\lambda(R)]\,\Xi_\lambda(R;\Omega) = 0. \tag{8}$$

We now choose R_0 such that the adiabatic approximation expressed by

$$\left.\frac{\partial\Xi_\lambda}{\partial R}\right|_{R_0} \ll 1, \quad \left.\frac{\partial^2\Xi_\lambda}{\partial R^2}\right|_{R_0} \ll 1, \tag{9}$$

is valid for all λ, and the inhomogeneous term can be neglected.[†] As a result, the hyperradial channel functions $G_\lambda(R)$ satisfy, in the vicinity of R_0, the following

[†]The latter condition is easily met by any R_0 exceeding the range of the initial state. The former is much more demanding. In fact, non-adiabatic couplings are known to be important at avoided crossings between adiabatic potential curves $E_\lambda(R)$. Since the latter are located approximately on the $-Z(\pi/4,\pi)/R$ curve - see section IV.A and [1],

set of *uncoupled* differential equations

$$\left[\frac{\partial^2}{\partial R^2} + p_\lambda^2(R_0)\right] G_\lambda(R) = 0, \tag{10}$$

where the channel momenta are given by

$$p_\lambda(R_0) = \sqrt{2\,(E - E_\lambda(R_0))}, \qquad p_\lambda(R_0) = \mathrm{i}\sqrt{2\,(E_\lambda(R_0) - E)}, \tag{11}$$

for open and closed channels respectively. The solution consists of the ingoing and outgoing hyperspherical waves associated to the channel momenta $p_\lambda(R_0)$. Imposing the outgoing wave boundary condition then determines each channel function within a normalization factor and the relation we hoped for follows naturally as

$$G'_\lambda(R_0) = \mathrm{i}p_\lambda(R_0)G_\lambda(R_0). \tag{12}$$

Putting together (4), (12), and the frame transformation which takes the initial angular basis $\Phi_i(\Omega)$ into the adiabatic angular basis $\Xi_\lambda(R_0;\Omega)$ at R_0, we define a system of linear inhomogeneous equations that can be solved for the channel functions $F_i(R_0)$. The solution over the full inner region follows according to the standard $\mathcal{R}$-matrix technique.

C. A property of the adiabatic channels at the boundary

At this point, it is important to point out that the solution is searched for and obtained in the form given by (5), where the $\Phi_i(\Omega)$ are analytical angular basis functions, and the channel functions $F_i(R)$ are expanded over analytic hyperradial basis functions (for details see the bibliography). This is different from the close-coupling type expansions used in current $\mathcal{R}$-matrix implementations, where the physical outgoing channels are included explicitly. Therefore, once we have got the photoabsorption wavefunction, we are not done: there still remains to disentangle the various physical outgoing channels from each other. This is one more difference compared to the usual $\mathcal{R}$-matrix experience.

---

it turns out that for large R, the possibly significant non-adiabatic couplings involve high-lying adiabatic channels, which are likely to play a minor role in the dynamics. To this extent, it is possible to find a value of R_0 that complies with the requirements of (9).

Let us now state a property of the adiabatic channels at R_0 which is important in this respect. Namely, the successive adiabatic channels λ, defined at R_0, ordered according to increasing adiabatic energies $E_\lambda(R_0)$, can be identified with the single ionization channels with excitation of the ion to its successive Stark sub-levels labelled by n and the parabolic quantum number K, the degeneracy of which is removed by the influence of the ionized electron located a distance R_0 away. If this identification could be pushed up to infinite values of n, the problem would be fully solved right at R_0, but this of course is not the case. In fact, this identification stops at n_0 such that the range of the n_0^{th} ionic state, which scales as n_0^2, remains much smaller than R_0. Typically, with $R_0 = 60$ a.u., which is the largest inner region we have considered so far, ionization-excitation channels up to n=3 included can be clearly disentangled from each other and from the bulk of the wavefunction.

D. An interesting application: the study of doubly excited states

Once the wavefunction $\tilde{\Psi}_n^+$ corresponding to ionization with excitation to the level n is identified, its outgoing total and differential fluxes through the hypersphere $R = R_0$ can be computed, and the partial cross section σ_n and asymmetry parameter β_n follow by dividing by the ingoing photon flux. The very possibility of identifying these channels demonstrates their *decoupling* from each other and from the bulk of the wavefunction: this in turn implies that the cross sections are converged at R_0, something that looks a bit surprising at first sight, given the relatively moderate value of R_0. Note anyway that this computational technique, based on the very definition of the cross sections, does not rely upon any approximation and provides accordingly very accurate data.

This property opens the route to an interesting application of the raw inner region treatment. Indeed, despite being designed primarily to deal with the double ionization problem, our approach can be applied below the double ionization threshold as well, notably in the region where doubly excited states are formed, which decay, among other channels, via auto-ionization. These states can be observed accordingly on the ionization cross sections, the more visibly *the more partial and differential the cross section is*, and may sometimes appear as *very narrow* Fano resonances. Our method, which provides accurate partial and differential ionization cross sections, and can produce them on a very dense energy grid to almost no cost due to the analytic energy dependence of the $\mathcal{R}$-matrix scheme, therefore turns out to be very convenient for studying these very intriguing states.

Finally, the property reported above is also essential regarding the initialization of the outer region propagation, as explained below.

IV. OUTER REGION PROPAGATION

Although our inner region $\mathcal{R}$-matrix approach has interesting applications, in particular to the study of doubly excited states, it cannot provide all the physical quantities of interest: cross sections for single ionization with excitation to the levels $n > n_0$ of the ion and for double ionization remain out of reach due to the limited size of the inner region. This is why we have developed an outer region treatment.

A. A semiclassical ansatz wavefunction

The main idea of the later is to look for the photoabsorption wavefunction in the following product form:

$$\tilde{\Psi}_1(R,\Omega) = \frac{1}{\sqrt{p(R)}} \exp\left[\mathrm{i}\int_{R_0}^{R} p(R')dR'\right] \times \Phi(R;\Omega). \tag{13}$$

The first term, which depends only on R, is a hyperspherical semiclassical outgoing wave associated to a local momentum $p(R)$. The later is supposed to satisfy the validity condition for a semiclassical approximation, that is to say, the first derivative of the associated wavelength is small compared to 1. The second term, by contrast, depends on all coordinates, yet not on the same footing: we call it the *reduced wavefunction* and we assume that it varies slowly with R. More precisely, we suppose that the hyperradial kinetic energy associated to this reduced function is very small compared to its counterpart arising from the semiclassical outgoing wave. To summarize,

$$\frac{p'}{p^2} \ll 1, \qquad \frac{\partial^2\Phi}{\partial R^2} \ll p^2\Phi. \tag{14}$$

The idea behind this approximation is that for large R, the dynamics becomes much less sensitive to the size of the system, measured by the hyperradius, than to its shape, which is controlled by the angular coordinates, notably the radial correlation angle $\alpha = \tan^{-1}(r_2/r_1)$ and the angular correlation angle $\theta_{12} = \cos^{-1}(\hat{r}_1 \cdot \hat{r}_2)$. So that an approximate treatment of the hyperradial motion becomes relevant.

To better understand the approximate treatment proposed here, let us compare our approach with the adiabatic by sector propagation that is more familiar to the CCP2 community. In the latter, the hyperradial channel functions $G_\lambda^{(i)}(R)$ defined with respect to the adiabatic angular basis $\Xi_\lambda(R_i;\Omega)$ are propagated within the adiabatic approximation from R_i to R_{i+1}, where a frame transformation is performed from $\Xi_\lambda(R_i;\Omega)$ to $\Xi_\lambda(R_{i+1};\Omega)$, and so on

iteratively. This method thus allows for a specific hyperradial motion in each adiabatic channel. Recalling that the adiabatic channels can be interpreted asymptotically as ionization-excitation and double ionization channels, it turns out that the adiabatic method accounts for the various excess energies available in the various physical outgoing channels. This is certainly needed if all outgoing channels are considered, from single ionization without excitation to double ionization, these two channels being energetically separated by as much as 2 a.u.. But it is much less so if, for instance, the three lowest ionization excitation channels are discarded: indeed, the lowest remaining channel, $n = 4$, is then only 0.125 a.u. away from the highest one. Accordingly, our approximation, which assumes that the bulk of the hyperradial motion is common to all channels, sounds reasonable if applied to the photoabsorption wavefunction stripped off the three lowest ionization-excitation channels. Luckily enough, the later decouple from the bulk of the wavefunction right at R_0, as explained above.

We still have to define the local momentum $p(R)$. To this end, we consider the bulk hyperradial motion to be that of an electron of energy E in a model potential $-Z_{eff}(R)/R$ which approximates the true 3-body potential $-Z(\alpha, \theta_{12})/R$. The local momentum follows as

$$p(R) = \sqrt{2\left(E + \frac{Z_{eff}(R)}{R}\right)}. \tag{15}$$

The effective charge is then defined by interpolating between the two following boundary values: (i) $Z_{eff}(R_0)$, obtained by matching the outer region wavefunction to the inner region wavefunction stripped off the identified ionization-excitation channels at R_0; and (ii) $Z_{eff}(\infty) = Z(\pi/4, \pi)$. It is easy to show that these two values provide relevant approximations of the true 3-body potential in the limiting cases considered. At fixed R indeed, the later takes the well known shape of a saddle [1], that is to say a flat plateau around the saddle point at $(\alpha = \pi/4, \theta_{12} = \pi)$, with an infinite barrier at $(\alpha = \pi/4, \theta_{12} = 0)$ corresponding to the bielectronic repulsion, and two infinite wells at $\alpha = 0$ and $\pi/2$ corresponding to the electron-nucleus attraction. When R tends towards ∞, the range spanned by these singularities in the $\alpha \times \theta_{12}$ plane tends towards zero: accordingly, this potential can be approximated by a plateau located at the saddle point value $-Z(\pi/4, \pi)/R$. At $R = R_0$, we can still forget the repulsive singularity which determines a forbidden region without influencing the dynamics in the accessible part of configuration space. Besides, matching the outer region wavefunction to the *stripped off* inner region wavefunction implies that we suppress the lowest levels supported by the attractive wells: this amounts to fill up these wells up to the level of the most excited discarded state, in just the same way as adding a repulsive core potential suppresses the core levels of a complex molecule in quantum chemistry. As a result, the approximate potential behind $Z_{eff}(R_0)$ reduces once again to a plateau, which is now located

slightly below the saddle point value of the potential. Accordingly, $Z_{eff}(R_0)$ is only slightly above $Z_{eff}(\infty)$, so that the detailed interpolation procedure used to complete the definition of $Z_{eff}(R)$ for the intermediate values of R does not matter. For this reason, the *ab initio* character of our approach is maintained.

B. Hyperradial propagation

Having completed the definition of our semiclassical ersatz, we carry it into the outer region equation -which is the homogeneous counterpart of (2). Due to the second inequality in (14), the second order derivative with respect to R can be neglected, and we obtain a partial differential equation which is first order over R. The change of variable defined by

$$d\tau = \frac{dR}{Rp(R)} \tag{16}$$

allows one to rewrite this equation into the following standard form of a propagation equation:

$$\mathrm{i}\frac{\partial}{\partial\tau}\Phi(\tau;\Omega) = \tilde{H}(\tau;\Omega)\Phi(\tau;\Omega). \tag{17}$$

So finally, the semiclassical treatment of the hyperradial motion has brought us back to a 5D propagation problem with respect to the 6^{th} variable $\tau(R)$, which plays the role of a mock time. This has many advantages. One may indeed benefit from the refined algorithms developed for time-dependent studies to solve a problem of lower dimensionality than its genuine time-dependent counterpart: not only is the wavefunction to propagate 5D instead of 6D, but in addition, the 5 variables are angles ranging over finite intervals. This enables us to propagate the wavefunction to quasi macroscopic distances, of the order of 10^6 a.u., within reasonable times. This peculiarity makes our approach very convenient for near threshold studies where one has to describe the dynamics over very large distances. Moreover, it allows us to reach the asymptotic region where the outgoing fluxes attached to the various processes converge, so that we can compute the cross sections from their plain definition without relying upon any approximate finite range formula. This is a distinctive signature of the method.

V. DISENTANGLING THE VARIOUS OUTGOING CHANNELS

Now that we have produced the photoabsorption wavefunction over an extended region, we still have to identify the various outgoing channels, which do

not appear explicitly in the expansion of this wavefunction. To disentangle these physical channels from each other, we use two different tools, namely projectors and propagators.

Let us first introduce the projector

$$P_n^2 = \sum_{\ell m} |2; n\ell m\rangle\langle n\ell m; 2| \tag{18}$$

onto the subspace of two-electron states in which electron 2 is in the n^{th} ionic level, composed of well known hydrogenic states $(n\ell m)$. Applying this projector implies that one integrates over $\vec{r}_2$ at fixed $\vec{r}_1$, something that looks rather uncomfortable as our coordinate system combines *collective* variables, namely R and α, with *particle* coordinates $\hat{r}_1 = (\theta_1, \varphi_1), \hat{r}_2 = (\theta_2, \varphi_2)$. However, on a hypersphere the radius R_n of which is large compared with the range r_n of the n^{th} ionic state, say $R_n \simeq 10^2 r_n$ to be more specific, integrating over r_2 at fixed r_1 amounts to integrate over α at fixed R_n, the tangent to the arc and the arc itself being undistinguishable over the distance of interest r_n. This leads us to introduce the projector applied at $R = R_n$, noted $P_n^2(R_n)$, its generalization

$$P_n(R_n) = P_n^1(R_n) + P_n^2(R_n) - P_n^1(R_n)P_n^2(R_n), \tag{19}$$

which takes account of the indiscernability of the electrons, as well as the function

$$\Psi_n^+(R_n; \Omega) = P_n(R_n)\Psi_1(R_n; \Omega). \tag{20}$$

We then check that the total and differential outgoing fluxes of Ψ_n^+ through the hypersphere $R = R_n$ are converged with respect to R_n. They give indeed, after renormalization by the ingoing photon flux, accurate values of the cross section and asymmetry parameter for ionization with excitation to the level n. The function given by (20) is then referred to as the n^{th} ionization-excitation wavefunction.

Let us next introduce the propagator $\mathcal{P}(R_n, R_{n+1})$ of (17) from R_n, where the n^{th} ionization-excitation channel can be projected out by applying $1-P_n(R_n)$, to R_{n+1}, where the same operation can be performed for the $(n+1)^{th}$ channel. The double ionization wavefunction is then determined from the photoabsorption wavefunction at the border of the inner region by applying, alternatively, propagators and anti-projectors, according to

$$\Psi^{2+}(R_\infty; \Omega) = \left\{ \prod_{n=1}^{\infty} (1 - P_n)\mathcal{P}(R_{n-1}, R_n) \right\} \Psi_1(R_0; \Omega). \tag{21}$$

The photoabsorption wavefunction is thus stripped off the successive ionization-excitation channels in the course of propagation, leaving at the end a pure

double ionization channel, from which every double ionization cross section can be extracted via a flux calculation.‡

VI. CONCLUSION

We have discussed above the most subtle aspects of our approach in reference to the common $\mathcal{R}$-matrix background of the community. No illustration has been given of the performances of the method -which are excellent: the interested reader is invited to consider the bibliography proposed below.

Acknowledgements

The authors acknowledge the support of the CNRS computer center IDRIS (Orsay, France).

---

[1] Fano U 1983 *Rep. Prog. Phys.* **46** 97
[2] Malegat L, Selles P and Kazansky A 1999 *Phys. Rev. A* **60** 3667
[3] Malegat L, Selles P and Kazansky A 2000 *Phys. Rev. Lett.* **85** 4450
[4] Selles P, Malegat L and Kazansky A 2002 *Phys. Rev. A* **65** 032711
[5] Citrini F, Malegat L, Selles P and Kazansky A K 2003 *Phys. Rev. A* **67** 042709
[6] Malegat L, Selles P and Kazansky A in *Many Particle Quantum Dynamics in Atomic and Molecular Fragmentation* eds. Ullrich J and Shevelko V P (Springer, Heidelberg, 2003)
[7] Selles P, Malegat L, Huetz A, Kazansky A K, Seccombe D P, Collins S A and Reddish T J 2004 *Phys. Rev. A* **69** 052707
[8] Bouri C, Selles P, Malegat L, Teuler J M, Kwato-Njock M and Kazansky A K 2005 *Phys. Rev. A* **72** 042716
[9] Bouri C, Selles P, Malegat L and Kwato-Njock M G 2006 *Phys. Rev. A* **73** 022724
[10] Bouri C, Selles P, Malegat L and Kwato Njock M G 2006 *Phys. Rev. A* **74** 032704

---

‡To be rigorous, the product in (21) should start with $n = 4$, and the photoabsorption wavefunction at R_0 should be Ψ_1 with the three lowest ionization excitation channels suppressed as explained in section III.C. In addition, n cannot exceed 50 in practice, so that at the end of the propagation, the double photoionization wavefunction is still contaminated by the ionization-excitation channels $n > 50$. Other methods have been developed to get rid of this residual pollution.

[11] Bouri C, Selles P, Malegat L and Kwato Njock M G 2007 *J. Phys. B: At. Mol. Opt. Phys.* **40** F51

M Plummer, J D Gorfinkiel and J Tennyson (eds.)
Mathematical and computational methods in R-matrix theory

Analysis of anionic molecular complexes within the *R*-matrix framework

Bernd M. Nestmann[1] and Michal Tarana[2]

[1] *Institute of Physical and Theoretical Chemistry, University of Bonn, Wegelerstraße 12, 45115 Bonn, Germany*
[2] *Institute of Theoretical Physics, Charles University Prague, V Holešovičkách 2, 180 00 Praha 8, Czech Republic*

I. CONCEPT

During the last decades the rapidly increasing capability of computers has opened new possibilities in the theoretical treatment of atoms and molecules. In particular, quantum chemical *ab initio* methods including electron correlation to a large amount became applicable to molecular systems. The agreement with experimental findings which can be achieved in such calculation is usually taken as a measure of the quality of the applied method.

Even though high precision is a desired goal, the main advantage of *ab initio* methods is their reliability even in cases where experimental results are not available. Moreover, since model assumptions are not included, the contribution of an *ab initio* calculation to the understanding of the process under consideration is free from any presupposition. However, in order to obtain such an understanding a close consideration of the intermediate results may be more important than a look at the final result.

Within the R-matrix approach scattering cross sections as well as bound state energies can be obtained from close-coupling calculations for an electron in the field of the molecule, moving outside of some sphere Ω around the molecule. In the calculations boundary conditions have to be taken into account in order to ensure the regularity of the solution. These conditions are determined by the Hamiltonian H_Ω describing the collision complex inside Ω. While a comparison with the experimental cross sections requires a complete R-matrix calculation, some phenomena like resonances, large values in elastic and excitation cross sections close to threshold as well as the appearance of bound states may be predetermined by properties of the collision complex inside Ω.

II. *R*-MATRIX POLES AND AMPLITUDES

The radius r_0 of the sphere Ω has to be chosen large enough so that outside the sphere the scattering wave function can be decomposed into contributions of the scattering channels. In particular, the eigenfunctions Ψ_k of H_Ω at the sphere Ω can be written in the form

$$\Psi_k|_\Omega = \sum_\rho \mathcal{A}\left(\Phi_\rho \times \sum_{lm} Y_{lm}(\theta,\phi)\frac{1}{r} f_{\rho lm;k}(r)\right)\Bigg|_{r=r_0}; \tag{1}$$

the Φ_ρ represent the target states as functions of the spin and spatial coordinates of the target electrons, the positions of the nuclei and the spin of the scattered electron. r, θ and ϕ are the spherical coordinates of the scattered electron. The Φ_ρ are assumed to be completely inside Ω so that the restriction of H_Ω only affects the functions $f_{\rho lm;k}(r)$. In order to conserve the hermiticity of H_Ω the kinetic energy operator applied to these functions has to be modified by adding Bloch terms – in our calculations, by adding the term $\delta(r-r_0)\,\frac{1}{2}\,\frac{d}{dr}$.

Due to the arguments given above the scattering wave functions outside Ω corresponding to a certain energy E are of the form

$$\Psi_E|_{out} = \sum_\rho \mathcal{A}\left(\Phi_\rho \times \sum_{lm} Y_{lm}(\theta,\phi)\frac{1}{r} f_{\rho lm;E}(r)\right)\Bigg|_{r\geq r_0}.$$

The $f_{\rho lm;E}(r)$ have to satisfy the boundary conditions

$$f_{\rho' l' m';E}(r_0) = \sum_{\rho lm} R_{\rho' l' m';\rho lm}(E)\ \frac{df_{\rho lm;E}(r)}{dr}\Bigg|_{r_0}.$$

These conditions are completely determined by the R-matrix amplitudes $\langle \rho lm r_0|\Psi_k\rangle = f_{\rho lm;k}(r_0)$ and the R-matrix poles E_k:

$$R_{\rho' l' m';\rho lm}(E) = \frac{1}{2}\sum_k \frac{\langle \rho' l' m' r_0|\Psi_k\rangle\langle\Psi_k|\rho lm r_0\rangle}{E_k - E};$$

the E_k are the eigenvalues of H_Ω corresponding to Ψ_k.

III. *R*-MATRIX POLES AND AMPLITUDES IF THE ELECTRON-MOLECULE INTERACTION IS NEGLECTED

Information about the energy-dependent electron-molecule interaction can be obtained by comparing the R-matrix poles and amplitudes with the poles and amplitudes of the interaction-free problem. Since the corresponding Hamiltonian H_Ω does not couple the different scattering channels its eigenvalues and -vectors can be assigned to the channels ρlm and to some "quantum number" n. In analogy to Eq.1 we can write

$$\Psi^0_{\rho lmn} = \Phi_\rho \times Y_{lm}(\theta,\phi)\frac{1}{r} f^0_{\rho lmn}(r);$$

with

$$f^0_{\rho lmn(r)} = N_{ln}\, j_l(p_{ln} r)$$

Here, the $j_l(x)$ are the Bessel functions, $n = 0, 1, \cdots$ are the number of nodes of $j_l(p_{ln}r)$ between $r = 0$ and $r = r_0$. p_{ln} is determined by n and the boundary condition of $j_l(p_{ln}r)$ at $r = r_0$ determined by the Bloch terms; in our case by

$$\left.\frac{dj_l(p_{ln}r)}{dr}\right|_{r_0} = 0.$$

N_{ln} provides the correct normalization of Ψ^0_k. Then, for the R-matrix poles and amplitudes we obtain

$$E^0_{\rho ln} = \epsilon_\rho + \frac{1}{2}\, p^2_{ln} \quad \text{and} \quad \langle \rho' l' m' r_0 | \Psi^0_{\rho lmn}\rangle = \delta_{\rho'\rho}\, \delta_{l'l}\, \delta_{m'm}\, N_{ln}\, j_l(p_{ln} r_0);$$

the ϵ_ρ are the target state energies. It is meaningful to express the the ϵ_ρ relative to the energy of the target ground state. In columns $2 \cdots 6$ of figure 1 the $E^0_{\rho ln} < 18\,\text{eV}$ are shown for $l = 0 \cdots 4$ and a single target state. r_0 has been set to 10 Bohr.

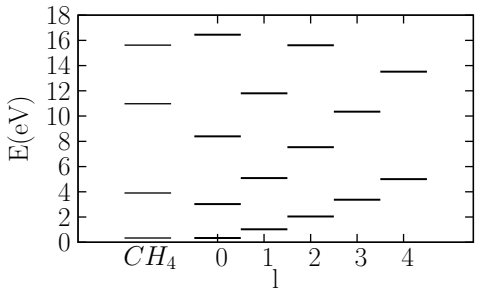

FIG. 1. R-matrix pole positions, first column: ${}^2A_1$ of $e^- + CH_4$, column $2 \cdots 6$: free particle problem

IV. *R*-MATRIX POLES IN THE CASE OF WEAKLY COUPLED CHANNELS

The following consideration is based on the assumption that the (E_k, Ψ_k) can clearly be assigned to some scattering channel $(\rho_k l_k m_k)$ which dominates in the corresponding R-matrix amplitudes, and to some n_k determined by the position of E_k in the increasing order of the poles belonging to the same scattering channel. One can now establish a relationship between the differences $E_k - E_{\rho_k l_k n_k}$, the corresponding scattering eigenphases and partial cross sections, and the angular and energy-dependent electron-molecule interaction. For small energy differences the corresponding electron-molecule interaction can be assumed to be small and the eigenphases as well as the partial cross sections are close to zero. If the difference is positive the electron-molecule interaction is repulsive and the eigenphase becomes negative. A negative energy difference indicates an attractive electron-molecule interaction and a positive scattering eigenphase. In both cases the cross sections increase with increasing values of $|E_k - E_{\rho_k l_k n_k}|$. In the first column of figure 1 the lowest poles are shown appearing in the *fixed nuclei* calculations of $e^- + CH_4$ in ${}^2A_1$ symmetry [1]. The comparison with the s-wave free particle poles indicates low cross sections for collision energies below 1eV. It has been shown in [1] that the s-type eigenphase close to threshold are positive and decrease to negative values with increasing collision energy, passing zero at approximately 0.5 eV.

V. RESONANCES INTERACTING WITH WEAKLY COUPLED CHANNELS

In general, resonances provide strong coupling between different scattering channels. However, in many cases it is possible to apply the Fano-Feshbach projection operator formalism in order to separate resonant scattering from the scattering background, which has the property as discussed in section IV. This property of the background can be used to construct the projection operators $\mathcal{P}$ and $\mathcal{Q}$ projecting the complete Hilbert space to subspaces representing the background scattering and the resonant scattering, respectively [2]. The construction is based on the following assumptions:

1. The projection onto the resonance subspace is of the form

$$\mathcal{Q} = \sum_j |\Phi_j\rangle\langle\Phi_j|, \qquad \text{with } \Phi_j = \sum_{k|E_k \le E_{max}} c_{jk}\Psi_k \qquad \text{and } \langle\rho l m r_0|\Phi_j\rangle = 0.$$

   The Φ_j are the so called discrete components of the resonances below E_{max} and are assumed to be completely inside Ω.

2. For the construction of the $\mathcal{P}$ operator we assume that the eigenvalues and -functions of the background R-matrix Hamiltonian H_Ω^{back} can be written in the form $(E^{back}_{\rho_h l_h n_h}, \Psi^{back}_{\rho_h l_h m_h n_h})$. Then, the $\mathcal{P}$ operator restricted to the inner of Ω can be expressed by

$$\mathcal{P}\Psi_k = \sum_h |\Psi^{back}_{\rho_h l_h m_h n_h}\rangle\langle\Psi^{back}_{\rho_h l_h m_h n_h}|\Psi_k\rangle$$

   with

$$\langle\Psi^{back}_{\rho_h l_h m_h n_h}|\Psi_k\rangle = \frac{\langle\rho_h l_h m_h r_0|\Psi_k\rangle}{E_k - E^0_{\rho_h l_h n_h}} \left(\sum_{h'} \delta_{\rho_h\rho_{h'}}\delta_{l_h l_{h'}}\delta_{m_h m_{h'}} \frac{\langle\rho_h l_h m_h r_0|\Psi^0_{\rho_h l_h m_h n_h}\rangle}{E_k - E^0_{\rho_{h'} l_{h'} n_{h'}}}\right)^{-1}.$$

The Φ_j are obtained by solving the equation $\mathcal{P}\mathcal{Q} = 0$ and diagonalizing $\mathcal{Q}H_\Omega\mathcal{Q}$. The energy-dependent resonance widths $\Gamma_j(E)$ and the level shifts $\Delta_j(E)$ are determined within the Fano-Feshbach projection operator formulism by the Φ_j and the R-matrix representation of the background scattering problem.

VI. THE $^2A_1$ SHAPE RESONANCE OF O_3

The $^2A_1$ shape resonance of O_3 characterized by the leading configuration $\{\cdots 1b_1^2 1a_2^2 4b_2^2 6a_1^2 7a_1\}$ is a good example to demonstrate the procedure described

in section V. In figure 2 the R-matrix poles in $^2A_1$ symmetry below 5eV for O–O bond length R=2.6 Bohr and the bond angle $\alpha = 116^\circ$ are shown together with the background poles (bg), the free-particle poles, and the eigenvalues of $\mathcal{Q}H_\Omega\mathcal{Q}$ (res). In the energy region considered there are two more poles of the electron scattering problem than in the free particle problem (in a_1 symmetry employed there are one p and two d components). Applying the resonance-background separation we get two discrete components: the resonance mentioned above and one bound state state, characterized by the configuration $\{\cdots 1b_1^2 1a_2^2 4b_2^2 6a_1^2 2b_2^2\}$. The background poles still differ considerably from the free particle poles indicating large background cross sections.

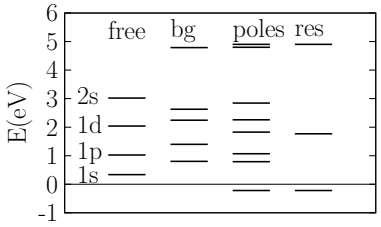

FIG. 2. Pole positions for $^2A_1(e^- + O_3)$ at R=2.6 Bohr and $\alpha = 116^\circ$

However, figure 3 shows that the R-matrix amplitudes are well separated which allows an assignment between the background poles and the free particle poles. Exceptions are the two d-amplitudes [(20) and (22)] which show strong mixing due to the small separation of the corresponding poles.

The inspection of figures 2 and 3 allows us to predict properties of the cross sections shown in figure 4 – in particular the large background cross sections at threshold are due to the large difference between the lowest (s-)pole and the lowest free-particle pole. Despite the large background cross sections the separation between resonance and background scattering works very well as can be seen in figure 4. Moreover, the different nature of resonant and background scattering can be observed by comparing the results

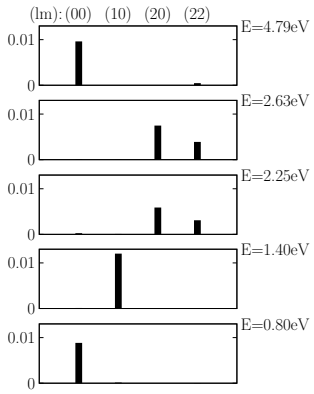

FIG. 3. Squares of the R-matrix background amplitudes for $^2A_1(e^- + O_3)$

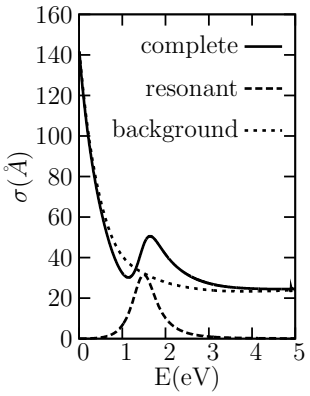

FIG. 4. Cross sections for ${}^2A_1(\mathrm{e}^- + \mathrm{O}_3)$ at R=2.6 Bohr and $\alpha = 116°$

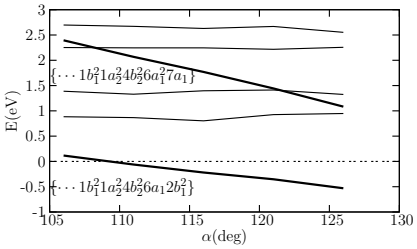

FIG. 5. Eigenvalues of $\mathcal{P}H_\Omega\mathcal{P}$ (thin lines) and $\mathcal{Q}H_\Omega\mathcal{Q}$ (thick lines) for ${}^2A_1(\mathrm{e}^- + \mathrm{O}_3)$ as functions of α at R=2.6 Bohr.

at different internuclear geometries. Figure 5 shows that the background results depend very weakly on the internuclear distance, in contrast to the eigenvalues of $\mathcal{Q}H_\Omega\mathcal{Q}$.

VII. NON-RESONANT COUPLED SCATTERING CHANNELS

e^-+HF scattering does neither belong to the cases described section IV nor to those described in section V. It is one of the most discussed examples of electron-molecule scattering. The interest is focused on the conspicuous threshold peaks appearing in the vibrational excitation cross sections. These peaks have been observed in experiments by Rohr and Linder in 1976 [3]. The question discussed is to which extent these peaks are caused by ionic bound states, virtual states, resonances, non-adiabatic effects, the strong dipole field of the target or by a combination of some of these possibilities. Figure 6 shows *fixed nuclei* R-matrix poles in ${}^2\Sigma^+$ symmetry as functions of the internuclear distance [4]; r_0 has been set to 10 Bohr. Configuration-interaction (CI) energies of HF^- and energies of the same system obtained within the R-matrix approach, neglecting the electron-molecule interaction outside Ω, are added to the figure. For comparison, the free-particle poles are included. All energies are relative to the ground-state energy of HF. The lowest pole of e^-+HF is clearly below the corresponding free-particle pole indicating large cross sections close to threshold. With increasing internuclear distance this pole becomes stabilized and approaches the ground-state energy of the anion for $\mathrm{R}_{\mathrm{H-F}} > 2.8$ Bohr. However, the most surprising

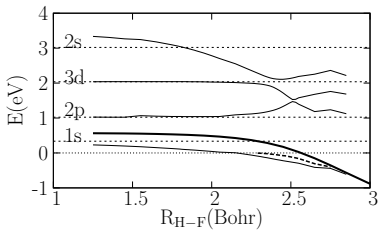

FIG. 6. R-matrix poles of $e^- + HF$ (thin solid line), CI results (thick solid line) and R-matrix results (dashed line) of HF^- (adapted from [4])

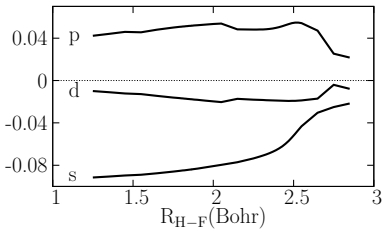

FIG. 7. R-matrix amplitudes corresponding to the lowest pole of $e^- + HF$ as a function of the internuclear distance (adapted from [4])

result of the *fixed-nuclei* R-matrix calculation is the unusual large p contribution in the amplitudes of the lowest pole as can be seen in figure 7. Therefore, the consideration of section IV cannot be applied to this case. Moreover, there is no way to remove the coupling in the channels by separating some resonance from the background as discussed in section V.

The reason for the strong s-p coupling at low collision energy is obviously the polarization of the electronic charge in the HF molecule which is also responsible for the large dipole momentum of the molecule. Our question is how the short-range electron-molecule interaction, reflected in the R-matrix pole and amplitudes affect the asymptotic behavior of the electron, in particular the existence of anionic bound states. Similar to the R matrix which characterizes the regular (n+1)–electron functions in the inner of Ω we will construct a matrix $R^\infty(E)$ which characterizes the scattering functions with respect to their asymptotic behavior. In the present case we will consider eigenfunctions of the Hamiltonian with no electron-molecule interaction, in analogy to section III. Let us consider the functions

$$\Psi^\infty_{\rho lm;E} = \Phi_\rho \times Y_{lm}(\theta,\phi)\frac{1}{r}g_l(E-\epsilon_\rho, r)$$

similar to Eq.1, but with

$$g_l(E,r) = \begin{cases} n_l(kr) & \text{for } E \geq 0, k = \sqrt{2E} \\ b_l(\kappa r) & \text{for } E < 0, \kappa = \sqrt{-2E}, \quad b_l(\kappa r) \to e^{-\kappa r} \text{ for } r \to \infty. \end{cases}$$

Figure 8 shows the logarithmic derivatives (in atomic units) of $g_l(E,r)$, $l = 0 \cdots 4$ at r=10 Bohr. $R^\infty(E)$ is given by the matrix elements

$$R^\infty_{\rho' l' m';\rho lm}(E) = \delta_{\rho'\rho}\,\delta_{l'l}\delta_{m'm} \quad g_l(E-\epsilon_\rho), r)/\left.\frac{dg_l(E-\epsilon_\rho), r)}{dr}\right|_{r_0}.$$

Solving the generalized eigenvalue problem

$$R(E)\,\vec{c}_j(E) = \lambda_j(E)\,R^\infty(E)\,\vec{c}_j(E)$$

one can define the functions

$$p_j(E) = \vec{c}_j^{\,T}(E) R^{\infty}(E) \vec{c}_j(E) \quad \text{and} \quad q_j(E) = \vec{c}_j^{\,T}(E) R(E) \vec{c}_j(E) = \lambda_j(E)\, p_j(E).$$

Of particular interest are energies E_0 with $p_j(E_0) = q_j(E_0)$ for some j, which is equivalent to $\lambda_j(E_0) = 1$. In such cases then we have a bound state of the anion, if $E_0 < \epsilon_\rho$ for all ρ considered, or a pole of the K-matrix otherwise.

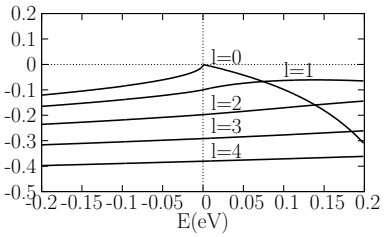

FIG. 8. Logarithmic derivatives of $g_l(E, r)$

For $e^- + HF$ scattering, the quantities $\arctan(p_j(E)^{-1})$ and $\arctan(q_j(E)^{-1})$ at $R_{H-F} = 1.85\,\text{Bohr}$ and $R_{H-F} = 2.35\,\text{Bohr}$ are shown in figures 9 and 10 respectively. The energy is given relative to the target ground state energy. In figure 10 we find a bound state for j=1 with an energy $E_0 \approx -0.02eV$.

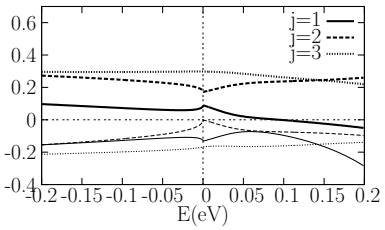

FIG. 9. At $R_{\mathrm{H-F}} = 1.85\,\text{Bohr}$: $\arctan(p_j(E)^{-1})$ (thin lines), $\arctan(q_j(E)^{-1})$ (thick lines)

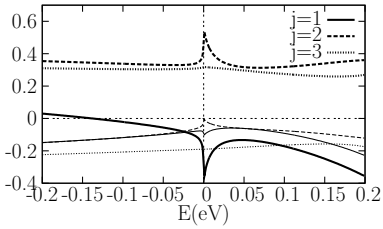

FIG. 10. The same as in figure 9 but at $R_{\mathrm{H-F}} = 2.35\,\text{Bohr}$

Notably conspicuous are the sharp structures of $q_j(E)^{-1}$ for $j = 1$ and $j = 2$ in the neighborhood of $E = 0$. We explain these structures by the s-p coupling observed for the lowest R-matrix pole and the centrifugal forces due to p-wave contribution in the wave function of the scattered electron.

As a next step we want to study the effect of long-range electron-molecule interaction after including it in $R^{\infty}(E)$.

Acknowledgements

We want to thank Vincent Brems and Roland Lindh for their contribution to the implementation of the R-matrix code in the MOLCAS and DIESEL package. The financial support of the Deutsche Forschungsgemeinschaft is gratefully acknowledged.

[1] B. M. Nestmann, K. Pfingst, and S. D. Peyerimhoff. *J. Phys. B: At. Mol. Opt. Phys.*, 27:2297–308, 1994.
[2] B. M. Nestmann. *J. Phys. B: At. Mol. Opt. Phys.*, 31:3929–48, 1998.
[3] K Rohr and F Linder. *J. Phys. B: At. Mol. Opt. Phys.*, 9(14):2521–2537, 1976.
[4] B. M. Nestmann and T. Beyer. *Chem. Phys.* in press, 2007.

M Plummer, J D Gorfinkiel and J Tennyson (eds.)
Mathematical and computational methods in R-matrix theory

Orthogonal and non-orthogonal radial orbital methods in *R*-matrix electron–atom scattering

M Plummer

Computational Science and Engineering Department,
STFC Daresbury Laboratory, Daresbury, Warrington WA4 4AD, UK

I. INTRODUCTION

The aim of this article is to provide a lead-in to understanding the use of orthogonal and non-orthogonal radial orbitals in R-matrix calculations. The talk given at the workshop described work by other speakers and people we were unable to invite for financial reasons as well as relevant work by the author. The article should thus be read as a 'starter' template for further study using the references provided, especially with regard to the work by other people. The implementation of the non-orthogonal orbital method described here uses B-splines to construct the orbitals. We also point the reader to some references to work using B-splines as described in the talk by Dr Hugo van der Hart.

II. BASIC THEORY AND THE ORTHOGONAL ORBITAL *R*-MATRIX METHOD

For illustration we consider non-relativistic electron–atom scattering. In the R-matrix inner region the trial wavefunction is made up of combinations of one-electron spin orbitals:

$$\Psi_k^{LS\pi} = \mathcal{A} \sum_{j=1}^{M_{LS\pi}} \sum_{i=1}^{N_{\rm c}} c_{kji}^{LS\pi}\, \overline{\Phi}_j^{LS\pi}(1,2,..,N,\hat{\boldsymbol{r}}_{N+1},\sigma_{N+1}) r_{N+1}^{-1} u_{il_{(j;[LS\pi])}}(r_{N+1}) + \sum_{q=1}^{Q_{LS\pi}} d_{kq}^{LS\pi}\, \phi_q^{LS\pi}(1,2,..,N+1) \quad . \tag{1}$$

$\overline{\Phi}_j^{LS\pi}(1,2,..,N,\hat{r}_{N+1},\sigma_{N+1})$ is an antisymmetrized combination of the 'scattering' electron spherical harmonic and spin function with the close-coupling

expansion target atom/ion states $\Phi_m^{LS\pi}(1,2,..,N)$ (note that we are not specifically distinguishing here between the scattering wavefunction as used in direct variational calculations and the inner-region-eigenfunction wavefunction as described in the article by P G Burke: however the codes and applications discussed below all use 'inner-region diagonalization' R-matrix theory). The $\Phi_m^{LS\pi}(1,2,..,N)$ are diagonalized approximations to the target states made up of $LS\pi$ 'configuration state functions' (CSFs) built from one-electron components $P_{nl}(r)$ and an associated spherical harmonic and spin function. $P_{nl}(r)$ and $u_{il}(r)$ are radial target orbitals (zero on the boundary $r = a$) and continuum functions (non-zero on the boundary) respectively. The $\phi_q^{LS\pi}(1,2,..,N+1)$ are $(N+1)$-electron CSFs.

The R-matrix calculation is a variational calculation for the scattering phase shifts or eigenphase sums. If all the open-channel target states in the close coupling expansion are exact, then the variational calculation is bounded: we have a minimum principle (Hahn *et al* 1964, Gailitis 1965). This is not the case for many-electron atoms.

In the orthogonal orbital R-matrix methods the $P_{nl}(r)$ and $u_{il}(r)$ are orthogonal to each other for each l: ie we have one large set of radial orbitals from which to build all the N-electron target states. The $P_{nl}(r)$ may be Roothan-Hartree-Fock orbitals for particular target states or other STO-based pseudo-orbitals, either optimized on target state energies or perhaps long-range dipole polarizabilities using (for example) CIV3/CIVPOL (Hibbert 1975, Le Dourneuf 1976), or included as a pseudostate expansion for given l (nb: numerical orbitals etc are also possible).

In RMATRX1 (Berrington, Eissner and Norrington 1995) and 'traditional' RMATRXII (Burke *et al* 1994) and RMATRIX95/PRMAT*(Sunderland *et al* 2002, Burke and Noble 2008), the $u_{il}(r)$ are orthogonal to each other and Lagrange orthogonalized to some of the $P_{nl}(r)$ (equation 2) and subsequently Schmidt orthogonalized to the rest. The logarithmic derivatives of $u_{il}(r)$ are fixed at the boundary and Buttle corrections (Buttle 1967) are needed.

$$(\frac{d^2}{dr^2} - \frac{l(l+1)}{r^2} - 2V(r) + k_{il}^2)u_{il}(r) = \sum_n \lambda_{nl} P_{nl}(r) \qquad (2)$$

The choice between Lagrange and Schmidt orthogonalization is a matter of taste. In this context, the $u_{il}(r)$ are meant to be realistic lower-level members of an expansion of the one-electron continuum states: the higher level component is represented by the Buttle correction. Therefore Lagrange-orthogonalization

*RMATRIX95/PRMAT is a package containing modernized, modular, up-to-date and parallelized versions of RMATRXII and FARM (Burke and Noble 1995).

is often restricted to 'physical' (HF) orbitals as the Lagrange-orthogonalization process can lead to mimicking of an exchange interaction with the orthogonalized orbitals (Gorczyca and Badnell 1997). If many pseudo-orbitals are included, we may have linear dependence between the pseudo-orbitals and the $u_{il}(r)$: the $u_{il}(r)$ can be Schmidt-orthogonalized to 'zero', leading to 'infinite' normalization coefficients. Also, the Buttle correction, which is normally only needed for diagonal elements of the R-matrix, becomes more complex with off-diagonal elements required. Gorczyca and Badnell (1997) developed techniques for dealing with this problem.

An alternative method (Plummer and Noble 1999, following Tennyson *et al* 1987), utilized in RMATRXII and RMATRIX95, expands the $u_{il}(r)$ in a basis of functions with arbitrary boundary conditions on the R-matrix sphere. The proto-$u_{il}(r)$ are prediagonalized, then Lagrange-orthogonalized to the $P_{nl}(r)$ (equation 3). The $u_{il}(r)$ and $P_{nl}(r)$ together then ideally represent a 'complete' basis: Buttle corrections are not needed.

$$(\frac{d^2}{dr^2} - \delta(r-a)\frac{d}{dr} - \frac{l(l+1)}{r^2} - 2V(r) + k_{il}^2)u_{il}(r) = \sum_n \lambda_{nl} P_{nl}(r) \qquad (3)$$

A third alternative is to use a B-spline basis. We refer the reader to van der Hart (1997), Zatsarinny and Froese Fischer (2000), Bachau *et al* (2001), Zatsarinny (2006) and references: B-spline basis sets are sets of piecewise polynomials, defined using a set of knot points. At the knot points, B-splines satisfy user-defined smoothness criteria. The choice of knot points can be adapted to the type of problem under investigation, and therefore B-spline basis sets are flexible: they can describe short-range, long-range and highly oscillatory orbitals. B–spline bases do not have fixed logarithmic boundary conditions at $r = a$ and Buttle corrections are not needed. B-spline bases are used in the non-orthogonal method of the next section and have been adapted to be consistent with the orthogonal methods of this section (van der Hart *et al* 2007). van der Hart and co-workers have used B-splines for studies of helium two-photon double-ionization (Feng and van der Hart 2003) and of multiphoton ionization of atoms in laser fields using both quasi-time-independent (Floquet) and time-dependent methods (for example, van der Hart *et al* 2005, 2007).

The second expansion in equation 1 contains $(N + 1)$-electron CSFs built up from the $P_{nl}(r)$. These functions can fulfill various purposes in RMATRX1 and have a more restricted purpose in RMATRXII. The main purpose of the second expansion is to 'fill in the gaps' in the first expansion caused by the orthogonalization process (for example, by replacing $u_{il}(r)$ by each $P_{nl}(r)$ in turn in the first expansion). Historically, it has also been used to include additional square-integrable correlation functions built from the set of $P_{inl}(r)$ (and possibly other orthogonal orbitals). This approach has worked well for e^-–H scattering (Burke and Taylor 1966) at energies for which all open target states are included explicitly, but at higher energies in e^-–H scattering and for many-electron

calculations with approximate target states generally there are dangers. The purpose of additional short-range correlation functions is to account for closed channels not included in the first expansion (an effective optical potential). With approximate target states there is no minimum principle associated with the variational calculation and thus no guarantee that pseudoresonances associated with additional functions in the second expansion will not appear in the open-channel energy range of interest.

Pseudoresonances are a 'necessary evil' associated with incomplete L^2 representation of continuum functions[†]. As long as this representation is restricted to the construction of pseudo-target states then pseudoresonant behaviour is broadly understood and occurs around the threshold for pseudostate excitation (compare, for example, Burke *et al* 1969 with Burke and Taylor 1966). Broadly speaking, we suggest modern opinion is that attempts to represent the real wavefunction and atomic behaviour should be included in the first expansion, with the second expansion 'completing' the approximate wavefunction.

RMATRX1 allows the user to pick configurations and orbitals for each expansion separately. It also allows the user to pick and choose target CSFs in the first expansion, eliminating those with expansion coefficients below a certain magnitude, to maintain a manageable calculation. This is fine in expert hands but can lead to undercompletion, overcompletion and general mismatching between the two expansions. For example, we refer to Berrington *et al* (1988, Fig. 1), an Fe^+ calculation in which an unbalanced 4p orbital in the second expansion causes a giant resonance to appear: balancing the two expansions removes the pseudoresonant behaviour.

The method of Gorczyca *et al* (1995) copes with these problems with linear transformations of the second sum so that it corresponds exactly to replacing $u_{il}(r)$ by each $P_{nl}(r)$ in turn in the chosen first expansion, thus making the calculation a particular 'close-coupling' calculation. RMATRXII produces the second expansion automatically from the target expansion, allowing $(N+1)$-electron configurations in which the target configurations are augmented by one electron in each of the $P_{nl}(r)$. Thus the second expansion 'completes' the first and also models closed-channel behaviour of higher-energy target states of the same symmetry and CSF composition as those included in the first expansion. All necessary CSFs for a particular calculation are included: RMATRXII and RMATRIX95/PRMAT rely on efficient computation and memory distribution to make calculations feasible (plus very fast angular integral calculation: Burke *et al* 1994, Burke 1998).

[†]There is an extensive body of work on pseudostate expansions in electron scattering which we cannot hope to reference adequately here. We suggest the recent review by Stelbovics *et al* (2004, see also Bartlett 2006) as a useful starting point for references.

This leads to a major problems with the orthogonal orbital method: is it possible to choose one manageable set of orbitals to represent accurately all the different target states, even with CI? The balance between the two expansions in equation 1 must be maintained. For systems with target states that are noticeably 'term-dependent', the second expansion can become very large for certain L-values, as can the first expansion for all L in ambitious calculations such as open d-shell systems. Nevertheless, RMATRIX95 (for example) has 'risen to the challenge': calculations of ions of iron peak elements Fe and Ni (also Sn) are ongoing, with 100s/1000s of channels and certain relativistic effects now included (for example, Scott *et al* 2006, Ramsbottom *et al* 2005, Lysaght 2006)

III. THE NON-ORTHOGONAL ORBITAL METHOD

A convenient summary (and program description) of the non-orthogonal orbital method and code BSR may be found in Zatsarinny (2006) and references. This method was developed by Zatsarinny (1996) and Zatsarinny and Froese Fischer (2000) and has a simple basic concept. The target orbitals and continuum orbitals do not have to be orthogonal. Each target state can be constructed from customized, term-dependent orbitals. Highly accurate target states/energies allow detailed study of, for example, particular resonances. The second expansion is not needed. In principle we have the possibility of a minimum basis for each target state and scattering symmetry without compromising on accuracy.

Possible problems with the method include: very complicated integrals (solved by Zatsarinny and Froese Fischer 2000), possible linear dependance between different orbitals and any associated B-spline problems. In particular, the 'variational principle but not minimum principle' problem of balance and possible unphysical behaviour is still present, but 'hidden'.

The method has been applied variously (see Zatsarinny 2006 for explicit references) over a wide range of energies to scattering and photodetachment involving sulphur, oxygen, carbon, boron, inert gases and recently (Zatsarinny and Bartschat 2005) Fe^+ (cf Ramsbottom *et al* 2005 using RMATRIX95: there is generally good agreement between the two methods).

IV. COMPARISON: TWO EXAMPLES

We consider two particular examples (these are not exhaustive). As a first example, consider Gibson *et al* (2003): K-shell photodetachment from C^-, both experiment and theory (non-orthogonal, RMATRX1 incorporating the method of Gorcyzca *et al* 1995). Fig. 2. of Gibson *et al* (2003) shows perfect agreement between experiment and the two theoretical methods over a resonant peak in the

cross section (the theoretical curves continue to overlap on either side, within the noise-envelope of the experimental results).

For our second example we consider electron-oxygen scattering at low energies. 'Detective' work on the elastic cross section has been performed by, among others: Le Dourneuf et al (1976, 1977 and references), Zatsarinny and Tayal (2001, see also Wu and Yan 2003), Plummer *et al* (2004) and Zatsarinny *et al* (2006). There is a contrast between very low-energy behaviour of the elastic scattering cross section as found by Le Dourneuf *et al* and as calculated by Zatsarinny and Tayal, who reported a near-threshold resonance which was not found in the earlier calculations.

Plummer *et al* (2004) were able to vary RMATRIX95 calculations to switch on and off the resonance (the experimental values of Williams and Allen (1989) are not dense enough to distinguish between the calculated results). Zatsarinny and Tayal used a very sophisticated scattering wavefunction with 26 target states, each independently derived with accurate energies, plus augmentation by additional pseudostates. This lead to a large value of the R-matrix sphere radius. Their ground state included spd orbitals. Plummer *et al* reproduced the threshold resonance by deliberately including excited state orbitals which give rise to a large radius, but were able to remove it by increasing the complexity of the ground state, or by using 'ground-state-friendly' orbital bases that did not extend so far.

The resonance arises mainly from s-wave scattering symmetries. There are no known O^- bound states in these symmetries and R-matrix poles become closer and closer to zero as scattering correlation is increased: phase shifts and eigenphase sums pass from negative to positive with no 'minimum-principle limit' on the final value. The resonance is an indication of over-correlation, or an incomplete representation of the ground state. This can be quite subtle, as the Zatsarinny and Tayal (2001) ground state is elaborate.

Plummer *et al* (2004) also showed in a model calculation, with target state CI restricted to single excitations from basic configurations, that the resonance occurs if an spd orbital basis is used, but disappears if an spdf orbital basis is used, ie if the basis is closer to a 'complete' expansion. The inclusion of f orbitals had a very small effect on the target state energies, dipole polarizability and the scattering cross section above the threshold region. Zatsarinny *et al* (2006) revisited elastic oxygen scattering with even more sophisticated term-dependent target states: the range of the calculations here neatly demonstrates the strengths of the non-orthogonal orbital method. They also found that they could make the resonance appear and disappear with 'incomplete' ground states. With their most elegant ground states the resonance disappeared. We note that a recent experimental determination of the electron affinity of the known bound state $^2P^o$ O^- (Blondel *et al* 2001) reported a very low e^-–O scattering cross

section in the zero-energy limit[‡].

Otherwise, the Plummer *et al* and Zatsarinny *et al* elastic cross sections are similar. At higher low-energies both calculations are somewhat over correlated as may be seen by comparing differential cross sections with experiment (Williams and Allen 1989): whereas total cross sections agree apparently well, calculated differential cross sections show marked depression of forward scattering compared to experiment above the lowest energies. The non-orthogonal calculations can represent resonances in the cross section which the orthogonal calculations cannot (yet) without more elaborate orbital bases. Happily, calculated excitation cross sections to the lowest spin-forbidden 'same-configuration' states are in excellent agreement with each other, better than current experiment: see Johnson *et al* (2005) for a recent comprehensive review (some earlier theoretical results for these cross sections have unphysical pseudoresonant behaviour due to mismatching of the first and second expansions in 1). The Johnson *et al* (2005) review also contains summaries and references for e^-–O excitation to higher excited states by Tayal and co-workers using the non-orthogonal orbital method.

V. CONCLUSIONS

The non-orthogonal and orthogonal methods can both give excellent results and can both give wrong results. Agreement between the two sets of calculations is welcome, particularly in cases (such as open d-shell atoms) where very little experimental data is available. Both methods are currently being adapted to include relativistic effects.

As calculations become larger, we suggest that RMATRX1 users who 'pick and choose' CSF components of target states should make use of the Gorczyca *et al* (1995) modification to make sure they do not introduce pseudoresonances. Aside from scientific/functional developments, the emphasis of the Daresbury/Queen's-Belfast group developing RMATRIX95/PRMAT

[‡]It could be argued that the appearing and disappearing threshold resonance is an indication of hitherto-undiscovered O^- bound states, rather than pseudoresonant behaviour. In the case of e^-–N scattering a very narrow above-threshold resonance occurs, which was also interpreted as a bound state (see, for example, Le Dourneuf 1976, 1977). However, the nitrogen threshold resonance has been observed experimentally (Cowan *et al* 1997, Wijesundera and Parpia 1998 and references). Further investigation of the threshold behaviour of S-matrix poles in the Plummer *et al* model is underway to finish this particular investigation and will be reported in the near future.

must be efficient parallelization and memory distribution, to cope with the very large orbital bases needed for sophisticated calculations.

Bachau H, Cormier E, Declava P, Hansen J E and Martín F 2001 *Rep. Prog. Phys.* **64** 1815

Bartlett P L 2006 *J. Phys. B: At. Mol. Opt. Phys.* **39** R379

Berrington K A, Burke P G, Hibbert A, Mohan M and Baluja K L 1988 *J. Phys. B: At. Mol. Opt. Phys.* **21** 339

Berrington K A, Eissner W B and Norrington P H 1995 *Comput. Phys. Commun.* **92** 290

Blondel C, Delsart C, Valli C, Yiou S, Godefroid M R and Van Eck S 2001 *Phys. Rev. A* **64** 052504

Burke P G, Burke V M and Dunseath K M 1994 *J. Phys. B: At. Mol. Opt. Phys.* **27** 5341

Burke P G, Gallagher D F and Geltman S 1969 *J. Phys. B: At. Mol. Phys.* **2** 1142

Burke P G and Mitchell J F B 1974 *J. Phys. B At. Mol. Phys.* **7** 665

Burke P G and Taylor A J 1966 *Proc. Phys. Soc.* **88** 549

Burke V M 1998 *Comput. Phys. Commun.* **114** 210

Burke V M and Noble C J 1995 *Comput. Phys. Commun.* **85** 471

Burke V M and Noble C J 2008 *Comput. Phys. Commun.* to be submitted

Buttle P J A 1967 *Phys. Rev.* **160** 719

Cowan R D, Froese Fischer C, Hansen J E and Kempter V 1997 *J. Phys. B: At. Mol. Opt. Phys.* **30** 1457

Feng L and van der Hart H W 2003 *J. Phys. B: At. Mol. Opt. Phys.* **36** L1

Gailitis M 1965 *Sov. Phys. JETP* **20** 107

Gibson N D, Walter C W, Zatsarinny O, Gorczyca T W, Ackerman G D, Bozek J D, Martins M, McClaughlin B M and Berrah M 2003 *Phys. Rev. A* **67** 030703(R)

Gorczyca T W and Badnell N R 1997 *J. Phys. B: At. Mol. Opt. Phys.* **30** 3897

Gorczyca T W, Robicheaux F, Pindzola M S, Griffin D C and Badnell N R 1995 *Phys Rev A* **52** 3877

Hahn Y, O'Malley T F and Spruch L 1964 *Phys. Rev.* **134** B397, B911

Hibbert A 1975 *Comput. Phys. Commun.* **9** 141

Johnson P V, McConkey J W, Tayal S S and Kanik I 2005 *Can. J. Phys.* **83** 589; corrigendum **83** 1071

Le Dourneuf M 1976 *Doctorat d'Etat* (University of Paris VI, available from CNRS under registration AO12658). The CIVPOL code, upgraded in 1992 by Plummer M and Le Dourneuf M to allow combinations of eigenstates and pseudostates of the same symmetry and in 2004 by Plummer M to calculate polarizabitilities from combinations of (pseudo-)eigenstates as well as from long-range polarization pseudostates, is not published.

Le Dourneuf M, Vo Ky Lan and Burke P G 1977 *Comm. At. Mol. Phys.* **7** 1
Lysaght M A 2006 *PhD Thesis*, University College Dublin, Ireland
Plummer M and Noble C J 1999 *J. Phys. B: At. Mol. Opt. Phys.* **32** L345
Plummer M, Noble C J and Le Dourneuf M 2004 *J. Phys. B: At. Mol. Opt. Phys.* **37** 2979
Ramsbottom C A, Noble C J, Burke V M, Scott M P, Kisielius R and Burke P G 2005 *J. Phys. B: At. Mol. Opt. Phys.* **38** 2899
Scott M P, Ramsbottom C A, Noble C J, Burke V M and Burke P G 2006 *J. Phys. B: At. Mol. Opt. Phys.* **39** 387
Stelbovics A T, Bartlett P L, Bray I and Kadyrov A S 2004 *Physica Scripta* **T110** 247
Sunderland A G, Noble C J, Burke V M and Burke P G 2002 *Comput. Phys. Commun.* **145** 311
Tennyson J, Burke P G and Berrington K 1987 *Comp. Phys. Commun.* **47** 207
van der Hart H W 1997 *J. Phys. B: At. Mol. Opt. Phys.* **30** 453
van der Hart H W, Doherty B J S, Parker J S and Taylor K T 2005 *J. Phys. B: At. Mol. Opt. Phys.* **38** L207
van der Hart H W, Lysaght M A and Burke P G 2007 *Phys. Rev. A* **76** 043405
Wijesundera W P and Parpia F A 1998 *Phys. Rev. A* **57** 3462
Williams J F and Allen L J 1989 *J. Phys. B: At. Mol. Opt. Phys.* **22** 3529
Wu J-H and Yuan J-M 2003 *Chin. Phys.* **12** 1391
Zatsarinny O 1996 *Comput. Phys. Commun.* **98** (1996) 235
Zatsarinny O 2006 *Comput. Phys. Commun.* **174** (2006) 273
Zatsarinny O and Froese Fischer C 2000 *Comput. Phys. Commun.* **124** 247; *J. Phys. B: At. Mol. Opt. Phys.* **33** 313
Zatsarinny O and Bartschat K 2005 *Phys. Rev. A* **72** 020702(R)
Zatsarinny O, Bartschat K and Tayal S S 2006 *J. Phys. B: At. Mol. Opt. Phys.* **39** 1237
Zatsarinny O and Tayal S S 2001 *J. Phys. B: At. Mol. Opt. Phys.* **34** 1299

M Plummer, J D Gorfinkiel and J Tennyson (eds.)
Mathematical and computational methods in R-matrix theory

2DRMP: fast computation of the Slater integrals

N S Scott[1], M P Scott[2], L Gr Ixaru[3] and C Denis[4]

[1] School of Electronics, Electrical Engineering and Computer Science,
The Queen's University of Belfast, Belfast BT7 1NN, U.K.
(ns.scott@qub.ac.uk)
[2] School of Mathematics and Physics,
The Queen's University of Belfast, Belfast BT7 1NN, U.K.
(m.p.scott@qub.ac.uk)
[3] Institute of Physics and Nuclear Engineering,
Magurele, Bucharest, R-76900 Romania
(ixaru@theory.nipne.ro)
[4] Laboratoire d'Informatique de Paris 6,
Université Pierre et Marie Curie - Paris 6,
4 place Jussieu, 75252 Paris Cedex 05, France
(Christophe.Denis@lip6.fr)

Slater integrals are two dimensional radial integrals whose integrand is constructed from normalized eigenfunctions of the Schrödinger equation. These integrals occur in many atomic structure and scattering computations. However, in 2-dimensional R-matrix propagation they represent a significant computational bottleneck. The problem involves two steps: numerical solution of the Schrödinger equation followed by computation of the Slater integrals. By exploiting the oscillatory nature of solutions of the Schrödinger equation we have devised a two stage computational strategy where the second stage is influenced and informed by the first. In particular, we have developed extended frequency dependent quadrature rules (EFDQR) that both improves the accuracy of the integrals and results in a performance gain of over two orders of magnitude.

I. INTRODUCTION

Based on the work of Burke, Noble and Scott [1] and Le Dourneuf, Launay and Burke [3] we have developed 2DRMP, a suite of two-dimensional R-matrix propagation programs aimed at creating virtual experiments on HPC and Grid architectures to study electron scattering from H-like atoms and ions at

intermediate energies [2,5,9–11]. This code is complementary to one developed by Dunseath et al [4]. The essence of this technique is as follows. The two-electron configuration space (x_1, x_2) is divided into square sectors as illustrated in Fig.1 (adapted from [8], Fig. 1).

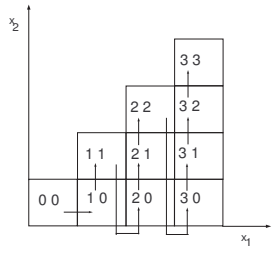

FIG. 1. Subdivision of the configuration space (x_1, x_2) into a set of connected sectors.

The two-electron wavefunction describing the motion of the target electron and the colliding electron is expanded within each sector in terms of one-electron basis functions, $\{y_{nl}\}$, that are eigenfunctions of the Schrödinger equation, solved subject to certain fixed boundary conditions. The expansion coefficients are determined by diagonalizing the corresponding Hamiltonian matrix. The R-matrix may then be propagated across the sectors at each scattering energy and the scattering properties of interest determined.

II. THE PROBLEM

An advantage of the technique is that the construction of the sector Hamiltonian matrices can be computed in parallel, with one sector per processor. However, in large scale virtual experiments, involving around 210 sectors, efficient exploitation is severely impeded by a significant load imbalance between the construction of the Hamiltonian matrix on diagonal and off-diagonal sectors. The root of the bottleneck is the millions of two dimensional radial integrals, the so called Slater integrals, that are required on each diagonal sector. On a diagonal sector, $I_j = (X_j,\ X_{j+1})$ these integrals are of the form,

$$R = \int_{X_j}^{X_{j+1}} dz\, y_{n_3 l_3}(z) y_{n_4 l_4}(z) I(z, \lambda, \phi), \tag{1}$$

where

$$I(z,\lambda,\phi) = [\frac{1}{z^{\lambda+1}} J_1(X_j,\, z,\, \lambda,\phi) + z^{\lambda} J_2(z,\, X_{j+1},\, \lambda,\phi)], \tag{2}$$

$$J_1(a,\, z,\, \lambda,\phi) := \int_a^z dx\, x^{\lambda}\phi(x), \quad J_2(z,\, b,\, \lambda,\phi) := \int_z^b dx\, \frac{1}{x^{\lambda+1}}\phi(x), \tag{3}$$

and

$$\phi(x) = y_{n_1 l_1}(x) y_{n_2 l_2}(x).$$

The functions, y_{nl}, are solutions of the Schrödinger equation,

$$y''_{nl} = (V(x) - E_{nl}) y_{nl}(x), \quad x \in I_j, \tag{4}$$

in the Coulomb field,

$$V(x) = \frac{l(l+1)}{x^2} - \frac{2Z}{x}. \tag{5}$$

Using standard "off the shelf" Newton-Cotes quadrature formula, Hamiltonian matrix construction on each diagonal sector, to approximately 7 figures of accuracy, can take **of the order of hours** while each off-diagonal sector takes only tens of seconds. This is illustrated in table I.

III. THE SOLUTION

We attacked this problem by designing numerical methods which advantageously exploited as many characteristic features of the problem as possible. In particular, we constructed hand crafted quadrature formula that would both improve the accuracy and significantly reduce the computation time of the Slater integrals.

Our analysis resulted in the development of a two stage computational strategy. In the first stage we used the method CMP{10,12} [7]. A key feature of the method is that the eigenfunctions, first derivative of the eigenfunctions and the normalization admit analytic solutions. Accordingly, CMP{10,12} allows us to produce, to an accuracy of about 12 figures, eigenvalues, frequencies, normalized eigenfunctions and the first derivative of the eigenfunctions in a few tens of steps using a fixed step size which is independent of n.

In the second stage, by using information from stage 1 and by exploiting the independence of the frequencies of eq. (4) on l, we were able to construct extended frequency dependent quadrature rules (EFDQR) for the

Slater integrals *using the same mesh.* These N-point extended frequency dependent rules are of the form,

$$\int_{x_1}^{x_N} dx\, y(x) \approx h \sum_{n=1}^{N} [a_n^{(0)} y(x_n) + h a_n^{(1)} y'(x_n)]. \tag{6}$$

A $N = 14$-point frequency-dependent rule this type is used to compute the outer integral, R, defined earlier in eq. (1). The x dependence of function $I(x, \lambda, \phi)$ on $x \in [X_j, X_{j+1}]$ is of the form,

$$y(x) = f_1^1(x)\sin(\omega_1 x) + f_2^1(x)\cos(\omega_1 x) + f_1^2(x)\sin(\omega_2 x) + f_2^2(x)\cos(\omega_2 x), \tag{7}$$

with $\omega_1 = f_{n_1} + f_{n_2}$ and $\omega_2 = |f_{n_1} - f_{n_2}|$. The other factor in the integrand, $y_{n_3 l_3}(x) y_{n_4 l_4}(x)$, is of the same form but with the frequencies $\omega_3 = f_{n_3} + f_{n_4}$ and $\omega_4 = |f_{n_3} - f_{n_4}|$. It follows that their product will be a function that is well described by a sum of eight functions of form,

$$y(x) = f_1(x)\sin(\omega x) + f_2(x)\cos(\omega x), \tag{8}$$

with the following eight possible frequencies: $|\omega_1 \pm \omega_3|$, $|\omega_1 \pm \omega_4|$, $|\omega_2 \pm \omega_3|$, and $|\omega_2 \pm \omega_4|$. Let these be Ω_k, $k = 1, \ldots, 8$ in descending order. The 14 coefficients are then constructed on the condition that the rule is exact for the set

$$\exp[\pm\Omega_k x]\,,\ x\exp[\pm\Omega_k x] \text{ (for } k = 1, \ldots, 6), \exp[\pm\Omega_7 x] \text{ and } \exp[\pm\Omega_8 x]. \tag{9}$$

This work is fully described in [8].

IV. THE RESULTS

The new algorithm was incorporated into the construction of the diagonal sector Hamiltonian matrices where the time taken for the construction is dominated by the computation of the Slater integrals. In table I we present three typical cases and compare the new EFDQR strategy against the Simpson's Rule (SR) approach implemented in the original 2DRMP code. Sector (0,0) takes longer because of the special treatment required at the origin.

Overall, we have found that the new computational strategy is more accurate, giving an accuracy of 10 rather than 7 figures, and is between one and two orders of magnitude faster than the original implementation.

TABLE I.

Timings computed on HPCx [11] for three typical cases. Case 1. $L = 0$, $S = 0$, $\Pi = even$, $n_{max} = 20$, $l_{max} = 7$. Case 2. $L = 2$, $S = 0$, $\Pi = even$, $n_{max} = 20$, $l_{max} = 9$. Case 3. $L = 4$, $S = 0$, $\Pi = even$, $n_{max} = 20$, $l_{max} = 11$.

Case	Sector where $i > 0$	No. of Slater integrals	Matrix size	HPCx(secs) SR	HPCx(secs) EFDQR	Speedup
1	$0, 0$	8187600	1680	943	38	25
	i, i	8187600	1680	943	30	31
2	$0, 0$	85741800	5090	9880	163	61
	i, i	85741800	5090	9880	128	77
3	$0, 0$	302869500	8900	34899	472	74
	i, i	302869500	8900	34899	373	94

The original 2DRMP code stored the diagonal sector matrices on disk after construction. In a subsequent job using one LPAR per sector, all diagonal sector matrices were read from disk, block cyclically distributed across their respective LPARs and diagonalized using ScaLAPACK. The EFDQR construction method was extended to use one LPAR per sector. Each diagonal sector matrix is built directly in its required block cyclic distribution, thereby allowing diagonalization to follow within the same job and avoiding disk IO and storage. Results for cases 1 and 2, as defined in table I, are now presented in table II. *This represents a real and very significant reduction in total cpu cycles particularly for larger cases.* For example in case 2, the number of processors is increased by a factor of 16 but the wall clock time is reduced by a factor of 350 and the total processor time, and therefore cost, by a factor of 25.

In summary, we have improved accuracy and transformed matrix construction from a long *capacity* job into a short *capability* job thereby increasing machine utilization, improving turnround and decreasing cost.

Acknowledgements

The authors are grateful to the UK EPSRC for their support through the grants GR/M01784/01 and GR/R89073/01. LGrI is indebted to the UK EPSRC for a Visiting Fellowship to Queen's University Belfast.

TABLE II.

Parallel EDFQR compared to SR. Speedup is given in the square brackets. Timings were computed on HPCx [11].

Case	Code	No. of diagonal sectors	processors per sector	total number of processors	wall clock time (secs)	total processor time (secs)
1	SR	20	1	20	943	18860
	$EFDQR$	20	16	320	4 [235]	1043 [18]
2	SR	20	1	20	9880	197600
	$EFDQR$	20	16	320	28 [350]	7610 [25]

[1] P. G. Burke, C. J. Noble and M. P. Scott, *Proc. Roy. Soc. A.* **410** (1987), 289–310.

[2] A. Carson, T. H. Harmer, N. S. Scott, V. Faro-Mazo, M. P. Scott and P. G. Burke, *2DRMP-G: Migrating a large-scale numerical mathematical application to a grid environment*, Lecture Notes in Computer Science, M. Daydé *et al* (Eds), **3402** (2005), pp. 233-246.

[3] M. Le Dourneuf, J. M. Launay and P. G. Burke, *J. Phys. B:At. Mol. Phys.* **23** (1990) L559–L564.

[4] K. M. Dunseath, M. Le Dourneuf, M. Terao-Dunseath, and J. M. Launay, *Phys. Rev. A.* **54** (1996), 561–572.

[5] J. W. Heggarty, P. G. Burke, M. P. Scott and N. S. Scott, *Comput. Phys. Commun.* **114** (1998) 195–209.

[6] HPCx, UK National Supercomputing Centre - http://www.hpcx.ac.uk/ .

[7] L. Gr. Ixaru, H. De Meyer, G. Vanden Berghe, *Journal Comp. and Appl. Math.* **88** (1998), 289–314.

[8] L. Gr. Ixaru, N. S. Scott and M. P. Scott, *SIAM J. Sci. Comput.* **28** (2006), 1252–1274.

[9] B.R. Odgers, $e^- + H$ *scattering at Intermediate Energies*, PhD Thesis, Queen's Univeristy of Belfast, (1995).

[10] N.S. Scott, L.Gr. Ixaru, C. Denis, F. Jézéquel, J.-M. Chesneaux and M.P. Scott, *High performance computation and numerical validation of e-collision software*, Lecture Series on Computer and Computational Sciences, "Trends and Perspectives in Modern Computational Science, Invited lectures," G. Maroulis and T. Simos (Eds), vol. 6, (2006) pp. 561–570

[11] T. Stitt, N.S. Scott, M.P. Scott and P.G. Burke, *2-D R-matrix propagation: a large scale electron scattering simulation dominated by the multiplication of dynamically changing matrices.*, Lecture Notes in Computer Science, J.M.L.M. Palma *et al* (Eds), **2565** (2003), pp. 354-367

M Plummer, J D Gorfinkiel and J Tennyson (eds.)
Mathematical and computational methods in R-matrix theory

Parallel diagonalization performance for R-matrix calculations

A G Sunderland

Computational Science and Engineering Department,
STFC Daresbury Laboratory, Daresbury, Warrington WA4 4AD, UK

I. INTRODUCTION

Efficient parallel diagonalization performance is essential for codes undertaking R-matrix calculations. Computations often involve matrices of dimension of tens or even hundreds of thousands that need to be solved quickly with manageable memory requirements on the latest large-scale high-performance computing platforms.

This presentation analyses the performance of parallel eigensolver library routines across a range of problem sizes and architectures. New developments of particular note include a ScaLAPACK implementation of the Multiple Relatively Robust Representations (MRRR) algorithm and the next generation series of high end parallel computers such as the Cray XT series and IBM's BlueGene. The results presented are based upon Hamiltonian matrices generated during external region calculations using the PRMAT code [1].

II. PARALLEL DIAGONALIZATION METHODS

A. The Symmetric Eigenvalue Problem

The standard eigenvalue problem is described as

$$A\boldsymbol{x} = \lambda\boldsymbol{x} \tag{1}$$

where A is a matrix and λ is the eigenvalue corresponding to eigenvector $\boldsymbol{x}$. For symmetric matrices this equation can be rearranged to give the equation describing the diagonalization of matrix A:

$$A = Q\Lambda Q^T \tag{2}$$

where the columns of the matrix Q are represented by the orthogonal eigenvectors of A and the diagonal matrix Λ represents the associated eigenvalues.

B. Underlying equations for matrix diagonalizations in PRMAT

The PRMAT code is based on the Baluja-Burke-Morgan [2] approach for solving the non-relativistic Schrödinger equation describing the scattering of an electron by an N-electron atom or ion:

$$H_{N+1}\Psi = E\Psi \tag{3}$$

where E is the total energy in atomic units and H_{N+1} is the $(N+1)$-electron Hamiltonian matrix.

In this approach the representative of the Greens function $(H + L - EI)^{-1}$ are diagonalized within a basis. The symmetric matrix $(H + L - EI)$ is reduced to diagonal form by the orthogonal transformation:

$$X^T(H + L - E)X = (E_k - E) \tag{4}$$

where the columns of the orthogonal matrix X^T represent the eigenvectors and E_k the eigenvalues of $(H + L)$.

C. Symmetric Eigensolver Methods

The solution to the real or hermitian dense symmetric eigensolver problem usually takes place via three main steps

1. Reduction of the matrix to tri-diagonal form, typically using the Householder Reduction.
2. Solution of the real symmetric tri-diagonal eigenproblem via one of the following methods:
   - Bisection for the eigenvalues and inverse iteration for the eigenvectors [3], [4],
   - QR algorithm [5],

- Divide & Conquer method (D&C) [6],
- Multiple Relatively Robust Representations (MRRR algorithm) [7],

3. Back transformation to find the eigenvectors for the full problem from the eigenvectors of the tridiagonal problem.

D. Eigensolver Parallel Library Routines

Several eigensolver routines for solving standard and generalized dense symmetric or dense Hermitian problems are available in the current release of ScaLAPACK [8]. These include:

- *PDSYEV* based on the QR Method
- *PDSYEVX* based on Bisection and Inverse Iteration
- *PDSYEVD* based on the Divide and Conquer method
- Also tested here is a new routine *PDSYEVR* [9] based on the MRRR algorithm. At the time of this analysis this routine is undergoing testing and development by the ScaLAPACK developers.

PDSYEV and *PDSYEVD* only calculate *all* the eigenpairs of a matrix. However *PDSYEVX* and the new *PDSYEVR* have the functionality to calculate subsets of eigenpairs specified by the user. All the eigensolvers listed require $O(n^3)$ operations to complete with associated memory overheads of $O(n^2)$. The potential advantages of the MRRR algorithm are both that theoretically only $O(kn)$ operations are required, where k is the number of desired eigenpairs, and the additional memory requirements are a relatively lowly $O(n)$. For reasons of conciseness only results obtained the latest parallel solvers *PDSYEVD* and *PDSYEVR* are reported in this paper. For a comparison of a fuller range of eigensolvers, readers are recommended to consult the HPCx Technical Report HPCxTR0608 [10].

III. TESTING ENVIRONMENT

A. Test Matrices

The matrices analysed here are derived from external sector Hamiltonian Ni^{3+} and Fe^{+} scattering calculations using the PRMAT code. They are all real symmetric matrices with dimensions ranging from 5280 to 20064. The eigenvalue distribution is fairly well-spaced with comparatively few degeneracies.

Due to somewhat limited access at the time of writing, for the cross-platform comparisons, matrices obtained from the package [16] have been used. CRYSTAL performs ab initio calculations of the ground state energy, electronic wave function and properties of periodic systems. The eigenvalue distribution of these real symmetric matrices is typically much more clustered than those obtained from the PRMAT code.

B. Test Platforms

The majority of the parallel timings presented are from runs undertaken on the current National Supercomputing facility HPCx [11] at STFC [12] comprising of 160 IBM p5-575 nodes, totalling 2536 processors. Figures also show timing comparisons of runs taken on HPCx with runs undertaken on other contemporary HPC platforms: an IBM Blue Gene/L machine [13], also sited at STFC and a Cray XT3 machine sited at the Swiss Supercomputing Centre CSCS [14].

IV. RESULTS

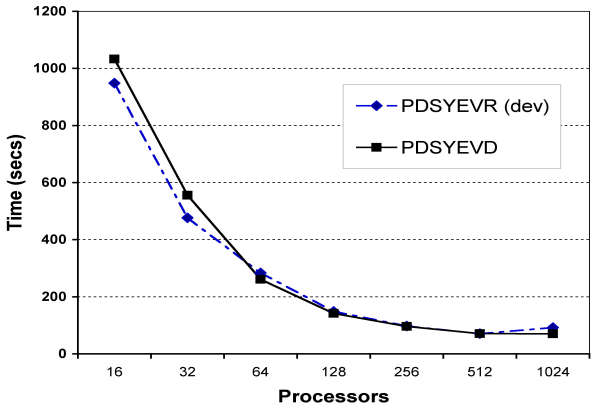

FIG. 1. Parallel Timings for PDSYEVD and PDSYEVR for Hamiltonian matrix, n=20064.

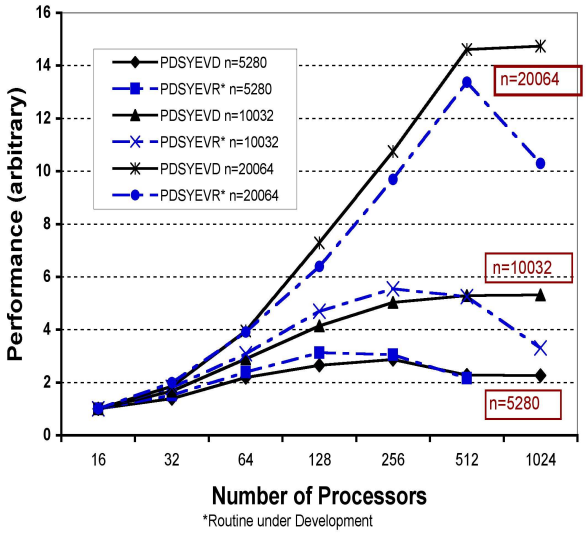

FIG. 2. Relative Scaling of PDSYEVD and PDSYEVR for a range of Hamiltonian matrix sizes.

Figures 1 and 2 show the scaling of performance for the diagonalization routines PDSYEVR and PDSYEVD for a range of problem sizes on HPCx.

Figure 2 shows how parallel scaling improves as the matrix size increases. The parallel performance of PDSYEVR is very close to that of PDSYEVD for all the problem sizes, though the performance on the highest processor count can degrade, possibly due to slightly uneven distributions of the eigenvalue representation tree amongst processors [15].

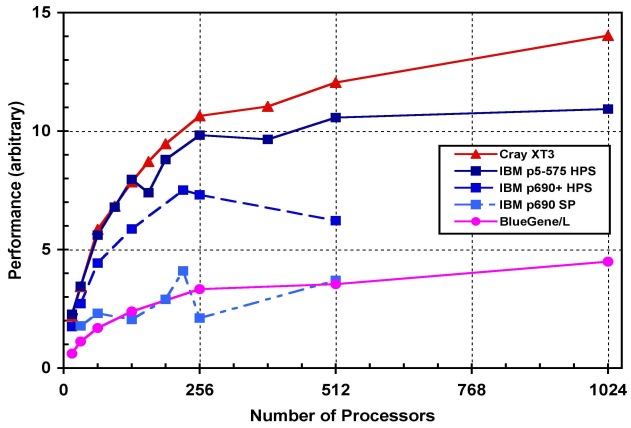

FIG. 3. Performance of PDSYEVD on the latest HPC architectures (CRYSTAL matrix, n=7194).

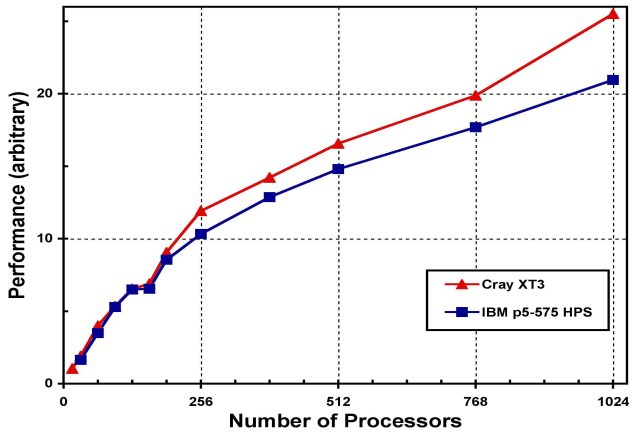

FIG. 4. Parallel Scaling for large problem size on Cray XT3 and IBM p5-575 (CRYSTAL matrix, n=20480).

Figures 3 and 4 show how the PDSYEVD routine scales with processor count on the high-end computing platforms detailed in section III B. Parallel performance is best on the Cray XT3 for both matrices tested here, relatively closely matched by the current configuration of HPCx (IBM p5-575 with the

High Performance Switch). The performance of the IBM BlueGene/L is around three times slower than the Cray XT3, roughly matching the performance of the orginal HPCx system.

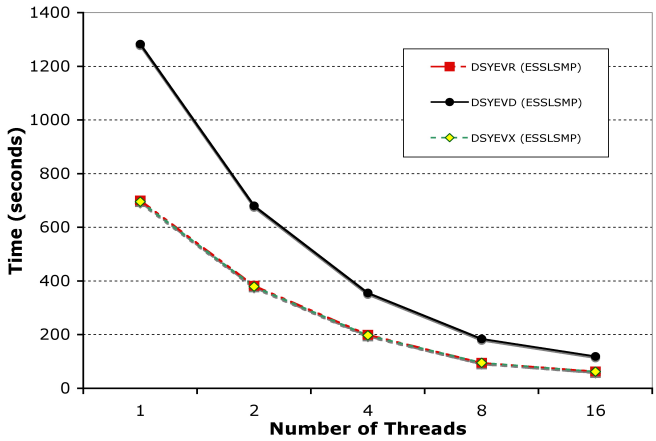

FIG. 5. Performance of Multithreaded Diagonalization Routines on HPCx (Hamiltonian n=10032).

Figure 5 compares the performance of several multithreaded eigensolver routines from the optimised IBM library `esslsmp` on one shared-memory processing node of HPCx. All the solvers now scale well within a node upto the maximum of 16 processors, though *DSYEVD* is now somewhat slower than *DSYEVR* and *DSYEVX*. At present the reasons for the relatively slow performance of multithreaded *DSYEVD* have not been determined.

V. CONCLUSIONS

The latest ScaLAPACK eigensolvers are generally reliable and perform well for the Hamiltonian systems central to PRMAT calculations. Typically, the parallel scaling improves for the larger problem sizes on all the platforms, as the computation to communication ratio increases. In other reports it has been established that both solvers generally perform preferably to the original ScaLAPACK solvers *PDSYEV* and *PDSYEVX* for the matrices under test here (see [10]). The parallel performance of the beta version of the MRRR-based solver *PDSYEVR* obtained from the developers for testing performs comparably to the divide-and conquer based *PDSYEVD* over a range of problem sizes. However it is apparent that the "holy grail" properties of $O(kn)$ operations and memory overheads of $O(n)$ are yet to be achieved for *PDSYEVR*. This is to be expected as the beta version relies on pre-exisiting underlying matrix and vector operations not necessarily optimised for the relatively low workspace requirements of the MRRR algorithm. It is expected that the fully developed version of *PDSYEVR* in the next release of ScaLAPACK will have performance properties matching closer to the theory. The performance of multi-threaded versions of these eigensolvers on HPCx also scales well within a node, in contrast to the performance obtained on earlier configurations of HPCx. Further work is underway to analyse some of the discrepencies between the multi-threaded eigensolvers investigated here.

---

[1] *A parallel R-matrix program PRMAT for electron-atom and electron-ion scattering calculations*, A.G. Sunderland, C.J. Noble, V.M. Burke, P.G. Burke, Computer Physics Communications 145 (2002) 311-340

[2] K.L. Baluja, P.G. Burke and L.A. Morgan, Comput. Phys. Commun. 27 (1982) 299

[3] *The numerical computation of the characteristic values of a real symmetric matrix*, Wallace J. Givens, Technical Report ORNL-1574, Oak Ridge National Laboratory, Oak Ridge, TN, USA, (1954)

[4] *The calculation of specified eigenvectors by inverse iteration, contribution II/18*, volume II of Handbook of Automatic Computation, pagesSpringer-Velag, New Yotk, Heidelberg, Berlin, (1971)

[5] *The QR transformation, parts I and II*, Computer J., 4:265-271, 332-345, (1961-62)

[6] *A parallel divide and conquer algorithm for the symmetric eigenvalue problem on distributed memory architectures*, F. Tisseur and Jack Dongarra, SIAM J. SCI. COMPUT, Vol.20, No. 6, pp. 2223-2236 (1999)

[7] *A Parallel Eigensolver for Dense Symmetric Matrices based on Multiple Relatively Robust Representations*, P. Bientinesi, I.S. Dhillon, R.UT CS Technical Report TR-03026, (2003)
[8] http://www.netlib.org/scalapack/scalapack_home.html
[9] *PDSYEVR. ScaLAPACKs parallel MRRR algorithm for the symmetric eigenvalue problem*, D. Antonelli, C. Vomel, Lapack working note 168, (2005). http://www.netlib.org/lapack/lawnspdf/lawn168.pdf
[10] *Performance of a New Parallel Eigensolver PDSYEVR on HPCx*, A.G. Sunderland, HPCx Technical Report (2006), http://www.hpcx.ac.uk/research/hpc/technical_reports/HPCxTR0608.pdf
[11] *The HPCx National Supercomputing Facility*, http://www.hpcx.ac.uk/
[12] *The Science and Technology Facilities Council*, http://www.stfc.ac.uk/
[13] *The IBM BlueGene/L*, http://www.research.ibm.com/bluegene/
[14] *The Swiss National Supercomputing Centre*, http://www-users.cscs.ch/xt4/
[15] *Lapack Working Note 168: PDSYEVR. Scalapack's Parallel MRRR Algorithm for the Symmetric Eigenvalue Problem*, Dominic Antonelli and Christof Voemel, http://www.netlib.org/lapack/lawns/lawn168.ps
[16] *CRYSTAL: A computational tool for solid state chemistry and physics*, http://www.crystal.unito.it/

M Plummer, J D Gorfinkiel and J Tennyson (eds.)
Mathematical and computational methods in R-matrix theory

The partitioned *R*-matrix method

Jonathan Tennyson and Gabriela Halmova

Department of Physics and Astronomy,
University College London, London WC1E 6BT, UK

I. INTRODUCTION

The R-matrix method is a well established computational procedure for treating electron collisions with atoms and molecules [1]. The basis of the method is the division of space into two regions: an inner region, defined by a sphere of radius a, typically $10\,\mathrm{a}_0$ to $15\,\mathrm{a}_0$ for molecular problems, and an outer region. The inner region must contain the entire electron density of the target system which means that it is only in this region that complicated correlation and exchange processes need to be treated in detail. The R-matrix, defined below, provides the link between the two regions.

In order to solve the inner region problem, which does not depend on the precise scattering energy of the electron, it is necessary to find solutions of the inner region Hamiltonian. This is usually done by expressing the vavefunction as a linear combination of configuration spin functions (CSFs), see [2], and diagonalising the resulting secular matrix problem. The eigenvalues, E_k, and eigenvectors are used to construct the R-matrix on the boundary a:

$$R_{il,i'l'}(a,E) = \sum_{k=1}^{M} \frac{w_{ilk}(a) w_{i'l'k}(a)}{E_k - E} + \delta_{ii'}\delta_{ll'} R^B_{il} \tag{1}$$

where $w_{ilk}(a)$ is the amplitude of partial wave l associated with target state i in eigenvector k at a. E is the scattering energy and R^B_{il} is the Buttle correction which can be introduced to correct for the incompleteness of the continuum basis in the inner region [1].

A serious computational drawback of this procedure is that the construction of $R_{il,i'l'}(a,E)$ requires all M solutions of the M-dimensional secular matrix. Since computer time for diagonalising a matrix increase as M^3 and the memory requirement increases as M^2, this puts a significant constraint on problems that can be addressed.

In practice many of the inner region solutions lie at energies which are very significantly higher than the scattering energy of interest. This is particularly

true for problems involving electron collisions with molecules where the region of interest is usually for electron collision energies below 20 eV.

Berrington and Ballance (BB) [3] derived a "partitioned R-matrix method" which only explicitly uses the lowest P inner region solutions and then approximated the higher solutions. Unfortunately the practical test given by BB required P to be about half M to give good results. This is too many solutions to provide any significant computational saving. This method was subsequently re-analysed and an alternative formulation of the partitioned R-matrix method was given by Tennyson [4]. These methods are discussed below.

II. PARTITIONED *R*-MATRIX THEORY

In BB's partitioned R-matrix method the R-matrix on the boundary is approximated as

$$R_{il_i,i'l_{i'}}(a,E) = \sum_{k=1}^{P} w_{ilk}(a) w_{i'lk}(a) \left(\frac{1}{E_k - E} - \frac{1}{E_0 - E} \right)$$

$$+ \delta_{ii'}\delta_{ll'} \left(\frac{s_{il}}{E_0 - E} + R^B_{il} + R^C_{il} \right) \tag{2}$$

where R^C_{il} is an error correction term discussed below. E_0 is an average or effective energy for the poles omitted when only the lowest P solutions are explicitly considered; it is defined as:

$$E_0 = \frac{(\sum_{I=1}^{M} H_{I,I} - \sum_{k=1}^{P} E_k)}{M - P}, \tag{3}$$

where the first sum is simply the trace of the Hamiltonian matrix. In (2), s_{il} is the total probability distribution of a given channel on the R-matrix boundary

$$s_{il} = \sum_{j=1}^{n_{il}} (u_{ilj}(a))^2, \tag{4}$$

where $u_{ilj}(a)$ is the amplitude of the jth function used to represent the continuum electron inside the R-matrix box, see [5] for example. BB's error correction term was also expressed as a function of these quantities:

$$R^C_{il} = \sum_{j=J_i}^{n_{il}} (u_{ilj}(a))^2 \left(\frac{1}{E_{ilj} - E} - \frac{1}{E_0 - E} \right). \tag{5}$$

where BB defined E_{ilj} as the energy of the continuum function $u_{ilj}(x)$ and the sum runs over those states for which $E_{ilj} > E_P$, the energy of the highest pole explicitly considered.

Tennyson [4] identified two problems with this formulation. The first was that the definition of E_0 was such that it increases as more L^2 terms are added to the inner region wavefunction expansion as most of these tend to be high in energy. However such terms have zero amplitude at a and therefore do not contribute to the R-matrix. Secondly BB's error correction term over-corrected since s_{il} summed all the probability for a channel even if some of this probability had already been accounted for in the P terms explicitly considered in the sum. Finally for molecular problems he observed that the energy of a continuum basis function is not really well defined. This latter problem was solved by using the appropriate diagonal element of the Hamiltonian matrix instead.

Tennyson redefined the effective energy, E_0, as the average of those diagonal elements of the Hamiltonian matrix between continuum orbitals, $H_{ilj,ilj}$, which are not among the lowest P diagonal elements, ie for $H_{ilj,ilj} > E_P$. This definition leaves E_0 unaffected by increasing the number of purely L^2 functions used. Secondly, he estimated the contribution of the continuum orbitals to the states not explicitly included in the sum (2) as:

$$X_{ilj} = 1 - \sum_{k=1}^{P} c_{iljk}^2. \tag{6}$$

where c_{iljk} is the coefficient of continuum orbital u_{ilj} in the kth eigenvector. This factor is then used to define a new error correction formula:

$$R_{il}^C = \sum_{j=J_i}^{n_{il}} (u_{ilj}(a))^2 X_{ilj} \left(\frac{1}{H_{ilj,ilj} - E} - \frac{1}{E_0 - E} \right). \tag{7}$$

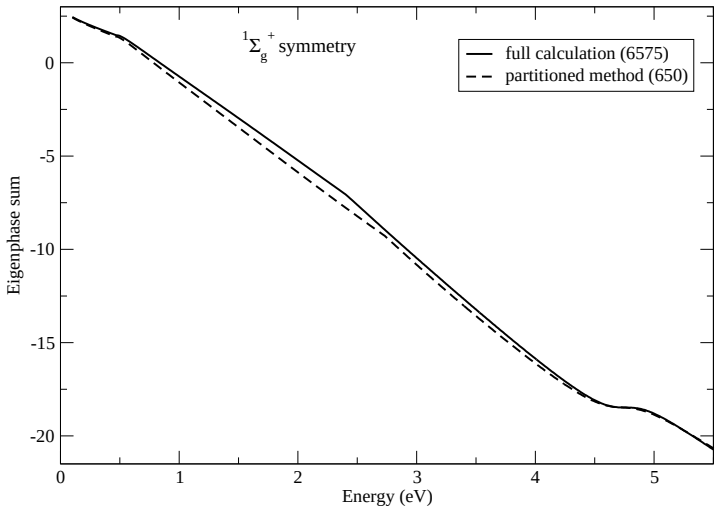

FIG. 1. Eigenphase sums for electron scattering from C_2^- for a full calculation (solid curve) and a partitioned R-matrix calculation (dashed curve).

III. TEST CALCULATIONS

In the initial work [4] tests were performed against previous calculations on electron collisions with water [6] and CF_2 [7]. These showed that not only did the reformulated theory perform very significantly better than the original theory but also the goal of getting good results for the case where P is 10 % or less of M was indeed achievable for low-energy (below 20 eV) studies. However these initial studies by their nature were all performed on problems for which it was possible to obtain all M eigenvalues and eigenvectors.

Recently we have been considering calculations on electron collisions with the C_2^- anion for collision energies of about 10 eV. Given that the electron detachment energy for this anion is below 5 eV, such calculations can only be performed using a method capable of treating the double continuum. Gorfinkiel and Tennyson [8,9] introduced a molecular R-matrix with pseudo states (MRMPS) procedure for treating precisely this class of problem. However their applications of the MRMPS procedure were only to two electron targets (H_3^+ and H_2). Attempts to use the procedure for many electron targets have proved difficult because of the very large number of configurations that need to be treated as a result of trying to treat the double continuum even if it is discretised by being localised inside a box.

We have therefore combined the MRMPS method with the partitioned R-matrix method to treat the problem of electron collisions with C_2^-. Figure 1

shows some test results for one of the smaller wavefunctions that we considered. Eigenphases are shown calculated using the full, $M = 6575$, solutions and with less than 10 % of that number, $P = 650$. It can be seen that the results are very similar. Indeed the resonance feature just below 5 eV is essentially unmoved between the two calculations. This result is typical of the more extensive (in both energy range and number of states P) tests that we have performed.

IV. CONCLUSIONS

The reformulation of the partitioned R-matrix method [4] provides a viable way of performing calculations on problems which are too large for full diagonalisation of the inner region Hamiltonian matrix to be computationally tractable. We are currently using this method to perform calculations on the electron impact detachment of C_2^- using molecular R-matrix with pseudo states models which give Hamiltonian matrices of dimension $M \sim 100,000$. For such calculations the partitioned R-matrix method represents a major saving. This is particularly true because the proportion of solutions required drops well below 10 %, indeed we anticipate obtaining good results with calculations which explicitly consider only about 1 % of the solutions of inner region Hamiltonian matrix.

P, the number of solutions explicitly obtained, is critical for the computational performance of the method but is perhaps the wrong parameter to focus on physically. Physically the important parameter is probably the energy span of the solutions which are explicitly calculated, as to get a good calculation it is clearly important to span the energy regime of the colliding electron. In this sense the key parameter should therefore be the eigenenergy of solution P, E_P. Our calculations on the C_2^{2-} system show that to get stable results for collisions energies of 15 eV, E_P should be at least 40 eV.

Finally we note one computational issue with implementing the partitioned R-matrix method. The outer region of the UK R-matrix codes is written in a highly modular fashion [10]. Communication between the various modules, which perform tasks such as R-matrix propagation [11,12] or resonance fitting [13], is achieved via a series of small input/output subroutines [10]. The partitioned R-matrix method requires significant extra information to be passed between these modules so that the error-corrected partitioned R-matrix can be constructed. The re-write of the communications routines makes it difficult for the new codes to be backwards compatible. There is no such problem with the only inner region code that needs amending, SCATCI [2].

Acknowledgements

The UK molecular R-matrix code has been supported over many years by UK Collaborative Computational Project 2 (CCP2).

[1] P. G. Burke and K. A. Berrington, eds., *Atomic and Molecular Processes, an R-matrix Approach* (Institute of Physics Publishing, Bristol, 1993).
[2] J. Tennyson, *J. Phys. B: At. Mol. Opt. Phys.* **29**, 1817 (1996).
[3] K. A. Berrington and C. P. Ballance, *J. Phys. B: At. Mol. Opt. Phys.* **35**, 2275 (2002).
[4] J. Tennyson, *J. Phys. B: At. Mol. Opt. Phys.* **37**, 1061 (2004).
[5] A. Faure, J. D. Gorfinkiel, L. A. Morgan, and J. Tennyson, *Comput. Phys. Commun.* **144**, 224 (2002).
[6] J. D. Gorfinkiel, L. A. Morgan, and J. Tennyson, *J. Phys. B: At. Mol. Opt. Phys.* **35**, 543 (2002).
[7] I. Rozum, N. J. Mason, and J. Tennyson, *J. Phys. B: At. Mol. Opt. Phys.* **35**, 1583 (2002).
[8] J. D. Gorfinkiel and J. Tennyson, *J. Phys. B: At. Mol. Opt. Phys.* **37**, L343 (2004).
[9] J. D. Gorfinkiel and J. Tennyson, *J. Phys. B: At. Mol. Opt. Phys.* **38**, 1607 (2005).
[10] L. A. Morgan, J. Tennyson, and C. J. Gillan, *Comput. Phys. Commun.* **114**, 120 (1998).
[11] K. L. Baluja, P. G. Burke, and L. A. Morgan, *Comput. Phys. Commun.* **27**, 299 (1982).
[12] L. A. Morgan, *Comput. Phys. Commun.* **31**, 419 (1984).
[13] J. Tennyson and C. J. Noble, *Comput. Phys. Commun.* **33**, 421 (1984).

M Plummer, J D Gorfinkiel and J Tennyson (eds.)
Mathematical and computational methods in R-matrix theory

Finite-elements R-matrix calculations: from molecules to the condensed phase

Stefano Tonzani

Department of Chemistry,
Northwestern University, Evanston, IL 60208-3113, USA

In the context of R-matrix theory, the present work describes an approach based on wavefunction expansion in a finite element basis set, targeted at calculations of electron-molecule scattering processes for large polyatomic targets. This method has been used successfully in various applications concerning gas phase molecules. When combined with multiple scattering theory, this can be also useful for processes at surfaces or in condensed phases.

I. INTRODUCTION

Amidst the large number of codes available to perform electron-molecule scattering calculations there is still a need for a simple tool that allows calculations for large molecules difficult to explore with more accurate treatments. Our approach contains a series of approximations that permit a fast treatment of large molecules, while limiting its applicability to elastic scattering, and its accuracy in terms of resonance positions to 1-2 eV when compared to experiment. We tested this approach on electron-molecule scattering from increasingly complex targets [1–5], photoionization [1] as well as strong field-molecule interactions [6].

It is neither feasible nor desirable, though, to use this approach for macromolecules like DNA because of computational requirements but also because the coupling between subunits is weaker than among atoms in a molecule, therefore a simpler approach like multiple scattering can be applied and it can be useful also by allowing the decomposition of the wavefunction over the various subunits. Combining multiple scattering with accurate phase shifts obtained *ab initio* is a powerful technique that can be exploited in many contexts, from electron-beam induced chemistry, to processes that take place in condensed phases. One of these processes is radiation damage to DNA [7] which we consider in more detail below and in Ref. [8].

II. *R*-MATRIX AND FINITE ELEMENTS

Starting from the fixed-nuclei electronic Schrödinger equation we simplify the problem using the static exchange approximation: we neglect all but the ground electronic target state, transforming the scattering problem into an effective 1-body problem, which features the electrostatic interaction, dependent on the target electron density and the nuclei positions, and the nonlocal exchange interaction. Using the local density approximation, the latter becomes [3]:

$$V_{ex}(\vec{r}) = -\frac{2}{\pi}k_F F(\eta) \qquad k_F(\vec{r}) = (3\pi^2\rho(\vec{r}))^{1/3} \qquad \eta = \frac{k}{k_F}. \tag{1}$$

where k_F is the Fermi momentum. Now we have to solve a potential scattering problem. The energy-dependent functional we use is the Hara exchange [9] where $k = \sqrt{2(E+I)+k_F^2}$ and I is the ionization energy of the molecule.

We add to static and exchange potentials a parameter-free local correlation-polarisation potential [10]. The long-range part of this potential is the dipole polarizability potential: $V_{pol} = -\frac{\alpha_0}{2r^4}$ where α_0 is the totally symmetric component of the polarisability tensor. This potential is nonlocal inside the molecule, but we use an approximate (local) form of the interaction based on the Lee-Yang-Parr potential of Ref. [11] which has been shown to give reliable results [10]. The short- and long-range potentials are matched unambiguously at their outermost crossing point, which is angle dependent. The final potential is continuous but not smooth. The electrostatic potential, electron density, gradient, laplacian, and polarizability are all calculated from *ab initio* codes (Gaussian, Gamess).

To calculate the scattering observables we use the R-matrix method, which consists in diagonalizing a continuum Hamiltonian inside a box (in our case a sphere of radius R_0), and having a separate long-range region where only simple interactions (Coulomb, dipole) are present. Rearranging the energy variational principle, we can obtain one for the logarithmic derivative of the wavefunction [12]:

$$b \equiv -\frac{\partial \log(r\Psi_\beta)}{\partial r} = 2\frac{\int_V \Psi^*(E-\hat{H}-\hat{L})\Psi dV}{\int_V \Psi^*\delta(r-r_0)\Psi dV}. \tag{2}$$

Expansion of Ψ in some basis set results in a generalized eigenvalue problem for b:

$$\underline{\Gamma}\vec{C} = (E - \underline{H} - \underline{L})\vec{C} = \underline{\Lambda}\vec{C}b \tag{3}$$

where $\underline{\Lambda}$ is the basis functions overlap on the surface of the sphere, $\hat{L}$ is the Bloch operator.

Partitioning the basis functions in two subspaces, closed and open, depending on whether their value at the surface of the box is zero or nonzero [12] we can reduce the burden of the solution of Eq. 3 to the easier task of solving a small eigenvalue problem: $\Omega\vec{C}_o = (\underline{\Gamma}_{oo} - \underline{\Gamma}_{oc}\underline{\Gamma}_{cc}^{-1}\underline{\Gamma}_{co})\vec{C}_o = \underline{\Lambda}_{oo}\vec{C}_o b$ and an associated very large linear system to get $\underline{\Gamma}_{cc}^{-1}$.

Our basis set is a cross product of finite element cubic polynomials [13] and it generates large (.5Mx.5M) sparse (.5% full) matrices. The task of solving the large linear system has to be tackled with fast and efficient parallel direct solvers [14]. The implementation of this approach is described in a previous work [1].

This approach has been applied to electron scattering from a series of molecules, as illustrated in Refs. [1–5]. In particular, we explored the DNA bases (interesting in the problem of radiation damage) as illustrated in Fig. 1. Resonant wavefunctions have been also calculated for these molecules [2] and they can be used in a first approximation to understand trends in dissociative electron attachment.

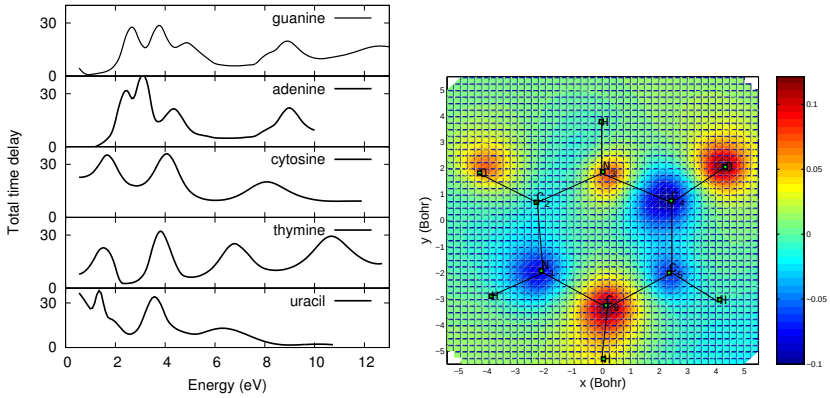

FIG. 1.

Total time-delay for the four main DNA bases, and the wavefunction for the first resonance of uracil at 1.3eV (adapted from Ref. [2], Figures 4 and 9).

III. MULTIPLE SCATTERING

In this framework, widely used in solids [15], molecules [16] and macromolecules [17] each molecular subunit has an incident plane wave of momentum $\vec{k}$ impinging on it plus the scattered waves of all other subunits. More specifically, the asymptotic form of the total wave function $\psi_{\vec{k}}^{(n)}(\vec{r})$ for a molecule centered at $\vec{R}_n$ outside the R-matrix shell is:

$$\psi_{\vec{k}}^{(n)}(\vec{r}) = 4\pi e^{i\vec{k}\cdot\vec{R}_n} \sum_{LL'} i^l B_{\vec{k}L}^{(n)} Y_{L'}\left(\Omega_{\vec{r}_n}\right) \Bigg[j_l\left(kr_n\right)\delta_{L'L} + \frac{1}{2}\left(S_{L'L}^{(n)} - \delta_{L'L}\right) h_{l'}^{(1)}\left(kr_n\right)\Bigg] \qquad (4)$$

where Y_L are spherical harmonics, j_l and $h_{l'}^{(1)}$ are the spherical Bessel function and Hankel function of the first kind respectively, $\vec{r}_n = \vec{r} - \vec{R}_n$, and $B_{\vec{k}L}^{(n)}$ are coefficients that contain the S-matrices of all the other scatterers, therefore Eq. 4 has to be calculated self-consistently. With this approach we have explored the interactions between neighboring bases in DNA and the role of coherence length (see Fig. 2), sequence disorder and structural conformation, to show that single molecule effects are not the only ones present and the effect of the environment has to be taken into account for a realistic description of DNA radiation damage [8]. At the same time the knowledge gathered in gas phase calculations can be very useful in establishing a model fit to describe the condensed phase environment.

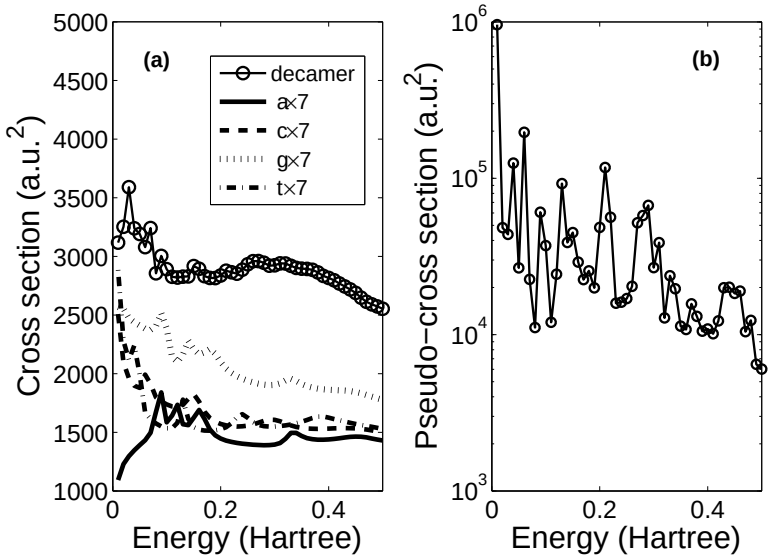

FIG. 2.

Interpolated total elastic cross section of the GCGAATTGGC B-form decamer at $\xi = 1000$ compared with the single adenine, cytosine, guanine, and thymine R-matrix cross section values (a) and at $\xi = 20$ (b) as a function of incident electron energy (adapted from Ref. [8], Figure 6).

Acknowledgements

This research has been supported by NSF, NSEC, and NERSC through supercomputing resources. We wish to thank C H Greene for the stimulus in undertaking this project and the continuous help and support given along the way, and L Sanche and L Caron, collaborators for the multiple scattering calculations.

---

[1] S. Tonzani, *Comput. Phys. Commun.* **176**, 146 (2007).
[2] S. Tonzani and C. H. Greene, *J. Chem. Phys.* **124**, 054312 (2006).
[3] S. Tonzani and C. H. Greene, *J. Chem. Phys.* **122**, 014111 (2005).
[4] S. Tonzani and C. H. Greene, *J. Chem. Phys.* **125**, 094504 (2006).
[5] S. Tonzani, Ph.D. thesis, JILA and Dept. of Chemistry, University of Colorado, Boulder (2006).
[6] Z. Walters, S. Tonzani, and C. H. Greene, *J. Phys. B: At. Mol. Opt. Phys.* **40**, F277 (2007).
[7] B. Boudaiffa, P. Cloutier, D. Hunting, M. A. Huels, and L. Sanche, *Science* **287**, 1658 (2000).
[8] L. Caron, S. Tonzani, C. H. Greene, and L. Sanche, *J. Chem. Phys: submitted* (2007).
[9] S. Hara, *J. Phys. Soc. Jpn.* **27**, 1009 (1969).
[10] F. A. Gianturco and J. A. Rodriguez-Ruiz, *Phys. Rev. A* **47**, 1075 (1993).
[11] C. Lee, W. Yang, and R. G. Parr, *Phys. Rev. B* **37**, 785 (1988).
[12] C. H. Greene, M. Aymar, and E. Luc-Koenig, *Rev. Mod. Phys.* **68**, 1015 (1996).
[13] Bioengineering Institute, The University of Auckland, New Zealand, *Fem/bem notes* (1997), http://www.bioeng.auckland.ac.nz/cmiss/fembemnotes/fembemnotes.pdf.
[14] Scientific Computing Group, University of Basel, *Pardiso*, http://www.computational.unibas.ch/cs/scicomp/software/pardiso/.
[15] G. A. Fiete and E. J. Heller, *Rev. Mod. Phys.* **75**, 933 (2003).
[16] D. Dill and J. L. Dehmer, *J. Chem. Phys.* **61**, 692 (1974).
[17] L. G. Caron and L. Sanche, *Phys. Rev. Lett.* **91**, 113201 (2003).